MONASH University

Particle Manipulation in Microfluidic System using Novel Surface Acoustic Wave Field

Jia Wei Ng

Bachelor of Engineering (Mechanical) (Hons.)

A thesis submitted for the degree of (*Doctor of Philosophy*) at
Monash University in 2020
Department of Mechanical and Aerospace Engineering

Copyright notice

Abstract

The study of fluid flow at the sub-millimetre scale, is known as microfluidics. It is an enabling technology that offers scaling down of common laboratory procedures into what is called lab-on-a-chip (LOC) devices. This offers many advantages like reduced size, cost, time and the amount of reagent and samples needed. Point-of-care (POC) applications can be successfully implemented using this technology. This is extremely useful especially in current times with the outbreak of the COVID-19 pandemic, where POC devices would radically improve the accessibility and affordability of medical diagnostics. However, due to the operational length scale of these devices being in order of magnitudes smaller than traditional fluid processing systems, specific phenomena not normally encountered in their macroscale counterparts have been created. Manipulation of micro-objects in closed microfluidic channels have been proven to be challenging. Surface acoustic waves (SAWs) offer great solution to this issue, where they can generate large but gentle force, providing the means to rapid manipulation in microfluidic systems. SAWs usually operate in high frequencies and correspondingly small length scales, allowing acoustic manipulation of micro-objects such as cells and bacteria, which is useful in biological applications. SAWs are excited by patterned electrodes, leading them to have acoustic fields that are highly localised and easily shaped, instead of having to rely on the resonance mode as in bulk acoustic wave (BAW) systems.

This doctoral thesis presents three particle manipulation platforms that are novel by exploiting the misconceptions typically made on the generation SAW fields used in micro-objects manipulations. Firstly, the classification of SAW systems is explored. They are usually categorised as using either travelling surface acoustic waves (TSAW) or standing surface acoustic waves (SSAW). However, aspects of both types of waves exist in any one system. We demonstrated this and developed a particle sorting platform that is size-deterministic. Next, we looked into the assumption of superposition of two counter-propagating waves forming a standing wave with periodic pressure nodes for particle trapping. The effect of exciting each of the two electrode sets with slightly different frequencies is examined. We showed theoretically, numerically, and experimentally that this frequency difference actuation scheme causes a new type of field

in which particles are not pushed as in a TSAW, or held in periodic locations as in a SSAW, but rather held in a single location which is easily controlled via relative amplitude modulation. Finally, by the combination of knowledge from the first two acoustic manipulation platforms and having a deeper understanding of the type of field obtained from distant electrodes sets, we examined the use of multiple sets of electrodes in close proximity and also slightly offset from each other laterally. We showed that the electrodes behave independently despite their proximity. There is little effect of acoustic streaming generated at the periphery of each electrode sets. The offset of the electrode set also accurately produced the pressure nodes offset in the sound field. We demonstrated that this results in the capability of using different actuation combinations to produce different sound fields to achieve multichannel acoustic sorting, enabling the integration to on-chip Fluorescence Activated Cell Sorter (FACS).

List of Publications

Articles in peer reviewed journals

1. Jia Wei Ng, David J. Collins, Citsabehsan Devendran, Ye Ai, Adrian Neild. Flow-rate-insensitive deterministic particle sorting using a combination of travelling and standing surface acoustic waves. Microfluidics and Nanofluidics, 2016;20(11). doi:10.1007/s10404-016-1814-2

2. Jia Wei Ng, Citsabehsan Devendran, Adrian Neild. Acoustic tweezing of particles using decaying opposing travelling surface acoustic waves (DOTSAW). Lab on a Chip. 2017;17(20):3489-3497. doi:10.1039/c7lc00862g

3. Jia Wei Ng, Adrian Neild. Multiple outcome particle sorting using cascaded surface acoustic wave (CSAW) manipulation. In review, 2020

4. David J. Collins, Citsabehsan Devendran, Zichao Ma, Jia Wei Ng, Adrian Neild, Ye Ai. Acoustic tweezers via sub–time-of-flight regime surface acoustic waves. Science Advances. 2016;2(7):e1600089. doi:10.1126/sciadv.1600089

Conference proceedings

1. Jia Wei Ng, David J. Collins, Citsabehsan Devendran, Ye Ai, Adrian Neild. Flow-rate-insensitive deterministic particle sorting using a combination of travelling and standing surface acoustic waves. *The 20th International Conference on Miniaturized Systems for Chemistry and Life Sciences, October 2016.*

2. Jia Wei Ng, Citsabehsan Devendran, Adrian Neild. Acoustic tweezing of particles using decaying opposing travelling surface acoustic waves (DOTSAW). *The 14th Conference on Acoustofluidics, August 2017.*

Thesis including published works declaration

I hereby declare that this thesis contains no material which has been accepted for the award of any other degree or diploma at any university or equivalent institution and that, to the best of my knowledge and belief, this thesis contains no material previously published or written by another person, except where due reference is made in the text of the thesis.

This thesis includes 2 original papers published in peer reviewed journals and 1 submitted publication. The core theme of the thesis is particle manipulation using surface acoustic waves within microfluidic systems. The ideas, development and writing up of all the papers in the thesis were the principal responsibility of myself, the student, working within the Laboratory for Micro Systems (LMS), Department of Mechanical and Aerospace Engineering, Faculty of Engineering, under the supervision of Prof. Adrian Neild and Dr. Tuncay Alan.

The inclusion of co-authors reflects the fact that the work came from active collaboration between researchers and acknowledges input into team-based research.

In the case of Chapters 3 and 4, my contribution to the work involved the following:

Thesis Chapter	Publication Title	Status
3	Flow-rate-insensitive deterministic particle sorting using a combination of travelling and standing surface acoustic waves.	Published
4	Acoustic tweezing of particles using decaying opposing travelling surface acoustic waves (DOTSAW)	Published

Nature and % of student contribution	Co-author name(s) Nature and % of Co-author's contribution	Co-author(s), Monash student Y/N*
Paper 1 (thesis Chapter 3): 80% Design, fabrication of devices, experimentation, numerical modelling, development, results analysis, interpretation and writing.	1) Citsabehsan Devendran (numerical modelling, review of drafts 6%), 2) David Collins (review of drafts 4%), 3) Ye Ai (review of drafts 3%), 4) Adrian Neild (Contributions to theory, overall supervision and review of drafts 7%)	N, N, N, N
Paper 2 (thesis Chapter 4): 85% Design, fabrication of devices, experimentation, numerical modelling, development, results analysis, interpretation and writing.	1) Citsabehsan Devendran (numerical modelling, review of drafts 5%), 2) Adrian Neild (contributions to theory, overall supervision and review of drafts 10%)	N, N

In thesis Chapter 5, the submitted publication with the title 'Multiple outcome particle sorting using cascaded surface acoustic wave (CSAW) manipulation'
Paper 3 (thesis Chapter 5):
85% Design, fabrication of devices, experimentation, numerical modelling, development, results analysis, interpretation and writing. 1) Adrian Neild (Contributions to theory, overall supervision and review of drafts 15%)

I have not renumbered sections of submitted or published papers in order to generate a consistent presentation within the thesis.

Student signature:

Student name: Jia Wei Ng

Date: 18 June 2020

Main Supervisor signature:

Main Supervisor name: Prof. Adrian Neild

Date: 18 June 2020

I hereby certify that the above declaration correctly reflects the nature and extent of the student's and co-authors' contributions to this work. In instances where I am not the responsible author, I have consulted with the responsible author to agree on the respective contributions of the authors.

x

Acknowledgments

First, I am profoundly grateful to my supervisor Professor Adrian Nield, who has been an unwavering source of encouragement and patience. Thank you for never giving up on me even though I felt like doing so myself. This thesis would not have been possible without your guidance. I would also like to thank my co-supervisor Dr Tuncay Alan for being supportive and providing invaluable insights into the matter in hand. I thank my current and former group members including Saab, Jason, Muhsincan, Amy, An, Nin, Sam, David, Ganaka, Emin, Bulut, Rui, Dariush, Yaqi, Joe, and Mahraz for all the fun and company throughout my PhD and being a massive help in the lab. I am very lucky to be a part of Lab for Microsystems (LMS), where everyone is so willing to help each other out. I would like to thank the Faculty of Engineering for the Postgraduate Research Scholarship (ERLA) to support the research carried out throughout my PhD. I would also like to thank the Department of Mechanical and Aerospace Engineering and the Monash Institute of Graduate Research, for the technical and administrative support given throughout my candidature. I also appreciate all the staff members from Melbourne Centre for Nanofabrication (MCN) for their help with the device fabrications. A huge thank you to my family. To my parents, Chai Yin and Yoke Leng, I wouldn't be here without all your support. To my siblings, Pei Ying, Jia Jun and Jia Yi, even from Malaysia, I've always felt your encouragement and support. To my coaches, teammates and friends at Southern Cross Cheerleading, you have kept both my body and my mind healthy over the years. To all my Malaysian friends that now reside in Melbourne, thanks for your support and friendships, but most importantly for bringing a little piece of home to this foreign land. I also would like to thank my housemate Rosie for all the cups of tea and companionship during the long, late nights of writing. Lastly, I would like to express my deepest gratitude to my amazing partner Saul. Even though I might have finished this thesis a lot earlier without you, these past years wouldn't have been filled with nearly as much love and fun. Though in all honesty, it would have been impossible to finish this PhD without you. Thank you for keeping me in line and showing me the light in some of the very dark times. I would be so lost without your unwavering love, support and understanding.

List of Figures

Contents

Chapter 1

Introduction

This chapter will introduce the general concept of microfluidics and discuss why it has become such a prominent field of research. This will be followed by a brief overview of the thesis outline and upcoming chapters.

1.1   Microfluidics

Microfluidics is a multidisciplinary field that studies fluids with volume ranging from femtoliters (fL) to microliters (μL) [1, 2]. The field has been revolutionary in life sciences research and industry and has received a great deal of research in recent times. Many devices are now capable of outperforming their classical ancestors.

While the study of microfluidics effects began over a century ago, such research only became truly viable with the development of microelectromechanical systems (MEMS) and the resultant microfabrication technology in the 1980s [3-5]. This microfabrication technology has allowed the creation of microscale devices which can take advantage of scaling law to allow for novel functionality and the study of phenomena that were elusive to macroscale devices [6]. These effects explain many of the advantages of a microfluidic system such as fast reaction time and small amount of reagent required.

The practical application of microfluidics is both broad in scope, ranging from ink jet printing [7-9] to chemical threat detectors [10] to the 3D printing of organs [11], and hold potential for great progress. Nowhere is this promise more apparent than in the area of biomedicine. Specifically, the development and successful implementation of lab-on-a-chip (LOC) technology, a microfluidic system that seeks to recreate the functions of a laboratory on a microchip. Successful implementation of this concept allows for point of care applications [12, 13]. This would radically improve the accessibility and affordability of medical diagnostics and monitoring. The current COVID-19 pandemic has only highlighted the need for advances in this vital area of public health. Further

elaboration and in-depth review of lab-on-a-chip (LOC) systems is presented in Chapter 2.

1.2   Thesis Overview

The purpose of the research in this thesis is to develop SAW manipulation techniques in microfluidic systems and to develop understanding of the physical principles that underlie these methods. The thesis is laid out as follows: a thorough literature review of SAW in microfluidic systems is performed in Chapter 2, the research is then presented in three separate publications, comprising Chapters 3-5. Finally, concluding remarks are made in Chapter 6. These chapters are described in more detail in the following subsections.

1.2.1   Chapter 2: Background, theory and fabrication

In Chapter 2, a thorough literature review is performed. The basic principles and scaling laws of a microfluidic system are discussed. This is followed by the discussion of the various microfluidic particle/cell manipulation techniques. The principles of acoustic manipulation method are then presented in-depth. Finally, the microfabrication procedures related to the production of both SAW devices and the microfluidic channels are described.

1.2.2   Chapter 3: Flow-rate-insensitive deterministic particle sorting using a combination of travelling and standing surface acoustic waves

Chapter 3 explores the use of unconventional acoustic pressure fields for continuous particle/cell sorting system. Particle and cell sorting are an important and necessary function in a wide range of pre-treatment and on-chip analysis applications. SAW sorting systems are usually classified as using either travelling (TSAW) or standing (SSAW) waves, and the separation is often temporal in nature rather than size deterministic. However, aspects of both types of waves exist in any one system. This

phenomenon is especially obvious when we combine SSAW with the highly significant attenuation which arises from the use of large microfluidic channel width. Here, we demonstrated this novel pressure field combining standing and travelling surface acoustic waves and used it to sort particles based on size. The key features of the acoustic field are modelled and also characterized with the experimental results.

1.2.3   Chapter 4: Acoustic tweezing of particles using decaying opposing travelling surface acoustic waves (DOTSAW)

Chapter 4 discusses the use of another unique sound field to perform acoustic tweezing of particles. Acoustic particle tweezing refers to the dynamic control of particle movement by translation of the sound field. A travelling wave is usually generated using a single set of electrodes, whilst the interference of counter propagating identical travelling waves from two electrode sets creates a standing wave. Standing surface acoustic wave has been commonly used to manipulate the movement of particles by first forming a periodic pattern of particles in the pressure node. Then the pattern is displaced by stretching or translating the standing wave which can achieved by changing the frequency of the pair of waves or their relative phase. However, we examined the effect of exciting each of the two electrode sets with different frequencies. Here, we showed theoretically, numerically and experimentally that this frequency shift causes a new type of field in which particles are not pushed as in a TSAW, of held in periodic locations as in a SSAW, but rather held in a single location which is easily controlled via relative amplitude modulation.

1.2.4   Chapter 5: Multiple outcome particle sorting using cascasded surface acoustic wave (CSAW) manipulation

In Chapter 5, like the previous chapters, we investigate the use of a novel and combinatorial SAW manipulation scheme to sort particles into multiple outcomes. This is especially important to on-chip fluorescent activated cell sorting applications. After the optical identification of a specific cell type, that particle is selectively displaced from the

incoming streamline into one of the multiple sort outcomes. For on-chip FACS, it is still a challenge to produce more than a binary outcome.

In this work, rather than exciting just a single opposing pair of electrodes, multiple pair of electrode sets, that are spatially offset from each other, are used in close proximity. By selectively actuating each the pair of electrode sets, a cascaded response is created. We show that the pairs of electrodes set behave independently, producing independent sound fields despite their close proximity. This experiment also demonstrates the multiple trajectory control by the use of different combinations of actuation of electrode pairs, enabling multiple outcome sorting.

1.2.5   Chapter 6: Conclusion and future work

In the final chapter, a summary of the contributions to SAW microfluidics by the research presented in this thesis is made. Finally, possible future work is presented.

Chapter 2

Background, theory and fabrication

2.1 Lab on a Chip

The goal of the lab-on-a-chip concept is to replicate and encapsulate a variety of laboratory processes into a singular miniaturized platform [14]. Lab-on-a-chip is a multidisciplinary field that receives contribution from fields ranging across mechanical engineering, material science, physics, chemistry and biology. Key features of LOC devices are: the small volumes reduce the time taken to synthesize and analyse a product; the unique behaviour of liquids at the microscale allows greater control of molecular concentrations and interactions; and reagent costs and the amount of chemical waste can be significantly reduced. LOC devices are being developed with more exciting functionalities and are starting to be constructed into highly integrated compact devices[15, 16].

Compact lab-on-a-chip devices can offer point-of-care diagnostic abilities that could revolutionize medicine and play an essential role in improving global health. Infectious diseases can be deadly and sometimes cause a global pandemic, as seen in the current COVID-19 crisis. Besides the immediate impact on global health, the COVID-19 pandemic has had significant social and economic effect worldwide, partially due to worldwide closure and implemented social distancing measures[17]. The key to prevent the spread of infection and improve patient outcome is having an improved molecular and serological diagnostic testing system in terms of testing availability and speed[18, 19]. As significant proportion of infected individuals are asymptomatic but still possess the capability of further spread of disease, testing availability has become progressively more important[20]. To evaluate the risk associated with reopening workplaces, educational institutions, and other social and cultural establishments, rapid diagnostic testing is essential. Even though the conventional diagnostic systems for viral disease are robust, but they are expensive, bulky, involves lengthy assays and their utilisation is labour intensive requiring skilled personnel to operate them, thus they are typically located in

centralised laboratories. By employing these portable, low cost LOC devices, more timely testing can be performed, allowing earlier containment of infected patients, thus, managing the spread of infection[21]. This is especially useful in developing countries where resources are limited. Such devices may also find uses in other areas, including a range of industrial applications and environmental monitoring.

The typical components in LOC includes pumps [22], valves [23], sorters [24], reactors [25, 26] and sensors [27]. Manipulation of micro-objects is one of the most important tasks in sample preparation in LOC that is required in many biological applications [28]. Lab-on-a-chip devices still suffer from system integration issues where the use of ancillary equipment such as fluidic pumps, high current power supplies, signal acquisition devices (microscopes, spectrometer, etc) are still required. Even though the chip itself is small, most of these devices are bulky and can take up a significant space on a laboratory bench. To combat this, further work in developing on-chip manipulation technique is required for some applications which require portability.

In the next subsections, the microfluidic concepts that affects the behaviour of fluid on the microscale that is used in LOC applications are discussed. This is then followed by a brief review of an on-chip actuation method that has the potential to address many issues preventing widespread implementation of LOC.

2.1.1 Scaling Effects

With shrinking dimensions, the surface to volume ratio increases, creating specific phenomena not normally encountered in macroscale systems. This section will cover characteristic microfluidic phenomena that are relevant to the work presented in Chapters 3-5 included in this thesis. Exploitation of the different length scales, L within microfluidic systems leads to a variety of interesting phenomena and thus different techniques [29]. Here we look at a few dimensionless numbers and the effects of scaling the length scales, L.

Reynolds number

The Reynold number, Re is a dimensionless term that relates inertial to viscous force and thus, a good description of the relative dominance of the forces experienced. Different flow patterns arise because of the interplay between inertia and viscosity. Inertia works as a mechanism to continue fluid movement when initiated while viscosity resists fluid motion. It is given by,

$$Re = \frac{\rho UL}{\mu} = \frac{inertial}{viscous} \tag{2.1}$$

where, ρ, U, and μ are the density, characteristic velocity and the viscosity of the fluid and L stands for the characteristic length scale. The Reynold number, Re is also used to differentiate fluid flow regime from either laminar, transient or turbulent. Turbulent flows occur at Re larger than about 4000 and flows at Re larger than about 1500 are often termed transitional flows. For a typical microfluidic system, viscous terms become more dominant as L is decreased, leading the Reynold number to be less than 100 or sometimes smaller than unity. This results in a laminar flow and greatly simplifies flow profile calculations. A laminar flow (as opposed to a turbulent flow) is characterised by the fluid flowing in "sheets" (laminae) with no intermixing of fluid between adjacent laminae and is stable against perturbations. Therefore, issues arising from mixing of fluids is eradicated, giving rise to high controllability of fluid flow without experiencing cross contamination. In the context of particle manipulation, this means that at low Reynolds numbers a particle will remain on a streamline unless an external force is used to displace it. In the work presented in Chapters 3, 4, and 5, particles are translated across multiple streamlines using SAW manipulation.

Péclet number

The Péclet number, Pe is the dimensionless number that dictates the relative importance of advection to diffusion. Pe is given as:

$$Pe = \frac{UL}{D} = \frac{advection}{diffusion} \qquad (2.2)$$

where, D is the diffusion constant.

The equation dictates the advective transport rate in comparison to the diffusive transport rate. Since the distance that a particle moves varies to the square power, as L is decreased, the diffusive rate becomes relatively dominant. This is shown by rearranging the diffusion length equation,

$$L = \sqrt{2D\tau} \qquad (2.3)$$

$$\tau = \frac{L^2}{2D} \qquad (2.4)$$

where, τ is the diffusion time.

This shorter diffusion time that stems from the smaller dimensions of the system, leads to faster reaction time in microfluidic devices. Péclet number can be used as a measure to compare the length of the system and the diffusion length. For a typical microfluidic device, the length scale involved is usually too large for a rapid diffusion, however too small to include mechanical agitation. For applications requiring rapid mixing, serpentine microfluidic channels can be used to stretch and fold fluid elements by chaotic advection [30].

Weber number

The Weber number, We is the non-dimensional number that shows the relative importance of inertial to surface forces in a two-phase flow and is given by,

$$We = \frac{\rho U^2 L}{\gamma} = \frac{inertial}{interfacial} \qquad (2.5)$$

where, γ is the surface tension of the interface considered.

The interfacial surface forces become relatively more dominant when L is reduced. Mini bioreactors utilising multiple emulsions can be realised by exploiting these dominant forces [26].

Capillary number

The Capillary number, Ca, characterises the relative effects of viscous forces to interfacial tension that acts across an interface of two immiscible fluids. It is defined as:

$$Ca = \frac{\mu U}{\gamma} = \frac{viscous}{interfacial} \tag{2.6}$$

where, μ, U and γ are the dynamic viscosity of the fluid, the characteristic velocity and the surface tension of the fluid.

The Capillary number is a very important parameter in microfluidic systems even though it is not strictly dependent of the characteristic length, L, because the characteristic velocity, U, of these systems are usually very small. The dominance of interfacial forces has been exploited in microfluidics to construct virtual walls and self-filling/pumping mechanisms [31, 32].

With the above phenomena in mind, researchers have been able to leverage these effects in LOC devices that can perform tasks with great value to biological and chemical studies.

2.2 Manipulation techniques

Microfluidic methods have been extensively used for cell/particle manipulation, where the scaling effects present in microsystems offer possibilities not present in macroscale systems. The microfluidic methods can be divided into passive and active manipulation techniques, where active methods rely on externally applied force fields, while passive methods do not. In the following subsections, different potential actuation methods are described in detail.

2.2.1 Passive Systems

Passive manipulation of particles or cells in microfluidic devices is a manipulation method that is not reliant of any externally applied force field. Instead, hydrodynamic viscous drag force plays a significant role in the cell/particle passive manipulation. At high Reynolds numbers, flowing cells/particles experience two significant directional forces: wall repulsion force, which pushes particles away from the wall, and shear-gradient lift force, which pushes particles away from the central axis. The balance of these two forces allows for cell/particle separation [33]. Whilst at lower Reynold's numbers the dominant forces which can be generated are related to direct interactions with physical obstructions.

Hydrodynamic separation is highly dependent on the particle-wall or particle-fluid interaction. For particle-wall interactions, the different types of wall can be either continuous wall or discreet wall. Continuous wall hydrodynamic based separation includes field flow fractionation (FFF) [34] and pinched flow fractionation (PFF) [35]. Discrete walls are usually obstacles in the microfluidic channel like posts and ridges. The ridges are usually used to guide the small particles while the posts are used to bump the large particles [36]. By arranging the posts in an array, size-based sorting can be achieved. This method is commonly known as deterministic lateral displacement (DLD). The separation size resolution can be very precise through iterated particle trajectory control by the spatial distribution of the posts. The pillar arrangements dictate the critical particle diameter that can be separated [37]. The array distribution and the cross-sectional shape

of the posts can be modified to allow for different applications and requirements. For particle separation using particle-fluid interactions, depending on the dominance of forces, they can be either be laminar flow based or inertial flow based. Inertial flow-based methods utilise a secondary flow in a curved microfluidic channel. Due to the momentum mismatch, fluid elements in the centre travel quicker than the ones near the channel walls, creating a pair of secondary flow known as Dean flow. Different sized cells experience a hydrodynamic force exerted by the Dean flow, in addition to the shear-gradient lift force and wall repulsion force, resulting in different size-based lateral equilibrium positions [38].

An advantage of passive manipulation methods is the potential and ability to perform complex individual processes. The inherent fast operating flow speed in passive manipulation systems also allows for high throughputs. Through parallelizing or stacking the single channels, the throughputs can be even further enhanced. However, the heavy reliance on sophisticated channel designs has limited flexibility and tunability, making them less robust. Furthermore, the multiple constrictions of the microfluidic channel causing them to be prone to clogging problems.

2.2.2   Active Systems

Active microfluidic methods utilise external force field for separation and handling of cells and particles. These active forces can be manipulated easily, leading to great flexibility and tunability according to the specific application required. The most widely used active methods for particle manipulation are optical micromanipulation, magnetic tweezers, acoustic manipulation and dielectrophoresis. In this subsection, a detailed review of these active methods is presented.

Magnetic

The magnetic field is a phenomenon being widely researched for microfluidic applications in biology and chemistry studies. The term magnetophoresis refers to the manipulation of microparticles and cells when exposed to an external magnetic field. Magnetophoresis is often used in particle/cell separation applications. The separation

process depends on an inhomogeneous magnetic field often directed perpendicular to the primary fluid flow. Paramagnetic particles/cells can be separated from non-magnetic particles or from each other. A critical requirement is that the samples should have either be natural or induced magnetisation. When a cell/particle does not possess any inherent magnetic properties, magnetic labelling is performed to allow magnetic manipulation. This is done by seeding or attaching the cells externally or internally with paramagnetic lanthanide ions [39] or magnetic micro- or nano-particles [40]. The magnetophoretic force that acts on the particle suspended within a magnetic field is given by [41],

$$
\begin{aligned}
\boldsymbol{F}_{eff} &= \boldsymbol{F}_p - \boldsymbol{F}_f \\
&= \chi_p V H \frac{dB}{d\boldsymbol{r}} - \chi_f V H \frac{dB}{d\boldsymbol{r}} \\
&= (\chi_p - \chi_f) V H \frac{dB}{d\boldsymbol{r}} \\
&= \Delta\chi V H \frac{dB}{d\boldsymbol{r}}
\end{aligned}
\tag{2.7}
$$

where, χ_p and χ_f are the volume magnetic susceptibility of the particle and suspending fluid respectively, V is the particle volume, H and B are the applied and local magnetic field respectively and their relationship is given by,

$$
\boldsymbol{B} = \mu_0 \boldsymbol{H}
\tag{2.8}
$$

where $\mu_0 = 4\pi \times 10^{-7}$ T mA^{-1} is the magnetic permeability of free space.

Magnetic sorting is mainly based on size and magnetic susceptibility. The advantage of the microfluidic system relying on magnetic force is that they are simple, cost-effective and can apply gentle forces that is suitable for biological handling. As the particles/cells are selected through specific markers, the selectivity and sensitivity for magnetophoresis is relatively high. This allows magnetic actuation method to be used in applications such as cell manipulation [42] and sorting [43], droplet handling [44], bioassay support [45-47], nucleic acid processing and detection [48-50]. Due to requirement of existence of magnetic species/marker, this technique can only be used in limited applications. Furthermore, magnetophoresis has a relatively weak force in

applications of interest and is subjected to the trade-off between the throughput and specificity of the system.

Dielectrophoresis

Dielectrophoresis (DEP) can be defined as the movement of dielectric microscale objects, such as microparticles and cells, when subjected to an inhomogeneous electric field. As a result, polarization effects in a suspended microscale object is achieved with respect to the suspension medium [51]. The time averaged dielectrophoretic force, F_{DEP} acting on micro-objects within alternating electrical field, E is given by, [52, 53],

$$\langle F_{DEP} \rangle = 2\pi r^3 \epsilon_m K(\epsilon_p, \epsilon_m, \omega) \nabla(E \cdot E) \tag{2.9}$$

where r is the particle radius, ϵ_m and ϵ_p are the complex permitivities of the particle and medium respectively.

The frequency dependence and differences in electrical properties are included in the Clausius-Mossotti factor, $K(\epsilon_p, \epsilon_m, \omega)$, and is given by,

$$K(\epsilon_p, \epsilon_m, \omega) = \frac{\epsilon_p(\omega) - \epsilon_m(\omega)}{\epsilon_p(\omega) + 2\epsilon_m(\omega)} \tag{2.10}$$

$$\epsilon_p(\omega) = \sigma_p + i\omega\epsilon_p \tag{2.11}$$

$$\epsilon_m(\omega) = \sigma_m + i\omega\epsilon_m \tag{2.12}$$

where ω is the angular frequency and σ is the electric conductivity.

Since DEP utilises non-uniform electric field, the electrode configuration geometry heavily affects the efficiency of DEP based microfluidic devices. An advantage of DEP is that it is conducted in a label-free manner, which can be useful especially when isolating rare cells with no known specific markers. Because the particle response

depends on the frequency and phase of the applied field, this allows them to be manipulated with great selectivity. DEP is also easily integrated with high-throughput microfluidic devices due to the inexpensive fabrication methods. Another advantage of DEP is the reachable precision and single-particle manipulation capabilities. These benefits allow DEP to be used in broad range of industrial, biomedical and life science applications, such as electrically controlled sorting [54], trapping [55, 56], focusing [57], concentration [58], and characterisation of chemical and biological analyses, particulate mineral suspended within a fluid medium [54]. Even though DEP is a popular actuation method within microfluidic systems, DEP based systems still have undesirable limitations. To generate the required gradients in the electric field and because of the short-range effect of DEP, the electrodes need to be located next to the trapping site or the shallow microchannel needs to be used, as a result, increasing the risk of clogging. Moreover, electric fields at DEP-relevant frequencies and amplitude has suggested in some results to cause significant stress in cells, leading to limited applicability to cell handling applications [59].

Optical

Optical manipulation is based on radiation pressure force arises from the momentum of the light itself [60]. These forces can be made large enough with the use of high intensity laser beam that induces high potential gradient. The force on the dielectric particle is caused by the transfer of momentum from the scattering of incident photons, which the momentum of each photons is given by,

$$P_{mom} = \frac{h_P}{\lambda_{light}} \qquad (2.13)$$

This force can be resolved into two forms as the scattering force, $F_{scattering}$, which pushes particles along the light propagation direction, while the gradient force, $F_{gradient}$, pulls particles in the spatial light intensity gradient direction. To decompose it even further, these forces acting on the suspended spherical particle with diameter, D, differ and changes formulation, depending on the regimes. The regimes are

influenced by the diameter, D, and can be split to two regimes, the Mie regime and the Rayleigh regime [61].

In the Rayleigh regime where $D \ll \lambda_{light}$, the scattering force, $F_{scattering}$, is given by [60],

$$F_{scattering} = n_m \frac{\sigma \langle S \rangle}{c} \tag{2.14}$$

where, n_m, c, and $\langle S \rangle$ represent the refractive index of the surrounding medium, speed of light and time averaged Poynting vector respectively. The particle cross section, σ, is defined as,

$$\sigma = \frac{8}{3} \pi (kr)^4 r^2 \left(\frac{n^2 - 1}{n^2 + 2} \right)^2 \tag{2.15}$$

Here k, r, n represent the light wave vector, particle radius and refractive index respectively. Whereas the gradient force, $F_{gradient}$, is given by,

$$F_{gradient} = \frac{1}{2 n_m \epsilon_0 c} \alpha \nabla I(\vec{r}) \tag{2.16}$$

where α and I represent the polarizability and light intensity respectively.

In the Mie regime where $D \gg \lambda_{light}$, the scattering and gradient forces are given by, [61]

$$
\begin{aligned}
F_{scattering} = \frac{n_m P_{ray}}{c} \Big\{ & 1 + R_{Fresnel} \cos(2\theta_i) \\
& - \frac{T_{Fresnel}^2 [\cos(2\theta_i - 2\theta_r) + R_{Fresnel} \cos(2\theta_i)]}{1 + R_{Fresnel}^2 + 2 R_{Fresnel} \cos(2\theta_r)} \Big\}
\end{aligned}
\tag{2.17}
$$

30

$$F_{gradient} = \frac{n_m P_{ray}}{c} \left\{ R_{Fresnel} \sin(2\theta_i) \right.$$
$$\left. - \frac{T_{Fresnel}^2 [\sin(2\theta_i - 2\theta_r) + R_{Fresnel} \sin(2\theta_i)]}{1 + R_{Fresnel}^2 + 2R_{Fresnel} \cos(2\theta_r)} \right\} \qquad (2.18)$$

where P_{ray} is the power of single ray. Fresnel reflection coefficient, $R_{Fresnel}$, and Fresnel transmission coefficient, $T_{Fresnel}$, is defined as,

$$R_{Fresnel} = \frac{1}{2} \left\{ \left(\frac{\tan(\theta_i - \theta_r)}{\tan(\theta_i + \theta_r)} \right)^2 + \left(\frac{\sin(\theta_i - \theta_r)}{\sin(\theta_i + \theta_r)} \right)^2 \right\} \qquad (2.19)$$

$$T_{Fresnel} = 1 - R_{Fresnel} \qquad (2.20)$$

Optical tweezers require the particle to be trapped at the beam focal point. In order to achieve this, the gradient force, $F_{gradient}$, needs to be more dominant than the scattering force, $F_{scattering}$. This particle collection occurs in one location in most systems, whereas multiple collection points in optical field proves to be challenging as it requires very complex systems [62].

The appealing features of the optical manipulation technique includes high spatial resolution, high controllability, high speed and responsiveness and high specificity. This allows non-invasive dynamic control of very small objects in the size range of tens of nanometres to tens of micrometres such as cells, bacteria and viruses, making them an extremely important research tool in physical chemistry, biophysics and biology [61]. Some of the application of the optical tweezer includes atom trapping [63], individualised biological particle manipulation [64] and mechanical characterisation of red blood cells [65].

However, the main limitation of the optical manipulation is the damaging of cells caused by the high intensity laser beams, leading to cell phototoxicity; therefore, it is not suitable for biological application. Several new strategies and approaches to optical tweezers are currently under development to minimise damage in biological experiments:

near infrared wavelength[66-69], spatial light patterns[70-72], exposure management[73, 74], oxygen depletion[75-77], and active thermal control[78]. Moreover, optical manipulation requires expensive, complicated sensitive setup, especially for complex manipulation, which in turn, making integration difficult with microfluidic platforms.

Thus, it is important to realise that microfluidic manipulation does not have one method which is superior than the others but knowing that it is a vast field with different tools suitable for different specific applications.

From these methods for particle manipulation, we now turn to the research this thesis is built on – acoustic manipulation. Detailed discussion of acoustics will be presented in the next section.

2.3 Acoustics

2.3.1 Acoustic Forces

Acoustic Radiation Force

The acoustic radiation force, F_{rad}, is the second order time average effect. It arises due to the scattering of the acoustic waves at interfaces, such as fluid particle boundaries and interface between two immiscible fluids. Acoustic force density can also be created in fluids with spatially inhomogeneous density and compressibility, which relocates and stabilises the fluid inhomogeneities[79-81]. Here, the primary acoustic radiation force is discussed, and is usually used for single isolated particles in a fluid. Due to the oscillatory nature of the first-order acoustic fields, the time average of these fields is zero. We define the time average $\langle X \rangle$ over a full oscillation period T_{osc} of a quantity $X(t)$ as:

$$X(t) = \sin(\omega t) \tag{2.21}$$

$$\begin{aligned} \langle X \rangle &= \frac{1}{T_{osc}} \int_0^{T_{osc}} \sin(\omega t)\, dT_{osc} \\ &= 0 \end{aligned} \tag{2.22}$$

where ω is the oscillation angular frequency, t is time.

Consequently, the acoustic radiation force must be the result of a non-zero time-averaged of a single second-order acoustic field, as shown in Equation 2.24.

$$X^2(t) = \sin^2(\omega t) \tag{2.23}$$

$$\begin{aligned} \langle X^2 \rangle &= \frac{1}{T_{osc}} \int_0^{T_{osc}} \sin^2(\omega t)\, dT_{osc} \\ &= \frac{1}{T_{osc}} \int_0^{T_{osc}} \frac{1}{2}[1 - \cos^2(2\omega t)]\, dT_{osc} \\ &= \frac{1}{2} \end{aligned} \tag{2.24}$$

Perturbation expansion theory is used to derive the second-order pressure and velocity fields [82]. The pressure, P, density, ρ, and velocity, $\boldsymbol{v}$ fields can be expanded as,

$$P = P_0 + P_1 + P_2 \tag{2.25a}$$

$$\rho = \rho_0 + \rho_1 + \rho_2 \tag{2.25b}$$

$$\boldsymbol{v} = \boldsymbol{v}_0 + \boldsymbol{v}_1 + \boldsymbol{v}_2 \tag{2.25c}$$

with $\boldsymbol{v}_0 = 0$. The subscripts 0, 1, and 2, denote the order of the expression.

From the isentropic speed of sound in the liquid, which is given by,

$$c_0^2 = \left(\frac{\partial P}{\partial \rho}\right)_s \tag{2.26}$$

pressure is given by,

$$P_1 = \rho_1 c_0^2 \tag{2.27}$$

In acoustofluidics, one typically considers time-harmonic fields at a single frequency. Hence, a simpler approach is to express the first order fields in complex notations as:

$$P_1 = P_1(x)e^{i\omega t} \tag{2.28a}$$
$$\rho_1 = \rho_1(x)e^{i\omega t} \tag{2.28b}$$
$$\boldsymbol{v}_1 = \boldsymbol{v}_1(x)e^{i\omega t} \tag{2.28c}$$

Physical, real-valued time average of two harmonically varying fields with the complex representation is given by the real-part rule:

$$\langle f\ g \rangle = \frac{1}{2} Re\ [f(x)\ g^*(x)] \tag{2.29}$$

where the asterisk denotes complex conjugation.

From the thermodynamic equations of state, we can express pressure, P in terms of density, ρ.

$$P = P(\rho) \tag{2.30}$$

The continuity equation and the Navier-Stokes equation are given as,

$$\frac{\partial \rho}{\partial t} = -\nabla \cdot (\rho v) \tag{2.31a}$$

$$\rho \frac{\partial \boldsymbol{v}}{\partial t} = -\nabla - \rho(\boldsymbol{v} \cdot \nabla)\boldsymbol{v} + \eta \nabla^2 \boldsymbol{v} + \beta \eta \nabla(\nabla \cdot \boldsymbol{v}) \tag{2.31b}$$

First order terms of the governing equation are given as,

$$\frac{\partial \rho_1}{\partial t} = -\rho_0 \nabla \cdot \boldsymbol{v}_1 \tag{2.32a}$$

$$\rho_0 \frac{\partial \boldsymbol{v}_1}{\partial t} = -\nabla P_1 - \rho(\boldsymbol{v}_1 \cdot \nabla)\boldsymbol{v}_1 + \eta \nabla^2 \boldsymbol{v}_1 + \beta \eta \nabla(\nabla \cdot \boldsymbol{v}_1) \tag{2.32b}$$

Second order terms of the governing equation are derived as,

$$\nabla \langle \rho_1 \boldsymbol{v}_1 \rangle = -\rho_0 \nabla \cdot \langle \boldsymbol{v}_2 \rangle \tag{2.33a}$$

$$\left\langle \rho_1 \frac{\partial \boldsymbol{v}_1}{\partial t} \right\rangle + \rho_0 \langle (\boldsymbol{v}_1 \cdot \nabla)\boldsymbol{v}_1 \rangle = -\nabla \langle P_2 \rangle + \eta \nabla^2 \langle \boldsymbol{v}_2 \rangle + \beta \eta \nabla(\nabla \cdot \langle \boldsymbol{v}_2 \rangle) \tag{2.33b}$$

Since the thickness of the viscous boundary layer is small with respect to the particle size, the viscous effects are negligible in the calculation of the acoustic radiation force. ($\eta \approx 0$), we get,

$$\nabla \langle P_2 \rangle = -\left\langle \rho_1 \frac{\partial v_1}{\partial t} \right\rangle - \rho_0 \langle (v_1 . \nabla)v_1 \rangle \tag{2.34}$$

Using the relationship stated below,

$$-\left\langle \rho_1 \frac{\partial v_1}{\partial t} \right\rangle = \frac{c_0^2}{2\rho_0} \nabla\langle \rho_1^2 \rangle \tag{2.35a}$$

$$\langle (v_1 . \nabla) v_1 \rangle = \frac{1}{2} \nabla\langle v_1^2 \rangle \tag{2.35b}$$

$$\kappa_f = \frac{1}{\rho_0 c_0^2} \tag{2.35c}$$

The second-order time-averaged pressure is now obtained and is expressed as,

$$\langle P_2 \rangle = \frac{1}{2} \kappa_f \langle P_1^2 \rangle - \frac{1}{2} \rho_f \langle v_1^2 \rangle \tag{2.36}$$

The acoustic radiation force, F_{rad}, on the particle can then be calculated as the surface integral of the time-averaged second-order pressure, P_2, as in given by the momentum flux equation,

$$F_{rad} = \int_S \langle P_2 \rangle (-\boldsymbol{n}) dS \tag{2.37}$$

where $\boldsymbol{n}$ is the normal vector. A momentum flux tensor is added to the integral to accommodate the fluctuating surface:(154)

$$F_{rad} = -\int_{S_0} \{ \langle P_2 \rangle \boldsymbol{n} + \rho_f \langle (\boldsymbol{n} \cdot v_1) v_1 \rangle \} \, dS$$

$$= -\int_{S_0} \left\{ \left[\frac{1}{2} \kappa_f \langle P_1^2 \rangle - \frac{1}{2} \rho_f \langle v_1^2 \rangle \right] \boldsymbol{n} + \rho_f \langle (\boldsymbol{n} \cdot v_1) v_1 \rangle \right\} dS \tag{2.38}$$

Theoretical studies of the acoustic force date back to Yiosoka and Kawasima [83] in 1955, and later derived in an alternative form by Gor'kov [84] in 1962. The analysis considers the force on a compressible particle in an inviscid ideal fluid in the long

wavelength limit where the particle radius, r, is much smaller than the acoustic wavelength, λ. The long wavelength limit can lead to assumption made in the optical force calculation in the Rayleigh regime. From the work summarised by Gor'kov, the acoustic radiation force can be calculated using the gradient of acoustic potential, U_{rad} [85],

$$F_{rad} = -\nabla U_{rad} \tag{2.39}$$

where the acoustic potential, U_{rad}, is given as,

$$U_{rad} = 2\pi r^3 \left[\frac{1}{3} f_1 \kappa_f \langle P_1^2 \rangle - \frac{1}{2} f_2 \rho_f \langle v_1^2 \rangle \right] \tag{2.40a}$$

$$f_1 = 1 - \frac{\kappa_p}{\kappa_f} \tag{2.40b}$$

$$f_2 = \frac{2(\rho_p - \rho_f)}{2\rho_p + \rho_f} \tag{2.40c}$$

where κ is the compressibility. Subscripts p and f denote the particle and fluid respectively. The potential is the greatest when there is a huge difference between the particles and the fluid in density and compressibility.

The acoustic contrast factor that dictates the direction of motion of the particles is given by,

$$\begin{aligned} \Phi &= \frac{1}{3} f_1 + \frac{1}{2} f_2 \\ &= \frac{1}{3} \left[\frac{5\rho_p - 2\rho_f}{2\rho_p + \rho_f} - \frac{\kappa_p}{\kappa_f} \right] \end{aligned} \tag{2.41}$$

The acoustic contrast factor, Φ, contains the effects of contrasts in material parameters in f_1 and f_2. Note that for positive acoustic contrast factors, $\Phi > 0$, the force is directed towards the pressure nodes (where $\langle P_2 \rangle$ is minimum), while for negative acoustic contrast factors, $\Phi < 0$, it is directed towards the anti-nodes. The is extremely useful in standing wave field, where there is a periodic distribution of the pressure field.

Acoustic Streaming Induced Drag Force

Acoustic streaming is the bulk fluid flow that accompanies the propagation of acoustic waves[86]. Streaming can be caused by one of two dissipation mechanisms. The first is dissipation in the viscous boundary layer, where the acoustic fluid velocity changes to match the velocity of boundary. This boundary-driven streaming is known as Rayleigh streaming in the bulk of the fluid and Schlichting streaming inside the boundary layers, and is typically observed in standing wave fields near walls or suspended objects [87-90]. The second dissipation mechanism is the attenuation of acoustic waves in the bulk of the fluid causes what is known as bulk-driven Eckart streaming [91]. They are typically observed in system much larger than the wavelength [92]. Eckart type streaming transforms into a Stuart-Lighthill type at very high frequencies (>100 MHz) as the dissipation length of acoustic waves shrinks considerably[86]. Stuart-Lighthill streaming is driven by a local and strong momentum transfer of a highly damped and rapidly decaying wave. Turbulent jet flow potentially emerges due to Stuart-Lighthill streaming because of the significant inertia for the induced flow[93, 94]. Streaming can be seen as undesirable in microfluidic manipulation processes, however, when used appropriately, they can be useful especially dealing with nano-sized particles where the acoustic streaming induced drag force are more dominant than the acoustic radiation force [95, 96]. Basic equations are governed from the Navier-Stokes equation by considering a small volume.

From the equation of continuity and momentum,

$$\frac{\partial \rho}{\partial t} + \nabla \cdot (\rho v) = 0 \tag{2.42a}$$

$$\rho \left(\frac{\partial v}{\partial t} + v \cdot \nabla v \right) = -\nabla \langle P \rangle + \eta \nabla^2 v + \left(\beta' + \frac{1}{3}\eta \right) \nabla (\nabla \cdot v) \tag{2.42b}$$

Note that $\beta' + \frac{1}{3}\eta$ is expressed as $\beta\eta$ in the Equation 2.31b.

Combining the equations above, we have

$$F = \frac{\partial (\rho v)}{\partial t} + \rho (v \cdot \nabla) v + v \nabla \cdot \rho v \tag{2.43}$$

F can be expressed in two terms, F_0 and $F_{Reynolds}$ [97].

$$F_0 - F_{Reynolds} = \frac{\partial(\rho v)}{\partial t} + \rho(v \cdot \nabla)v + v\nabla \cdot \rho v \qquad (2.44\text{a})$$

$$F_0 = \frac{\partial(\rho v)}{\partial t} \qquad (2.44\text{b})$$

$$-F_{Reynolds} = \rho(v \cdot \nabla)v + v\nabla \cdot \rho v \qquad (2.44\text{c})$$

Since F_0 time averages to zero, $F = -F_{Reynolds}$

$$\begin{aligned}\langle F \rangle &= \langle \rho_0(v_1 \cdot \nabla)v_1 + v_1\nabla \cdot \rho_0 v_1 \rangle \\ &= \rho_0 \langle (v_1 \cdot \nabla)v_1 + v_1\nabla \cdot v_1 \rangle\end{aligned} \qquad (2.45)$$

Second order steady state velocity field (acoustic streaming velocity) can then be evaluated based on the first order velocity and pressure fields,

$$\langle F \rangle = -\nabla\langle P_2 \rangle + \eta\langle \nabla^2 v_2 \rangle + \left(\beta' + \frac{1}{3}\eta\right)\langle \nabla(\nabla \cdot v_2) \rangle \qquad (2.46)$$

As a result of this acoustic streaming field, particle will experience a Stokes drag force. The motion of the particle can then be predicted using the following formula:

$$F_{drag} = 6\pi\eta r(\langle v_2 \rangle - u) \qquad (2.47)$$

Particles experience both acoustic radiation force and acoustic streaming induced drag force when subjected to a sound field. The dominance of the forcing mechanism determines how the particles will behave and hence change the way the particles are handled. The dominance of radiation force causes particles to drift, while particles will move in vortices when the streaming is dominant. Armaghan has investigated the effect of particle size and power on the particle behaviour. She showed that streaming is more dominant with the decrease of particle sizes and also showed the interplay of power and particle size create regimes where particle patterning occurs [98]. A deeper understanding is required to be able to create a particle handling platform that is predictable.

Bjerknes Force

Bjerknes force, also known as the secondary radiation force, is the interaction between the scattered wave from another surface, and the suspended microscale-object in the acoustic field [99, 100]. The surface studied can be split to other particles, wall or bubbles. They key parameter of the Bjerknes force is the acoustic wavelength, wave propagation direction, separation distance, and size ratio. The condition to make this secondary force significant is the distance between the other surface and the suspended matter is very small and the particle size is approaching the acoustic wavelength. Bjerknes force is also dependent on the orientation of the particles with respect to the direction of wave propagation, resulting the force to be either attractive or repulsive depending on their sign.

As particle size decreases, scaling laws show that the acoustic streaming induced drag force becomes dominant as discussed in the previous subsection. These swirling flows can be used to capture suspended objects that are very small (in the order of nanometres), but with limitations like low capacity limit and flow rate. Bjerknes force offers an alternative method in capturing nano-objects. This can be achieved by scattering waves off a cluster of microparticles [101-105].

2.4   Acoustic Excitation Methods

2.4.1   Bulk Acoustic Waves

Bulk acoustic wave (BAW) is defined as compressional waves in a solid that propagate through the bulk material. In BAW acoustophoresis, an ultrasonic standing wave is generated in a fluid-filled channel by a bulk piezoelectric transducer. The piezoelectric transducer is typically placed underneath the channel, either being glued on or coupled with gel/liquid, transforming a sinusoidal voltage into mechanical vibration at a tuneable frequency $f = \frac{\omega}{2\pi}$, and excites bulk waves and resonance in channels within an acoustically hard material, often glass or silicon. A large part of the bulk waves is reflected at the fluid/channel structure interface, resulting in superposition of travelling wave and counterpropagating reflected wave, leading to certain fluid resonance mode across the channel width. Resonance occurs when the channel dimension is tailored to match the half-integer multiples of the acoustic wavelength. The BAW field exerts acoustic radiation forces on micro-objects suspended in the continuous phase fluid and the force can be calculated with the Gor'kov potential. For a 1D standing wave field, the analytical calculation for the radiation force is given by,

$$F_{SSAW} = 4\pi r^3 E_{ac} k_{ac} \sin(2k_{ac}x)\Phi \qquad (2.48)$$

where r is the particle radius, x is the particle position in the wave propagation direction, Φ is the acoustic contast position as given in Equation 2.41. The wave number, k_{ac}, and the acoustic energy density, E_{ac}, are given as,

$$k_{ac} = \frac{\omega}{c_f} = \frac{2\pi f}{c_f} \qquad (2.49a)$$

$$E_{ac} = \frac{P_a^2}{4\rho_f c_f^2} = \frac{1}{4}\rho_f v_a^2 \qquad (2.49b)$$

where f and c_f are the frequency and fluid medium sound speed respectively. P_a and v_a are the absolute pressure and velocity fields.

BAW forms a distribution of minimum and maximum pressure regions called pressure nodes and antinodes in the fluid domain. Suspended particles in the fluid domain are pushed to either the pressure nodes or antinodes, depending on their acoustic contrast factor. Forces generated in this BAW field are used for particle and cell manipulation applications such as concentration, filtration, size separation and on chip FACS. In batch process mode, particle positioning and arraying has been shown in one or two dimensional.

BAW usually operates in kilohertz (kHz) to low megahertz (MHz) order frequencies, leading to a regime where acoustic wavelength is much larger than the diameter of the immersed micro-objects, making them having lower precision, rendering them less suitable for nanoparticle manipulation and tissue-engineering applications [106]. Due to the requirement of bulky piezoelectric transducers, BAW pose difficulty in integration with other microfluidic systems, making them less robust [107]. Most importantly, as BAW fields are resonant modes, and there are a limited number of modes available, it is very challenging to subsequently displace the field and as such the trapped particles, to enable tweezing. Although matching and backing layers can be used to suppress reflection in BAW devices to enable flexible manipulation of particles, careful calculation of the design parameter are required to achieve this[108, 109]. There are also other approaches that has been explored to remove chamber resonance in the manipulation device, in exchange for more complexity in the system[110, 111]. That being said, BAW has been well researched and developed and is moving to maturity. There have been multiple commercial systems like the Attune NxT flow cytometer[112] and Lumicks AFS® parallel single-molecule force spectrometer[113] that utilise BAW.

In our work presented in Chapters 3, 4, and 5, we are interested in generating more complex acoustic fields to achieve more unique microfluidic functionalities. We proposed the use of attenuation, displaced actuators and frequency difference actuation scheme, which will be difficult or even impossible with BAW due to its inherent nature. Hence, we explore the use of SAW devices to create these novel sound field.

2.4.2 Surface Acoustic Wave

As the name suggests, surface acoustic waves are nm-scale amplitude, MHz frequency acoustic waves propagating on a piezoelectric substrate [114]. The advantages presented with SAW microfluidics include simple fabrication, high biocompatibility, fast fluid actuation, versatile, compact and inexpensive devices and accessories, contact free, and compatibility with other microfluidic components. In contrast to standing waves produced by BAW transducers, acoustic fields produced by SAW can be generated in arbitrary locations and orientations with respect to microfluidic channels, with localised field widths on the order of 10's of microns [115]. This enables SAW to play an important role in fields like biology, medicine, and chemistry. SAW have been widely employed in many microfluidic applications such as particle/cell manipulation (i.e. separation [116, 117], focusing [118], and patterning [119]), droplet manipulation [120], and fluidic control (i.e. fluid pumping [121, 122], mixing [123-125], jetting [126], and atomisation [127-129]).

SAW is generated by a series of interdigitated transducers (IDTs) patterned on a piezoelectric substrate. IDTs consist of a set of connected metallic fingers interspaced with an opposite set of connected metallic fingers, forming what we call "finger pairs". By applying an AC signal across the pair of electrodes at resonant frequency, the surface displacement produced by each finger pair is reinforced by the subsequent one, generating SAW with displacement amplitude on the order of 10 Å, that will continue to travel along the substrate surface, in the direction orthogonal to the IDTs, until dissipated by either relaxation in the material itself or through leakage into a secondary material (i.e. intended fluid volume). The resonant frequency, f_{SAW}, is given by,

$$f_{SAW} = \frac{c_s}{\lambda_{SAW}} \tag{2.50}$$

where c_s is the phase velocity of the piezoelectric substrate and λ_{SAW} is the resonant wavelength of the IDTs.

The structure of the IDT determines the bandwidth and directivity of the generated SAW, whereas for BAW, acoustic waves depends on the geometry of the fluid chamber as the entire fluid volume is being resonated, making BAW devices less versatile. The characteristic of SAW can be altered by changing the number, spacing, and aperture (overlapping length of the finger pairs). The most common designs used in microfluidic application are the straight IDTs, focused IDTs, chirped IDTs and the slanted finger IDTs. Each of these produces different displacement field that results in a different pressure field in the fluid medium. Straight IDTs are the normal and most commonly used configuration in microfluidic device as they are the simplest and most efficient in terms of operation. A focused IDT [130] consists of pairs of annular electrodes that, as the name suggest, direct the wave and energy into a spatially small focal point. The chirped IDTs [131] and slanted finger IDTs [132] have a gradient of electrode finger width, in the direction along to the finger pairs for the former, and the latter in the direction perpendicular to the finger length. Both of these IDTs allow the use of frequency modulation to generate SAW with different characteristic, where chirped IDTs is used to generate SAWs over a wide frequency range; and slanted finger IDTs is used to produce narrow SAW beams of varying frequency at specific location along the finger pairs. In Chapter 5, the localisation of SAW beams is investigated and is proposed to sort particles with multiple outcomes by combining multiple displaced IDTs, making them really useful in on-chip FACS systems.

The SAW can be coupled to the adjacent fluid domain through a microfluidic channel so that the leaky SAWs excite longitudinal acoustic waves in the liquid at the Rayleigh angle, θ_R, given by, the Snell's law [133]:

$$\theta_R = \sin^{-1}\left(\frac{c_f}{c_s}\right) \tag{2.51}$$

where c_f is the sound speed in the fluid.

Due to the leakage of energy into the fluid, the leaky SAW, which is the wave travelling along the fluid-substrate interface, attenuates exponentially in the propagation direction with the attenuation coefficient, α_{LSAW}, given as [134],

$$\alpha_{LSAW} = \frac{\rho_f c_f}{\rho_s c_s \lambda_{SAW}} \tag{2.52}$$

where ρ_s is the piezoelectric substrate density.

SAW microfluidics are conventionally classified into two types: travelling SAW (TSAW) and standing SAW (SSAW) and will be explored in the next subsections.

Travelling Surface Acoustic Wave

The SAWs that propagate away from a single set IDTs are termed as travelling surface acoustic wave (TSAW). TSAW has been used to manipulate micro-objects suspended in a fluid, either using acoustic radiation forces or acoustic streaming induced Stokes drag acting on the micro-objects. The acoustic radiation force that is imparted by TSAW onto the small compressible spherical particle can be calculated using the formulation, given by Yosioka and Kawasima,

$$F_{TSAW} = 4\pi r^2 (k_f r)^4 \left(\frac{I_{aco}}{c_f}\right) \Phi \tag{2.53a}$$

$$I_{aco} = \frac{\rho_f c_f k_f^2}{2} \tag{2.53b}$$

$$k_f = \frac{2\pi}{\lambda_{ac}} \tag{2.53c}$$

where I_{aco} is the intensity of the incident acoustic wave and k_f is the wavenumber in the fluid medium.

Skowronek et. al. introduced a dimensionless coefficient, κ, to describe the effective acoustic radiation force for the manipulation of particles via travelling waves, and is what Destgeer et. al. [135] named as the "acoustic radiation force factor" as it described the acoustic radiation force per unit acoustic energy density per unit cross sectional area of a spherical object. And this is given by [136],

$$\kappa = k_f r$$
$$= \frac{2\pi r}{\lambda_{ac}} \qquad (2.54)$$

where λ_{ac} and r are the wavelength of acoustic waves in liquid medium and the radius of the solid particles respectively.

The critical value of the "acoustic radiation force factor" is explored experimentally and found to be 1.28 ± 0.20. When $\kappa < 1.28$, there is no net acoustic radiation force applied to the particles, as the wave is isotropic. When $\kappa \geq 1.28$, a net acoustic radiation force drives the translation of particles in the fluid flow. Through this parameter, TSAW has been shown to achieve submicron particle sorting [116] and size-selective particle manipulation in a microchannel anechoic corner that arises from longitudinal wave excited at an angle according to the Snell's law [117]. Furthermore, TSAW shows great potential in microfluidic fluorescent activated cell sorters (µFACS), especially for single particle level displacement as the TSAW field can be highly localised with the use of a focused IDT [115].

The interaction of TSAW with fluid produces a chaotic streaming flow that strongly depends on the dimensions of the microchannel (width and height). The effect is more pronounced at higher acoustic intensities due to the non-linearity. This acoustic streaming is harnessed for controlled and continuous mixing of fluids inside the microchannel. Two different fluids can be effectively mixed in a continuous flow resulting in a concentration gradient profiles modulated by changing the input power [137].

Standing Surface Acoustic Wave

Conventionally, the superposition of two counter-propagating TSAWs with same frequency produces standing surface acoustic wave (SSAW). The acoustic radiation force acting on the small compressible spherical particles is given by Equation 2.48 (Yosioka's formulation),

$$F_{SSAW} = 4\pi r^3 E_{ac} k_{ac} \sin(2k_{ac}x)\Phi \qquad (2.48)$$

r is the particle radius, x is the particle position in the wave propagation direction, Φ is the acoustic contrast position, k_{ac} is the wave number and E_{ac} is the acoustic energy density. Equation 2.48 can be written in terms of a velocity potential amplitude, Ψ_a, instead of the acoustic energy density as below,

$$F_{SSAW} = \Psi_a^2 \rho_f \pi (k_{ac}r)^3 \Phi \sin(2k_{ac}x) \qquad (2.55)$$

where the potential ψ is defined as,

$$\psi = \Psi_a e^{i(\omega t \mp k_{ac}x + \theta)} \qquad (2.56)$$

where t is time, the $\mp$ dictates the propagation direction, and θ is the phase of the wave. Note that both Equation 2.48 and Equation 2.55 has a sine term, representing the periodicity in the force equation. This shows that the SSAW can be used to trap particles using their periodic pressure nodes.

Suspended particles in a standing SAW field move to pressure nodes or antinodes according to their physical properties. SSAWs have been widely used for micro-object manipulations such as focusing, trapping, and sorting applications. A cytometer is realised through SSAW- based particle focusing [138, 139]. Since the size of the particles affects the magnitude of the force experienced and thus affecting the lateral displacement, they can be used in microparticle separation applications, mainly using one-dimensional SSAW with a single pressure node located at the centre of the microchannel [140]. SSAW with multiple pressure nodes can also be used in sorting micro-objects. A tilted-angle SSAW device has been shown to sort particles with enhanced separation distance [141, 142].

Unconventional SAW Actuation Schemes and Phenomena

A 2D interference pattern can be achieved by using two orthogonal pairs of IDTs [143]. They can be used to study cell-cell interaction. The trapping location can be changed in real time by exploiting the modulation of acoustic parameters (for example,

phase shifts, frequency shifts and amplitude modulation) [131, 144], enabling manipulation of particles. When operating SSAW approaching the size of the cells, one cell per acoustic well can be achieved and single cell studies can be performed [143], Single IDTs can be used to generate SSAW field for particle manipulation. This is achieved by positioning the microfluidic channel directly on top of the IDT. A size deterministic separation of particles have been realised using a virtual deterministic lateral displacement device that consist of single IDTs [145]. SSAW fields combined with a pulsed actuation has also shown to allow for spatially selective trapping location [146]. Due to diffraction effects, TSAW can be used to generate lateral patterning, while two-dimensional particle patterning can be accomplished with a one-dimensional SSAW. This is shown to be useful for continuous particle focusing [147].

Chapters 3, 4, and 5 of this thesis challenges the misconceptions typically made with SAW field generation where any SAW system is generally classified to be either TSAW or SSAW based. We show that there are indeed intermediate states in all systems and we examine the use of these more complex acoustic fields to create unique functionality to be used in many different application, expanding the range of acoustofluidics manipulations that can be performed.

2.5   Microfabrication

2.5.1   SAW Device Fabrication

A typical SAW device is made up of IDTs patterned on a piezoelectric substrate. For the work carried out throughout the thesis, a transparent, 0.5 mm thick, 128° Y-cut X-propagating, lithium niobate (LiNbO$_3$) substrate is used. LiNbO$_3$ has excellent electrical-mechanical coupling efficiency, resulting in high substrate displacements and surface velocities, and is often used in SAW microfluidic applications [148-150]. To fabricate SAW devices, IDTs and the contact pads are deposited on LiNbO$_3$ wafer and they consist of two different layers. The upper layer is a thick (up to 1 μm) conductive layer, made up of either gold (Au) or aluminium (Al), selected by their excellent conductivity. Sandwiched between the conductive layer and the piezoelectric substrate is a thin (5-10 nm) adhesion layer made up of metals like chromium (Cr) or titanium (Ti), used to prevent electrode lift-off.
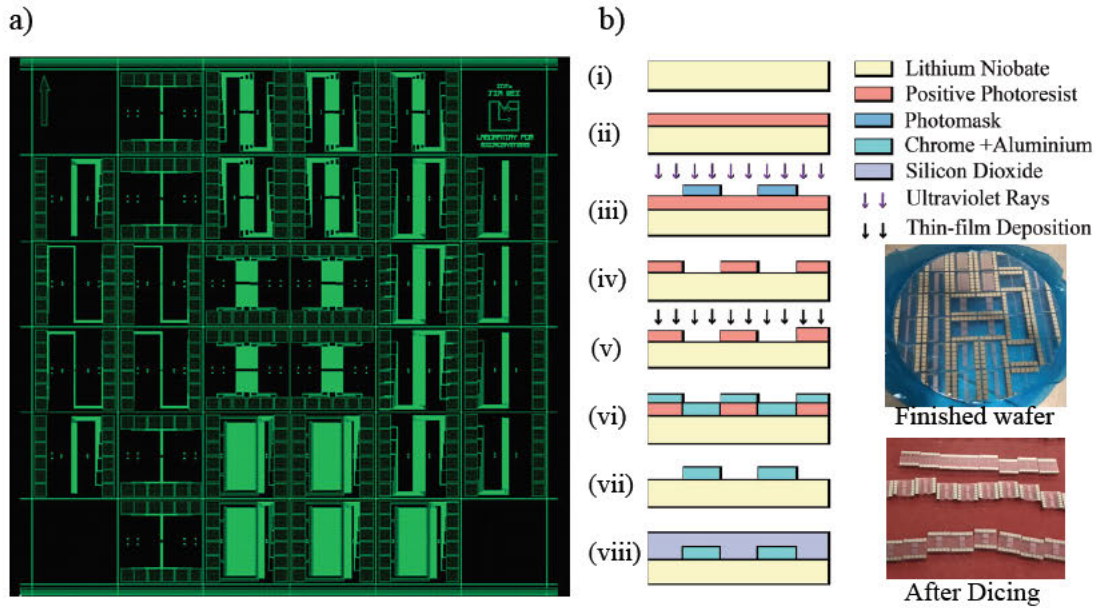
Figure 2.1: (a) An example of photomask design for IDTs using Layout Editor. (b) Process diagram of SAW device fabrication. (i-ii) A LiNbO$_3$ wafer is spin-coated with a positive photoresist and then (iii) selectively exposed to ultraviolet light using a photomask. (iv) Development of the patterned features is carried out, which is followed by (v-vi) metal deposition and (vii) lift-off to form the patterned metals on the LiNbO$_3$ wafers. (viii) A layer of SiO$_2$ is subsequently deposited on the wafer. SAW device fabrication finishes off with dicing of the wafer.

Photolithography is microfabrication technique used for micrometre and submicron feature patterning on a substrate. LiNbO$_3$ wafers are firstly spin coated with a photoresist layer, and then being heat treated to remove remaining solvent in photoresist. Next, to transfer the required design onto the spin coated wafers, a photomask is used when the substrates are exposed to intense ultraviolet (UV) light. The patterns in the wafers are then developed in appropriate developer bath. The exposure to light causes a chemical change that allows some of the photoresist to be removed. Positive photoresist, when exposed to light, are soluble in the developer, whereas the unexposed region of negative photo dissolves in the developer.

The adhesive and conductive metal layers of the IDTs are then deposited using high-vacuum electron beam evaporation. The deposition material is bombarded with an electron beam from a charged tungsten filament to be evaporated and converted into gaseous state. The atoms or molecules in a vapour phase is then precipitate and form a thin film coating of the substrate. After the deposition process, the excess metal layers that is not part of the design, which are not on the substrate surface, are removed, along with remaining photoresist in a process called "lift-off", by applying a solvent to the wafer. To promote bonding between the PDMS microchannel and the piezoelectric substrate, another thin layer of silicon dioxide (SiO$_2$) is coated on the surface of piezoelectric wafers, with the exception of the electrode pads. This coating also serves another function to protect the metallic electrodes from corrosion. The LiNbO$_3$ wafers now contains multiple arrays of SAW devices that can be diced into individual SAW chips using high speed cutting tool with small width blade.

2.5.2   Microfluidic Channel Fabrication

In the work contained in the thesis, the microfluidic channels are made of a polymer called polydimethylsiloxane (PDMS). PDMS is commonly used in microfluidic devices as it is transparent, which facilitate the observation of contents in the channels through microscope. They are also considered biocompatible, especially with properties like high gas permeability. The ease of pattern transference with high resolution allows for the lithography replication of microchannels.

To fabricate a PDMS microfluidic channel, a mould/master with the inverse design of microchannel is required. Microfluidic channel features are first patterned and developed on a silicon wafer using photolithography. Deep-reactive ion etching (DRIE) is then performed on the wafer to create deep and steep-sided trenches on the exposed region where photoresist is not covered. This process is time-multiplexed, and repeatedly alternates between two modes to achieve nearly vertical sidewalls. The two modes involve the etching step, which uses sulphur hexafluoride (SF_6) as the reactive gas; and the deposition step, where a thin passivation layer, made up of perfluorocyclobutane
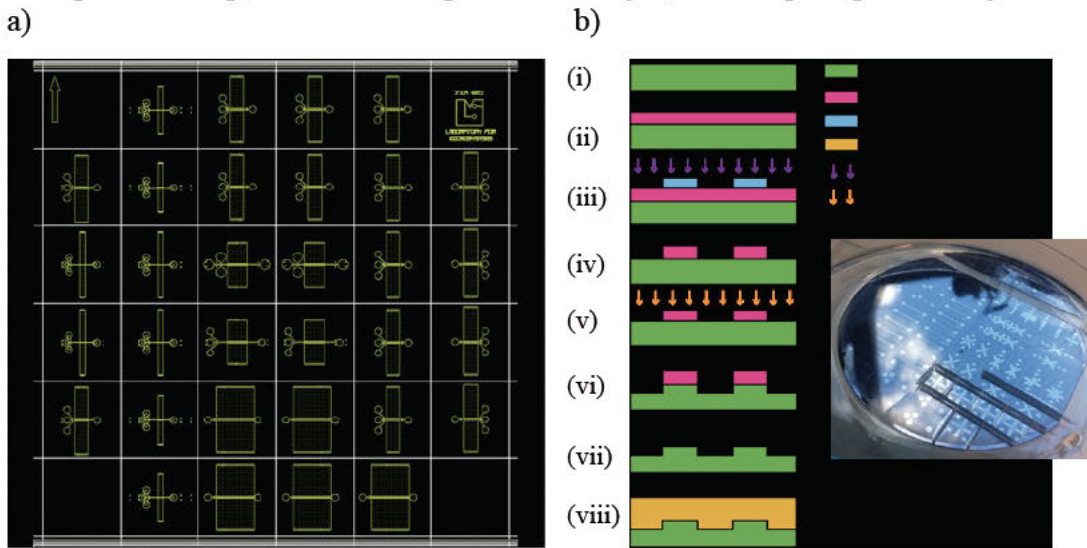

Figure 2.2: (a) An example of photomask design for microfluidic channels using Layout Editor. (b) Process diagram of the microchannel fabrication process. (i-ii) A Si wafer is spin coated with negative photoresist. (iii) With the use of a photomask, the wafer is selectively exposed with ultraviolet light, resulting in (iv) patterned features on Si wafer after development. (v-vi) The wafer then undergoes deep reactive ion etching (DRIE) process using the patterned features as a mask, resulting in (vii) a silicon mould for PDMS. (viii) Finally, the microfluidic channel patterns are transferred to the PDMS by filling the mould with PDMS.

(C_4F_8) is coated. When the mould is ready to use, a mixture of liquid PDMS and crosslinking agent is poured onto the mould. It is then degassed in a vacuum chamber to remove the air bubbles and is set to cure on a hotplate. Finally, we obtain a replica of the microchannels on the PDMS block after removing it from the mould once it is fully cured.

2.5.3   Device Assembly

By combining the SAW device and the PDMS microchannel, a fully functioning SAW actuated enclosed microfluidic device is produced. The assembly is done using a plasma activated bonding process. The surfaces of $LiNbO_3$ substrate and PDMS undergoes oxygen plasma treatment and is then brought together. The –OH surface termination on the PDMS surface, as a result of surface activation, forms a strong hydrogen bond with the SiO_2 layer on the LiNbO3, leading to an irreversible seal[151]. The bonding strength is determined by the density of silanol -OH groups on the treated surface. Delamination of the bonding interface can sometime occur when the surface is under-treated[152].
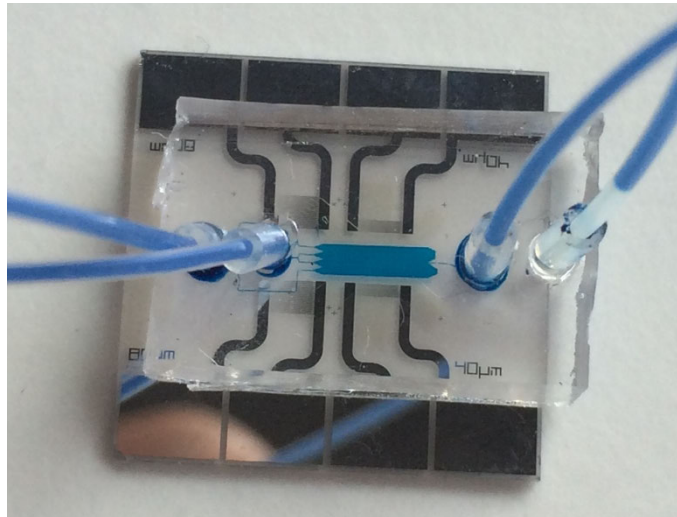
Figure 2.3: Assembled SAW actuated enclosed microfluidic device. This device was used to conduct experiments for research presented in Chapters 3 and 4.

Chapter 3

Flow-Rate-Insensitive Deterministic Particle Sorting using a Combination of Travelling and Standing Surface Acoustic Waves

3.1 Overview

For most SAW particle manipulation methods, the acoustic fields tend to be described as either travelling or standing in nature. In the former, TSAW acts predominately to push particles away from the source and in the latter, SSAW traps particles in multiple stable locations, in either the node or antinodes of the pressure field depending on material properties. In this work, we demonstrate that aspects of both types of waves exist in any SAW system, and, when the chip is designed to enhance this effect, this hybrid field is used for particle sorting. Due to the loss of energy from the substrate leaked into the adjacent fluid, the SAW displacements attenuate exponentially along the propagation direction. From the interference between two counter-propagating decaying SAWs, there is a spatial variation in amplitude of the resulting acoustic pressure field. The hybrid field has regions where standing wave is dominant (near the centre of microchannel) and where travelling wave is dominant (on the outer edge of the channel). By combining the favourable properties from both waves, it allows for size specific final trapping location. Hence the sort is deterministic based on size, rather temporal in nature. FEA modelling allows better understanding of the hybrid field sorting mechanism, showing both travelling wave dominant region and standing wave dominant region. the equilibrium trapping position is affected by particle size. The experiments show that particles with fractional size differences can be separated, with effective separation of 5.1 μm, 6.1 μm, and 7.0 μm using the same device. It is also demonstrated that the difference

in particle behaviour is insensitive to the flow rate provided a sufficient acoustic field strength is used, this is a direct result of the deterministic nature of the sorting mechanism.

3.2   Publication

The following publication was reproduced [153] with permission from Springer.

CrossMark

RESEARCH PAPER

Flow-rate-insensitive deterministic particle sorting using a combination of travelling and standing surface acoustic waves

Jia Wei Ng[1] · David J. Collins[2] · Citsabehsan Devendran[1] · Ye Ai[2] · Adrian Neild[1]

Abstract Manipulation of cells by acoustic forces in a continuous flow offers a means to sort on the basis of physical properties in a contactless, label-free and biocompatible manner. Many acoustic sorting systems rely on either standing waves or travelling waves alone and require specific exposure times to the acoustic field, fine-tuned by manipulating the bulk flow rate. In this work, we demonstrate a flow-rate-insensitive device for continuous particle sorting by employing a pressure field that utilises both travelling and standing acoustic wave components, whose non-uniform spatial distribution arises from the attenuation of a leaky surface acoustic wave. We show that in parts of the pressure field in which the travelling wave component dominates, particles migrate across multiple wavelengths. In doing so, they drift into areas of standing wave dominance, whereby particles are confined within their respective nodal positions. It is demonstrated that this final confinement location is dependent on the particle size and independent of the force field exposure time and thus the flow rate, permitting the continuous separation of 5.1-, 6.1- and 7.0-μm particles. Omitting the need to precisely control the bulk flow rate potentially enables sorting in systems in which flow is not driven by external pumps.

✉ Adrian Neild
adrian.neild@monash.edu

[1] Laboratory for Micro Systems, Department of Mechanical and Aerospace Engineering, Monash University, Clayton, VIC 3800, Australia

[2] Pillar of Engineering Product Development, Singapore University of Technology and Design, Singapore 487372, Singapore

1 Introduction

Sorting of biological cells and particles is essential in a number of research fields including analytical chemistry, food and chemical processing, cell biology, diagnostics and therapeutics (Riera-Franco de Sarabia et al. 2000; Tartaj et al. 2003; Davey and Kell 1996). For example, blood has a highly diverse cell population, largely consisting of erythrocytes (red blood cells), leucocytes (white blood cells) and thrombocytes (platelets). Isolation of specific cell types from unprocessed heterogeneous biological samples is usually a prerequisite for downstream analysis.

Label-free particle or cell sorting can be achieved based on its physical properties such as size, stiffness, density or electrical impedance (Shields et al. 2015). Microfluidic techniques enable the use of passive and active methods for particle and cell sorting. Passive particle sorting methods utilise the interaction between particles, flow field and channel structure. Such methods include hydrodynamic filtration (Yamada and Seki 2005; Di Carlo 2009), pinched flow fractionation (Morijiri et al. 2011), deterministic lateral displacement (McGrath et al. 2014; Huang et al. 2004; Loutherback et al. 2010; Morton et al. 2008) and the Zweifach–Fung effect (Morijiri et al. 2011; Wei Hou et al. 2012). In contrast, active techniques make use of forces arising from external fields of various forms such as dielectrophoretic (Kim et al. 2008; Gascoyne and Vykoukal 2002; Park et al. 2011; Wiklund et al. 2006), magnetic (Carr et al. 2009; Wang et al. 2007; Xia et al. 2006), optical (Lei et al. 2012; MacDonald et al. 2003) and acoustic (Collins et al.

🌀 Springer

2016; Shi et al. 2009) fields to manipulate the particles. For passive methods, static design for specific parameters renders sorting parameters unalterable, leading to limited device flexibility. In contrast, active methods are generally more versatile as the field strength can be arbitrarily modified to achieve high sorting efficiency and throughput (Lenshof and Laurell 2010; Sajeesh and Sen 2013).

Among active techniques, acoustic methods offer good biocompatibility, permitting the manipulation of living organisms, and have minimal impact on the viability and function of biological cells (Collins et al. 2015). Acoustic fields are typically generated using one of the two actuation methods: bulk acoustic waves (BAW) (Devendran et al. 2014; Neild et al. 2007; Glynne-Jones et al. 2012; Johansson et al. 2009; Leibacher et al. 2015) or surface acoustic waves (SAW) (Sesen et al. 2014; Collins et al. 2013; Miansari et al. 2015). The former employs an acoustic field that is produced using a piezoelectric ceramic transducer, bonded to a microchannel and actuated by an AC signal, the frequency of which is chosen to create a resonance condition and thus a standing wave within the fluid volume. BAW field strength is enhanced with the use of channel materials that have good acoustic reflection properties (Leibacher et al. 2014). A SAW, on the other hand, is generated by a series of interdigitated transducers (IDTs) patterned on a piezoelectric substrate. SAW devices offer minimal power consumption, low cost, rapid response time and easy integration with microfluidic devices (Collins et al. 2014b; Yeo and Friend 2009, 2014). In contrast to standing waves produced by BAW transducers, acoustic fields produced by SAW can be produced in arbitrary locations and orientations with respect to microfluidic channels, with localised field widths on the order of 10's of microns (Collins et al. 2016). Both travelling surface acoustic waves (TSAW) and standing surface acoustic waves (SSAW) can be generated by one or two pairs of IDTs, respectively, where standing waves result from the combination of two counter-propagating travelling waves. This permits flexibility in the type of pressure field excited, and the absence of acoustic reflection requirements means that channels can be fabricated from common, easily integrated microfluidic materials such as polydimethylsiloxane (PDMS).

Deterministic sorting on the basis of stiffness and density using acoustic forces is possible with certain particles migrating to pressure nodes and others to the pressure antinode (Petersson et al. 2005). However, this can only be achieved if the two particle populations have opposing acoustic contrast factors. More usually, it is the speed of migration to a certain location which is used to achieve sorting; for this, SAW-based acoustic separation has been shown using either TSAW- (Franke et al. 2010; Schmid et al. 2014; Destgeer et al. 2015; Behrens et al. 2015) or SSAW-dominant (Witte et al. 2014; Ding et al. 2012) systems.

In SSAW systems, particles such as red blood cells and white blood cells have a positive acoustic contrast factor within their respective mediums and so migrate to the pressure nodes. For this case, different-sized particles experience different acoustic radiation forces, albeit in the same direction, and therefore migrate to the pressure nodes at different rates (Shi et al. 2009). In TSAW systems, particles also experience different forces depending on their size and migrate at different lateral displacement velocities in the direction of acoustic propagation, unbounded due to the absence of an opposing acoustic force (Destgeer et al. 2013, 2014). Whilst positive acoustic contrast factor (non-Brownian) particles eventually migrate to the node (SSAW) or the opposing channel wall (TSAW), separation is achieved by limiting exposure time in a continuous flow. Comparing these approaches, SSAW has limited separation sensitivity and efficiency due to the shorter $1/4\,\lambda_f$ distance over which particles are separated, whilst TSAW permits migration distances up to the entire width of a microfluidic channel.

The overriding feature common in both cases, however, is the temporal rather than deterministic nature of the separation, relying on the differences in speed of migration for both types of system (Collins et al. 2014a). The exposure time is limited by a combination of the area over which the force field acts, and the bulk flow rate. Here, consideration of the drag force responsible for pulling the particle along the channel length and the force field that moves particles laterally across the channel width is required. A balance between these two forces can result in excellent separation, by fine-tuning the flow rate or field strength (Li et al. 2015; Collins et al. 2014a). Particle migration is also susceptible to the variations of flow rate due to parabolic flow profiles in the height and width directions. In systems where a high degree of flow rate control is not feasible or practical, as is the case with capillary-driven flow (Hitzbleck et al. 2013), temporal sorting is not appropriate. To circumvent this, we present a deterministic method of acoustic-based particle separation where particle migration is size specific regardless of exposure time.

We demonstrate this flow-rate-insensitive acoustic particle sorting through the imposition of a combined TSAW/SSAW field. This hybrid pressure field combines the favourable features of systems using either travelling or standing waves, such that particles are translated over long distances to the centre of the channel (akin to TSAW) and then "caught" at a stable location (akin to SSAW). Whilst Devendran et al. (2016b) utilised a combination of TSAW and SSAW created by a disparity in the power applied to opposing IDTs, the end location was not stable and a frequency swept signal was required to accentuate differences in particle response in the static fluid volume. In contrast, here we generate stable end locations for particles in the

SSAW-dominant region without the need for careful fine-tuning of applied power or flow rate. The spatial variation in amplitude of a SAW as energy is leaked into the fluid is key to separation in a combined TSAW/SSAW field. We employ two counter-propagating SAWs leading to regions of the channel in which the field is alternately dominated by travelling waves (near the channel edges) and standing waves (near the channel centre). We show that particles with fractional size differences can be separated, with effective separation of 5.1, 6.1, and 7.0 µm using the same device. It is also demonstrated that the difference in particle behaviour is insensitive to the flow rate, provided a sufficient acoustic field strength is used.

2 System principle

A surface acoustic wave (SAW) is generated by exciting a piezoelectric substrate with an alternating current (AC) electrical signal. A SAW propagates along the substrate surface and efficiently couples into contacting fluids. High-displacement SAW is produced by applying an AC signal across the IDT electrodes at resonant frequency, $f = c_s / \lambda_{SAW}$, where c_s is the speed of sound in the substrate and λ_{SAW} is the distance between periodic features in the IDTs. The mechanical displacements from each finger pair reinforce one another, resulting in a SAW (with displacements on the order of nanometres) that continues to propagate along the surface of that substrate until dissipated by either relaxation in the material itself or through leakage into a secondary material, i.e. the fluid in this case (Friend and Yeo 2011). When a SAW is travelling at a substrate–fluid interface, it leaks acoustic energy, resulting in a longitudinal wave being radiated into the fluid at the Rayleigh angle $\theta_R = \sin^{-1}(c_f / c_s)$, where c_f is the sound speed in the fluid. This wave travels through the fluid until it encounters an interface with a material of different acoustic property. Due to the loss of energy leaked into the fluid, the SAW displacements attenuate exponentially along the propagation direction. The decay length of a leaky SAW, over which the amplitude attenuates to $1/e$ in the propagation direction, is ~10 λ_{SAW} (Shiokawa et al. 1989; Dentry et al. 2014). In this work, two sets of $\lambda_{SAW} = 40$ µm IDTs are used to excite counter-propagating waves from either side of a 1200-µm-wide fluid channel. This width corresponds to ~3.25 times the decay length (over this distance, the wave amplitude drops to 3.89 % of its original value). This design, incorporating such a large contrast between the width of the channel and the decay length of the SAW, makes the role of attenuation highly significant (Devendran et al. 2016a). Uniquely, this design results in regions across the channel width where either travelling or standing waves dominate particle behaviour. TSAW is dominant near the

channel edges, where the counter-propagating wave is a fraction of the amplitude of the propagating wave. Conversely, SSAW is dominant in the channel central region, where comparable attenuation of incoming and interfering waves generates acoustic nodal positions to which particles migrate.

Particle separation is possible because of the different scaling relationships of acoustic radiation forces to travelling and standing waves, respectively. It is helpful to use the relationships developed by Hasegawa et al. to discuss this (though, note that these equations are only valid for either a pure travelling wave or standing wave, and for particles considerably smaller than used in this study, hence, they are only used as a concept here; different methods are used for the force calculations presented later in this work), which found that $F_{TW} \propto R^6$ and $F_{SW} \propto R^3$ for $R \ll \lambda$ and is nonlinear for $O(R/\lambda) \gtrsim 1$ (Hasegawa and Yosioka 1975). The dependence of particle size for each force type is also emphasised by Skowronek et al. (2013), showing the particle deflection by TSAW is most effective for parameter $\kappa \geq 1.28 \pm 0.20$, where $\kappa = k \times R$ and k is the wavenumber in the fluid. In the travelling wave-dominant channel region, there are no local force potential minima for the particle to settle in; hence, it will be pushed to the centre of the channel until it reaches force potential minima in the standing wave-dominant region that prevents further translation. As the standing and travelling wave forces scale differentially with particle size, the location at which the transition from travelling wave dominant to standing wave dominant occurs is also particle size dependant. As such, the location of the first stable force potential minima is size dependant and so offers a deterministic sorting mechanism—the stable lateral position in the combined TSAW/SSAW field is unique to every particle size. This operating principle is demonstrated here through both numerical modelling and experiments that conform to the modelled predictions.

3 Methodology

3.1 Device fabrication

The SAW device consists of two sets of opposing identical interdigitated transducers (IDTs) separated by a distance of 2 mm. Each set of IDTs has 12 finger pairs with the wavelength of 40 µm and aperture of 700 µm. The IDTs were fabricated by having a 250-nm-thick Al conductive layer on a 5-nm-thick Cr adhesive layer patterned on a 0.5-mm-thick transparent piezoelectric 128° Y-cut X-propagating lithium niobate (LN) substrate. LN is often used in SAW microfluidic applications due to its excellent electrical-mechanical coupling efficiency, resulting in large substrate displacements and surface velocities on the order of ~1 m/s

(Campbell and Jones 1968; Sivanantha et al. 2014). With the exception of electrode pads to which an AC signal is applied, the substrate is coated with a 200-nm layer of SiO_2 to prevent electrode corrosion and promote channel bonding.

The microfluidic channel, used to confine particle solutions in the acoustic field, is composed of polydimethylsiloxane (PDMS) (SYLGARD® 184, Dow Corning, 1:10 ratio of curing agent/ polymer). The 1200-μm-wide, 25-μm-high fluid channel was moulded on a silicon template etched using conventional Bosch process deep reactive ion etching (Oxford Instruments PLASMALAB100 ICP380). For improved removal from the mould, a hydrophobic surface layer was produced by finishing the etching process with a passivation step (C4F8). The PDMS fluid channel was then aligned and bonded to the LN substrate after exposure to an air plasma (Harrick Plasma PDC-32G, Ithaca, NY, 1000 mTorr, 18 W). The joined surfaces were heated (70°, 10 min) immediately after coupling to enhance the bonding of the activated surface. To maximise the acoustic energy transferred to the liquid in the chamber and minimise the amplitude attenuation due to the lossy SAW transmission at the LN-PDMS interface, an air-filled chamber was used to completely enclose the IDTs with a 90-μm-wide PDMS partition, which separates the air- and liquid-containing sections.

3.2 Experimental procedure

The opposing SAWs are generated by applying a sinusoidal voltage produced by a power signal generator (BelektroniG F20 Power Saw, Freital, Germany) that is split into two signals across the two sets of IDTs. Fluorescent polystyrene particles (Magsphere, Pasadena, CA, USA) with 5.1, 6.1 and 7.0 μm diameters were injected into the microfluidic channel using a syringe pump (KD Scientific Legato 210, Holliston, MA, USA). The beads are hydrodynamically focused to the sides of the main channel by a central sheath flow with a flow rate of 6 μl/min prior to the continuously applied SAW field. The buffer solution consists of deionised water (Milli-Q 18.2 MΩ cm, Millipore, Billerica, MA) with 2 % w/w polyethylene glycol (PEG) to prevent particle adhesion and was also flushed through the channels prior to use. During use, the device was mounted on a 3D printed platform for stabilisation and imaged using a 5-MP C-mount camera (PixeLink PL-B872CU, Ottawa, Canada) on a fluorescence microscope (Olympus BX43, Tokyo, Japan). The videos were post-processed and analysed using a custom MATLAB (MathWorks) program. The fluorescence intensity of the particles was profiled at the end of the working region to analyse particle separation efficacy for each video frame (over a time frame of approximately 1 min).
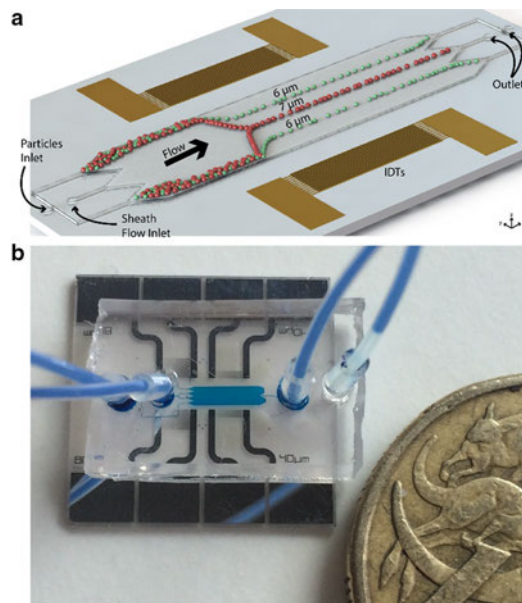
Fig. 1 **a** Sketch of the SAW device operating principle: particles with different sizes pass through an acoustic field created by two opposing sets of interdigitated transducers (IDTs) on a piezoelectric lithium niobate (LN) substrate. Attenuation of leaky SAW creates TSAW-dominant regions and SSAW-dominant region for each particle size in the microchannel. In the TSAW-dominant region, larger particles are more affected in the force field, causing them to migrate laterally further to the centre of the channel, as compared to smaller particles. The particles eventually reach a stable location in the SSAW-dominant region. **b** Here the chamber of the finished device is filled with blue dye for visualisation, with an Australian $1 coin for scale

A laser Doppler vibrometer (LDV, UHF-120, Polytec GmBH, Waldbronn, Germany) was used to measure the substrate displacement and velocity magnitudes. This allowed the mixture of TSAW and SSAW to be characterised across the width of the fluid-filled channel (Fig. 1).

3.3 Numerical procedure

To demonstrate the effect of a mixed wave field in a complex system, a simplified 2D model in COMSOL Multiphysics was used, as a full 3D model is prohibitively expensive computationally, whilst this does not fully represent the system, it does allow the interplay between key forces to be demonstrated. The model incorporates the effect of TSAW and SSAW forces allowing the fundamental principles of operation to be probed. In the experimental system, the IDTs act as a SAW source at either edge of the channel's width. The SAW propagates across the width, decaying in amplitude as energy is leaked into the fluid. In the model,
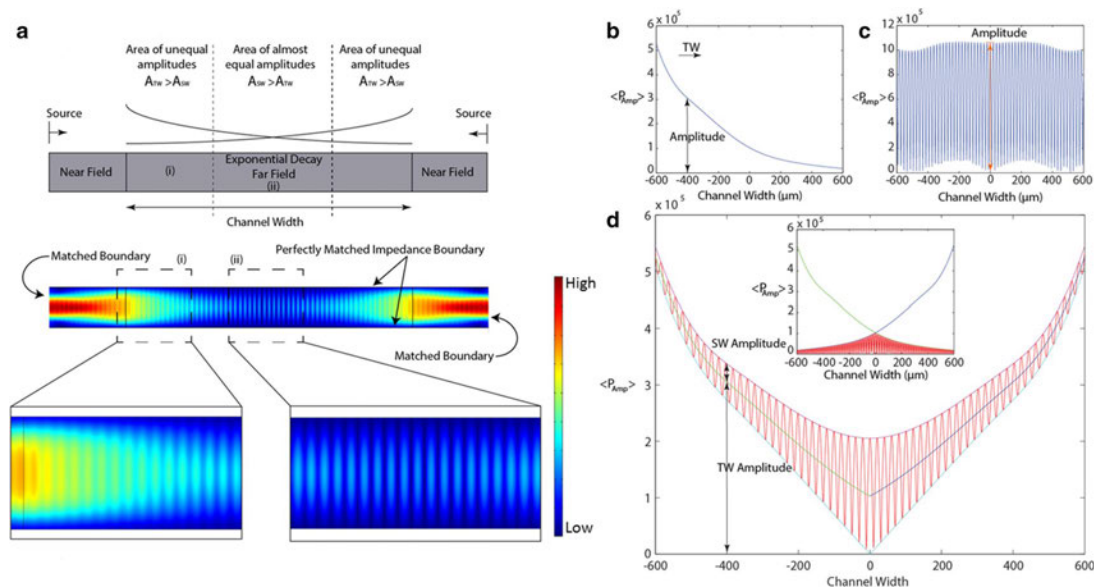
Fig. 2 Finite element model. **a** Shows the boundary conditions and second-order time-averaged pressure field from two counter-propagating (decaying) travelling waves. (**b**–**d**) Second-order time-averaged pressure along the centre line of the far-field chamber for various fields: **b** a pure attenuating travelling wave, **c** a pure standing wave and **d** combined elements of travelling waves and standing waves that corresponds to the pressure field in (**a**). The magnitude of the spatially periodic time-averaged pressure represents the degree of standing wave at any given location, whilst its offset from the *x*-axis shows the spatially varying amplitude of the travelling wave component. (*i*) Region with higher travelling wave-to-standing wave ratio. (*ii*) Region with higher standing wave to travelling wave ratio

this is mimicked by utilising two wave sources at each end of the simulated space, with a central region representing the channel's width between them (both being 1200 μm wide). The waves emerging from the two sources are attenuated to match the leaking decay of the SAW (using an attenuation coefficient of $(9.24\lambda_{SAW})^{-1}$ Nepers/m) (Shiokawa et al. 1989); see Fig. 2. The presence of a particle in the fluid results in scattering of the incident waves, where the effects of re-reflection of these waves back onto the particle have been minimised by imposing a perfectly matched acoustic impedance boundary to the upper and lower boundaries as depicted in Fig. 2a. To best represent the experimental system, sources of the waves are located beyond the ends of the central region of the model (i.e. beyond the edges of the physical channel used experimentally) such that near-field effects of the sources are eliminated. Finally, at both ends of the model space, a matched acoustic boundary condition permits waves of a defined wavenumber to traverse without reflection. The result is two counter-propagating travelling waves, one from each end of the chamber that establishes the pressure field shown in Fig. 2a. The time-averaged absolute pressure is shown for various fields in Fig. 2b–d generated in COMSOL. In a system with solely an

attenuating travelling wave, the pressure decreases exponentially (Fig. 2b), whilst for a pure standing wave, the shape of the time-averaged pressure is the modulus of a sinusoid (Fig. 2c—some numerical error can be seen). The pressure field shown in Fig. 2a combines elements of travelling and standing waves; likewise, its time-averaged pressure field, Fig. 2d, shows characteristics of both types of field with both decaying and fluctuating features. The height of this fluctuation represents the degree of standing wave at any given location, whilst its offset from the *x*-axis demonstrates the magnitude of the travelling wave component. To better understand the combined TSAW/SSAW sorting mechanism, the force experienced by the particle is evaluated at multiple locations orthogonal to the flow, every $\lambda_{SAW}/16$, from the centre to the side of the chamber (the force distribution is symmetrical about the centre of the channel). The particle size effect was also studied with three different diameters (5.1, 6.1 and 7.0 μm). The simulated material properties of the particles are the same as the polystyrene beads used in the experiments with a density of 1050 kg/m^3 and sound speed of 2350 m/s. Due to the low viscosity in our case (viscous damping factor, $\gamma \ll 1$) where acoustic streaming is not significant, it has a negligible influence on the

acoustic radiation forces on the large particles used in this work (Bruus 2008). As a result, the pressure and velocity field inside the microchannel are governed by simple linear acoustic of inviscid fluids, i.e. the Helmholtz wave equation for the pressure and potential flow for the velocity. Neglecting the viscosity of the fluid, the time-averaged force can be calculated according to (Dual et al. 2012)

$$F = - \int_{S_0} \left[\left(\frac{1}{2\rho_f c_f^2} \langle \boldsymbol{p}_1^2 \rangle - \frac{1}{2}\rho_f \langle \boldsymbol{v}_1^2 \rangle \right) n + \rho_f (n.\boldsymbol{v}_1)\boldsymbol{v}_1 \right] dS \quad (1)$$

where the integration is performed over the particle surface, S_0, due to the absence of the acoustic streaming terms. The mean square fluctuation of pressure and velocity is $\boldsymbol{p}_1^2$ and $\boldsymbol{v}_1^2$, respectively, and density of the fluid, ρ_f, and the sound speed in the fluid, c_f, are 1000 kg/m^3 and 1490 m/s, respectively. This simplified acoustic model will not fully describe the experimental system, but offers qualitative insight into the physical nature of the interaction between travelling and standing wave forces and how they determine particle behaviour. To obtain quantitative agreement
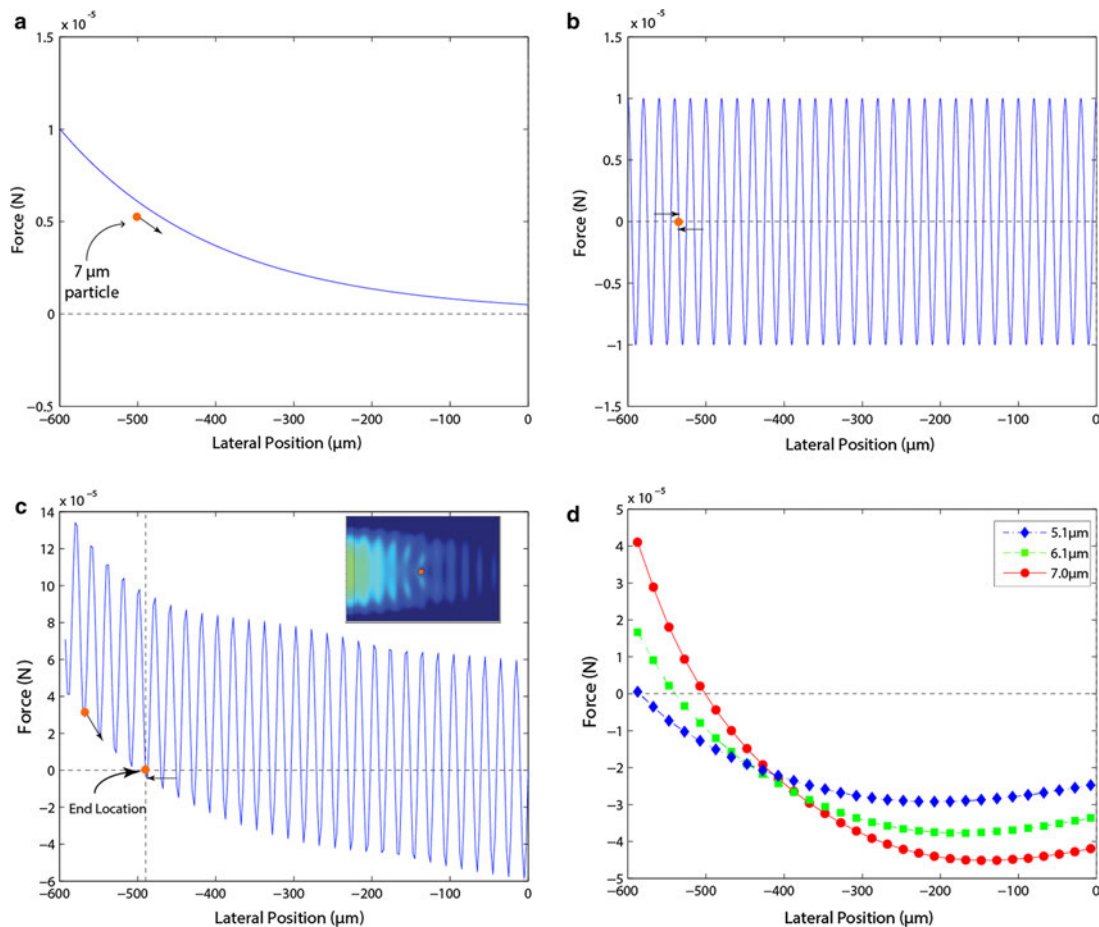

Fig. 3 Spatial variation of forces exerted on suspended particles. **a** Pure (decaying) travelling wave field. **b** Pure standing wave field. **c** Resultant force field from two counter-propagating (decaying) travelling waves. End location refers to the point where particles become trapped when the forces start to fluctuate sufficiently that they become negative. *Inset* shows the distortion of pressure waves by the particle with the size comparable to the wavelength, confirming that

linear superposition of forces in these force fields is not valid, and hence, direct evaluation of forces from numerical simulation is performed. The *circles* in the figures (**a–c**) represent the particle, and the *arrows* represent the particle motion. 7.0-μm particles and a pressure amplitude of 1 MPa are used in the simulation. **d** Force value at every λ/16 towards the right of a pressure node for different particle sizes. The end locations for each particle vary with particle size
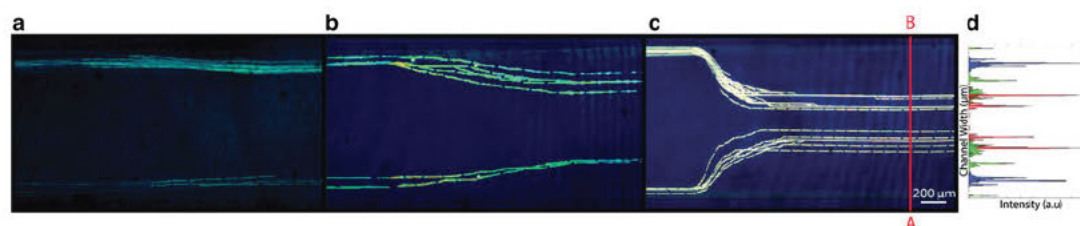
Fig. 4 Trajectories of particles of size **a** 5.1 μm, **b** 6.1 μm, **c** 7.0 μm. The intensity plot (**d**) along AB of stacked images of (**a**), (**b**) and (**c**) represents the stable lateral position of the beads after deflection
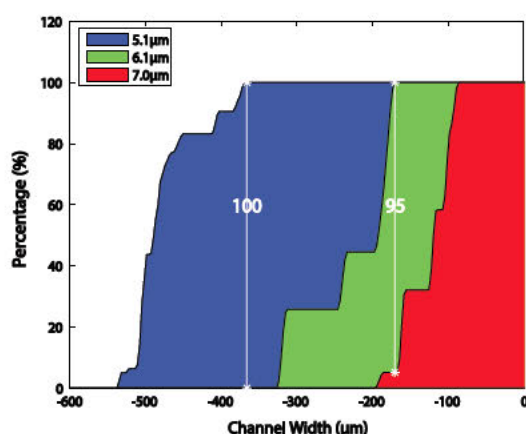
Fig. 5 Cumulative percentage of number of particles with respect to the channel width, showing the collection of each particle size is possible within a discrete range of channel width. The maximum percentage of collection of particles between the two pairs of particle sizes, with 5.1- and 6.1-sized particle and 6.1- and 7.0-sized particles, is plotted, showing high separation efficiency can be achieved. Flow rate and power input of 0.5 μl/min and 637 mW, respectively, were used. For reference, 58 particles with diameter of 7.0 μm are used in this experiment

between simulation and experiment, a 3D acoustic model along with time-dependent particle motion can be simulated, with the cost of additional computational resources.

4 Results and discussion

Figure 3 shows the spatial variation of forces exerted on suspended particles. For the purpose of comparison, the forces in a pure (decaying) travelling (a) and standing field (b) are shown. For the former, the force is of constant sign and, as such, always in the direction of wave propagation (Fig. 3a). In contrast, for the standing wave field, the force alternates in sign every quarter wavelength, such

that particles are trapped at periodic locations in the field (Fig. 3b). For a combined field, it is not necessarily valid to simply evaluate the sum of these force fields, as the forces are nonlinear in nature. Instead, the force is calculated directly based on the resultant pressure field obtained from the numerical simulations shown in Fig. 2a. The resulting force field is shown in Fig. 3c. Elements of both TSAW and SSAW force fields are present: a net decay in force with attenuation of the travelling wave with increasing distance from the acoustic source, and a periodically fluctuating force magnitude that is largest at the channel centre. Near the edge of the channel, the force is positive in sign; hence, whilst the magnitude of the force fluctuates, it always acts to move the particles towards the centre of the channel. However, towards the centre, the effect of the periodic, primarily standing wave, forces is sufficient to become negative (i.e. acts in the opposite direction). At this point, particles become trapped (labelled "end location" in Fig. 3c). Changing the input power in the model has no effect on the location where the force starts to act in the opposite direction, further confirming the unchanged predicted end location for the particles in Fig. 3c. In order to use the finite element model to demonstrate the principle of size-based deterministic separation of particles, we have examined the value of the force at every location $\lambda_{SAW}/16$ towards the right of a pressure node (each local minima). These values have been found over a spatial range for different particle sizes and are shown in Fig. 3d. It can be seen that the end locations (where the force equals zero) for each particle vary with particle size. The standing wave-dominant region for a larger particle is located further from the edge of the channel width when compared to a smaller particle, and is the key mechanism to deterministically sort particles by size.

Larger particles require a higher SSAW-to-TSAW ratio (i.e. closer to the central region of the channel) for the standing wave force to dominate over that of the travelling wave one (Devendran et al. 2016b). This is confirmed experimentally in Fig. 4, which illustrates the trajectories of the 5.1-, 6.1- and 7.0-μm-sized particles exposed to
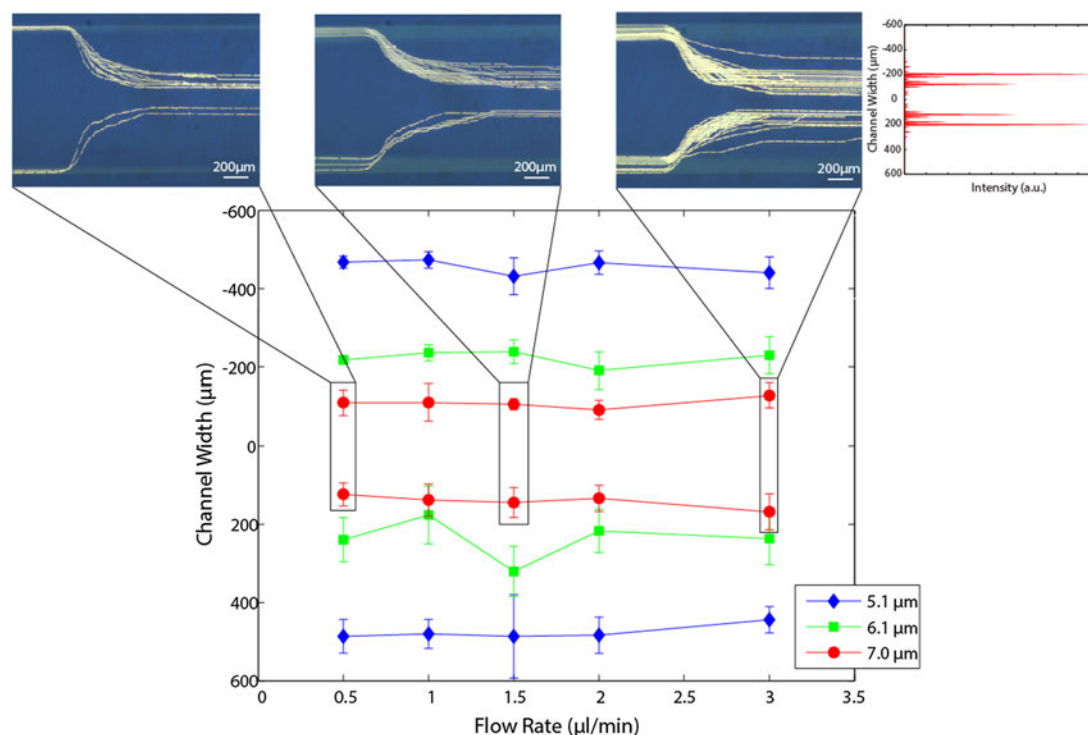
Fig. 6 a Lateral position of the polystyrene beads of size 5.1 μm (*diamond*), 6.1 μm (*square*) and 7.0 μm (*circle*) after their egress from the working region as a function of flow rate. Overlaid images of some of the experiments with different flow rates are shown at the top of the figure. For the 3 μl/min flow rate, the total number of particles that makes up each data points is 300, 574, and 550 for 5.1-, 6.1- and 7.0-μm particles, respectively

acoustic forces. The particles enter from each side of the channel and are deflected towards the channel centre by the TSAW and reach a stable location as the SSAW component becomes dominant. Each particle has their distinct band of exit location, with larger particles displaced towards more central regions. This agrees well with the numerical simulation where the first stable trapping location occurs at more central positions than for smaller particles. Each line does not correspond to a single particle trajectory rather; in some locations, multiple particles follow the same path, and a clearer representation of the spread of particles is shown in the intensity image in Fig. 4d. The frequency, the input power and the flow rate are 99 MHz, 637 mW and 3 μl/min, respectively. In order for easier analysis of particles with different diameters, this set of experiments was conducted with one particle size at a time. The intensity of particles at all exit locations was overlaid to obtain the final Fig. 4d depicting the possibility of deterministic sorting.

Figure 5 shows the cumulative percentage of particles counted from the outer edges of the channel moving towards the centre from the video; these data are a reanalysis of the intensity plot shown in Fig. 4. As expected, the exit location of larger particles is closer to the centre of the channel compared to the smaller particles. The maximum separation potential is shown by the difference in the percentage of a pair of particle sizes at any given lateral location.

In reported continuous particle separation work using acoustic forces, flow rate affects the exit location of the particles by changing the time they are exposed to acoustic force. Figure 6 shows the relationship between the flow rate and the exit location of the particles. Particle stream flow rates of 0.5, 1, 1.5, 2 and 3 μl/min were investigated at a constant input power of 637 mW. We observe that the flow rate has a negligible effect on the exit locations of the particles, establishing a unique and stable location for particles of different sizes after being deflected. The power input was also varied to characterise its effect on the particles' exit location, as shown in Fig. 7. A range of acoustic powers (200, 417, 637, 807 and 1020 mW) were used with a
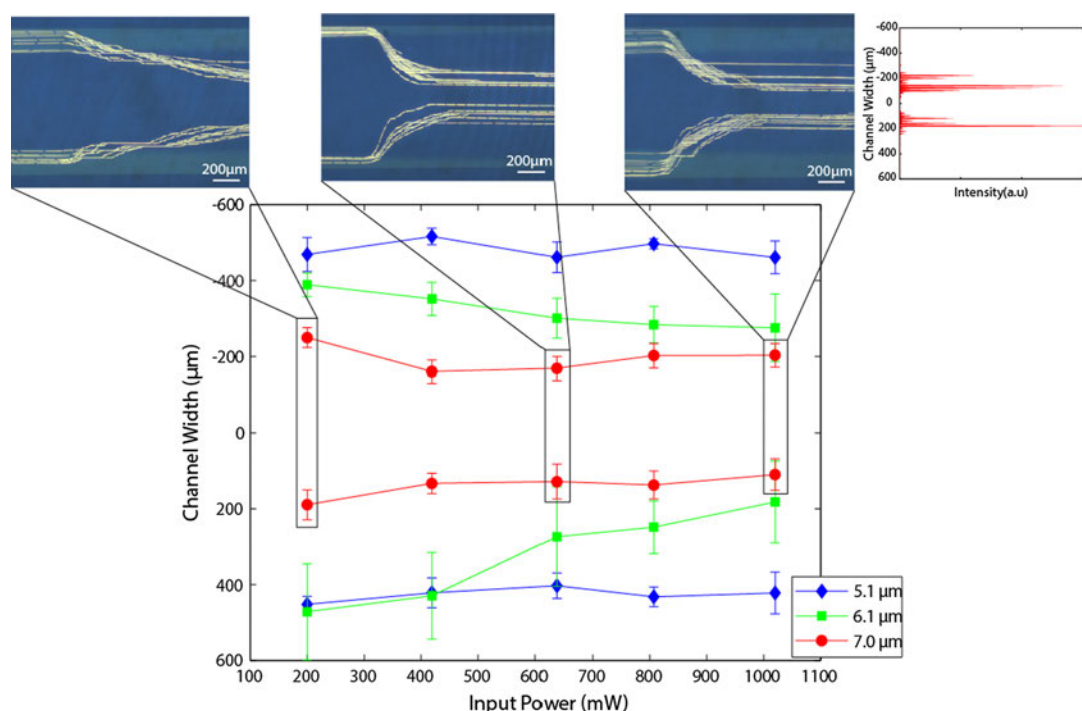
Fig. 7 a Lateral position of the polystyrene beads of size 5.1 µm (*diamond*), 6.1 µm (*square*) and 7 µm (*circle*) after their egress from the working region as a function of input power. Overlaid images of selected experiments with different input power are shown at the *top* of the figure

constant flow rate of 2 µl/min. Similar to the flow rate, the amount of power input does not substantively affect particle translation distances, especially for 5.1- and 7.0-µm particles.

As for 6.1-µm particles, the mean exit location is seen to be further from the centre of the channel at lower powers (below 600 mW). This is also the case for the lowest power applied to the 7.0-µm particles. The inset shows the trajectory of these latter particles, and it can be seen that the trajectory is such that the particles have not reached a stable end location prior to exiting the ultrasonic field (the image is aligned with the edges of the IDTs). In the context of flowrate, we showed how the end location is flow rate independent, but qualified this by stating that this is provided, an end location is reached. This requirement makes a link between applied power, flow rate, applied power and length of the ultrasonic field, the first governs the strength of the migration forces, the latter two the exposure time. At the lower powers, we are operating outside this condition for the middle-sized particles and at the lowest power also for the largest particles. Note that the time required to reach the end location is dependent on both the travelling wave force and the distance which needs to be travelled,

both increase with increased particle size, and the rate of these increases differ, so it is not unreasonable for it to be the middle-sized particles which require the most time to reach their stable end location. The second effect we notice with the 6.1-µm particles was that there were more collisions between incoming particles, creating particle clusters that are acoustically indistinguishable from larger particles, resulting in a stable location marginally further towards the centre of the channel at higher powers, at which there is a correspondingly larger attractive inter-particle force for larger displacement amplitudes (Collins et al. 2015). It is worth noting that the concentration of particles was kept constant measured by volume, so there are more 6.1-µm than 7.0-µm particles.

The exit location of a particle size forms a band rather than following a discrete pressure node as might be expected from the model. In this regard, the model is only considering a highly idealised case in which a single particle of exact size traverses the force field. In reality, each particle type will have a range of sizes (with ≈3 % coefficient of variation), and some inter-particle effects will be present when particles are in close proximity with each other within the ultrasonic field. In addition, there is
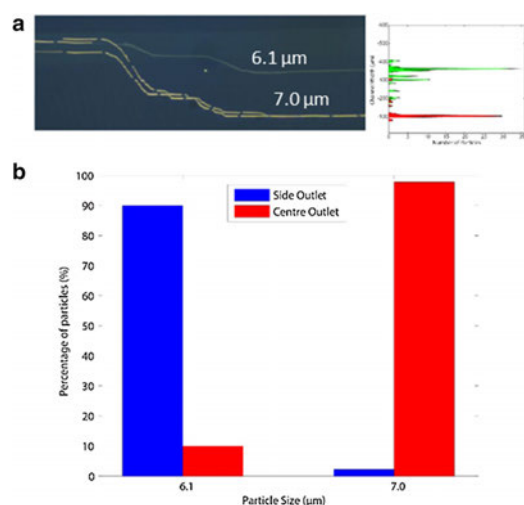
Fig. 8 Continuous separation of fluorescent polystyrene beads of 6.1 μm (*green*) and 7.0 μm (*yellow*) diameter. **a** Stacked images showing a single separation process along the flow direction of the microchannel, where the different-sized particles are expected to reach a stable position after sorting. The corresponding distribution of particles at the end of the working region is represented by the number of particles obtained from the fluorescent profile. **b** Shows the separation efficiency that is analysed by measuring the distribution of the fluorescence intensity. Flow rate and the input power in this case are 3 μl/min and 637 mW, respectively, with a SAW wavelength of 40 μm

usually a non-uniform distribution of displacement amplitudes across the face of the IDTs which will further contribute to the observed discrepancy.

The spatially variant pressure field with distinct travelling wave and standing wave-dominant regions is ultimately generated by the attenuation of leaky SAW into the liquid. The amount of attenuation incurred by a wave at a given point is a function of the distance over which energy couples into the bounding fluid. The width of the channel used in the experiment is selected to be 1200 μm (30 λ_{SAW}) as this will result in the amplitude of the leaky SAW to drop to approximately 20 % of the original amplitude at the centre of the channel and 4 % at the opposite end of the channel. For a given channel width, the stable location for each particle size remains unchanged regardless of the variation of flow rate and input power over the range examined (0.5–3 μl/min, 200–1020 mW). However, as long as the IDT aperture is large enough for the migration to take place fully, then the end location is flow rate independent. The stable end location is located further from the start of the IDTs for higher flow rates and lower input powers; hence, a larger IDT aperture is required. The IDT aperture can

thus be modified to suit given flow rate and applied power constraints.

As the underlying mechanism is based on attenuation at the liquid–substrate interface, no precise alignment is required as compared to conventional SSAW particle separation devices, where the centre of channel needs to be aligned with a single pressure node. Using the TSAW and SSAW combined approach, the simultaneous separation of 6.1- and 7.0-μm polystyrene beads was successfully achieved.

The sorting process and size-deterministic behaviour can be observed in Fig. 8, where the larger 7.0-μm particles were collected in the centre outlet channel, whereas the smaller 6.1-μm particles accumulate in the upper outlet channel. By splitting the top half of the channel outlet by three sections equally and classifying the first 200 μm as the centre outlet and the following 200 μm as the side outlet, the separation efficiency of the particles is found to be 90 % for 6.1 μm and 98 % for 7 μm beads, as shown in Fig. 8b. The separation efficiency is defined as $A/(A + B)$ for 6-μm particles and $B/(A + B)$ for 7.0-μm particles, where A and B are the number of the target particles collected at the side and centre outlet, respectively.

5 Conclusion

Continuous size-based deterministic particle sorting has been successfully demonstrated through the use of a pressure field that combines both standing and travelling waves. This phenomenon exploits the substantial attenuation observed at high frequencies within wide fluid channels. Such a hybrid pressure field utilises the best features of both to sort particles deterministically. The particles in the travelling wave-dominant region are deflected and sorted on the basis of size due to the large force scaling and are subsequently trapped at stable pressure node locations, resulting in distinct exit locations independent of flow rate. We demonstrate this principle with the separation of 5.1-, 6.1- and 7.0-μm-diameter particles. Submicron separation resolution can also be achieved using this TSAW/SSAW combined approach, which is a challenge for other particle separation techniques. With the ability to sort multiple particle population with a degree of insensitivity to flow rate, we anticipate that this system can be implemented in a broad range of applications, where size-deterministic sorting of particles or cells is required, especially in systems where flow rates cannot be controlled precisely.

References

Behrens J, Langelier S, Rezk AR, Lindner G, Yeo LY, Friend JR (2015) Microscale anechoic architecture: acoustic diffusers for ultra low power microparticle separation via traveling surface acoustic waves. Lab Chip 15(1):43–46. doi:10.1039/C4LC00704B

Bruus H (2008) Theoretical microfluidics. OUP, Oxford

Campbell JJ, Jones WR (1968) A method for estimating optimal crystal cuts and propagation directions for excitation of piezoelectric surface waves. Sonics and ultrasonics. IEEE Trans 15(4):209–217. doi:10.1109/T-SU.1968.29477

Carr C, Espy M, Nath P, Martin SL, Ward MD, Martin J (2009) Design, fabrication and demonstration of a magnetophoresis chamber with 25 output fractions. J Magn Magn Mater 321(10):1440–1445. doi:10.1016/j.jmmm.2009.02.064

Collins DJ, Alan T, Helmerson K, Neild A (2013) Surface acoustic waves for on-demand production of picoliter droplets and particle encapsulation. Lab Chip 13(16):3225–3231

Collins DJ, Alan T, Neild A (2014a) Particle separation using virtual deterministic lateral displacement (vDLD). Lab Chip 14(9):1595–1603. doi:10.1039/c3lc51367j

Collins DJ, Alan T, Neild A (2014b) The particle valve: on-demand particle trapping, filtering, and release from a microfabricated polydimethylsiloxane membrane using surface acoustic waves. Appl Phys Lett 105(3):033509. doi:10.1063/1.4891424

Collins DJ, Morahan B, Garcia-Bustos J, Doerig C, Plebanski M, Neild A (2015) Two-dimensional single-cell patterning with one cell per well driven by surface acoustic waves. Nat Commun 6:8686. doi:10.1038/ncomms9686

Collins DJ, Neild A, Ai Y (2016) Highly focused high-frequency travelling surface acoustic waves (SAW) for rapid single-particle sorting. Lab Chip 16(3):471–479. doi:10.1039/c5lc01335f

Davey HM, Kell DB (1996) Flow cytometry and cell sorting of heterogeneous microbial populations: the importance of single-cell analyses. Microbiol Rev 60(4):641–696

Dentry MB, Yeo LY, Friend JR (2014) Frequency effects on the scale and behavior of acoustic streaming. Phys Rev E: Stat, Nonlinear, Soft Matter Phys 89(1):013203. doi:10.1103/PhysRevE.89.013203

Destgeer G, Lee KH, Jung JH, Alazzam A, Sung HJ (2013) Continuous separation of particles in a PDMS microfluidic channel via travelling surface acoustic waves (TSAW). Lab Chip 13(21):4210–4216. doi:10.1039/c3lc50451d

Destgeer G, Ha BH, Jung JH, Sung HJ (2014) Submicron separation of microspheres via travelling surface acoustic waves. Lab Chip 14(24):4665–4672. doi:10.1039/c4lc00868e

Destgeer G, Ha BH, Park J, Jung JH, Alazzam A, Sung HJ (2015) Microchannel anechoic corner for size-selective separation and medium exchange via traveling surface acoustic waves. Anal Chem 87(9):4627–4632. doi:10.1021/acs.analchem.5b00525

Devendran C, Gralinski I, Neild A (2014) Separation of particles using acoustic streaming and radiation forces in an open microfluidic channel. Microfluid Nanofluid 17(5):879–890. doi:10.1007/s10404-014-1380-4

Devendran C, Albrecht T, Brenker J, Alan T, Neild A (2016a) The importance of travelling wave components in standing surface acoustic wave (SSAW) systems. Lab Chip 16:3756-3766. doi: 10.1039/C6LC00798H

Devendran C, Gunasekara NR, Collins DJ, Neild A (2016b) Batch process particle separation using surface acoustic waves (SAW):

integration of travelling and standing SAW. RSC Adv 6(7):5856–5864. doi:10.1039/c5ra26965b

Di Carlo D (2009) Inertial microfluidics. Lab Chip 9(21):3038–3046. doi:10.1039/b912547g

Ding X, Lin SC, Lapsley MI, Li S, Guo X, Chan CY, Chiang IK, Wang L, McCoy JP, Huang TJ (2012) Standing surface acoustic wave (SSAW) based multichannel cell sorting. Lab Chip 12(21):4228–4231. doi:10.1039/c2lc40751e

Dual J, Hahn P, Leibacher I, Moller D, Schwarz T, Wang J (2012) Acoustofluidics 19: ultrasonic microrobotics in cavities: devices and numerical simulation. Lab Chip 12(20):4010–4021. doi:10.1039/c2lc40733g

Franke T, Braunmuller S, Schmid L, Wixforth A, Weitz DA (2010) Surface acoustic wave actuated cell sorting (SAWACS). Lab Chip 10(6):789–794. doi:10.1039/b915522h

Friend J, Yeo LY (2011) Microscale acoustofluidics: microfluidics driven via acoustics and ultrasonics. Rev Mod Phys 83(2):647–704. doi:10.1103/RevModPhys.83.647

Gascoyne PRC, Vykoukal J (2002) Particle separation by dielectrophoresis. Electrophoresis 23(13):1973–1983. doi:10.1002/1522-2683(200207)23:13<1973:aid-elps1973>3.0.co;2-1

Glynne-Jones P, Demore CE, Ye C, Qiu Y, Cochran S, Hill M (2012) Array-controlled ultrasonic manipulation of particles in planar acoustic resonator. IEEE Trans Ultrason Ferroelectr Freq Control 59(6):1258–1266. doi:10.1109/TUFFC.2012.2316

Hasegawa T, Yosioka K (1975) Acoustic radiation force on fused silica spheres, and intensity determination. J Acoust Soc Am 58(3):581–585. doi:10.1121/1.380708

Hitzbleck M, Lovchik RD, Delamarche E (2013) Flock-based microfluidics. Adv Mater 25(19):2672–2676. doi:10.1002/adma.201204854

Huang LR, Cox EC, Austin RH, Sturm JC (2004) Continuous particle separation through deterministic lateral displacement. Science 304(5673):987–990

Johansson L, Nikolajeff F, Johansson S, Thorslund S (2009) On-chip fluorescence-activated cell sorting by an integrated miniaturized ultrasonic transducer. Anal Chem 81(13):5188–5196

Kim U, Qian J, Kenrick SA, Daugherty PS, Soh HT (2008) Multitarget dielectrophoresis activated cell sorter. Anal Chem 80(22):8656–8661. doi:10.1021/ac8015938

Lei H, Zhang Y, Li B (2012) Particle separation in fluidic flow by optical fiber. Opt Express 20(2):1292–1300. doi:10.1364/OE.20.001292

Leibacher I, Schatzer S, Dual J (2014) Impedance matched channel walls in acoustofluidic systems. Lab Chip 14(3):463–470. doi:10.1039/c3lc51109j

Leibacher I, Reichert P, Dual J (2015) Microfluidic droplet handling by bulk acoustic wave (BAW) acoustophoresis. Lab Chip 15(13):2896–2905. doi:10.1039/c5lc00083a

Lenshof A, Laurell T (2010) Continuous separation of cells and particles in microfluidic systems. Chem Soc Rev 39(3):1203–1217. doi:10.1039/b915999c

Li P, Mao Z, Peng Z, Zhou L, Chen Y, Huang P-H, Truica CI, Drabick JJ, El-Deiry WS, Dao M, Suresh S, Huang TJ (2015) Acoustic separation of circulating tumor cells. Proc Natl Acad Sci 112(16):4970–4975. doi:10.1073/pnas.1504484112

Loutherback K, Chou KS, Newman J, Puchalla J, Austin RH, Sturm JC (2010) Improved performance of deterministic lateral displacement arrays with triangular posts. Microfluid Nanofluid 9(6):1143–1149. doi:10.1007/s10404-010-0635-y

MacDonald MP, Spalding GC, Dholakia K (2003) Microfluidic sorting in an optical lattice. Nature 426(6965):421–424

McGrath J, Jimenez M, Bridle H (2014) Deterministic lateral displacement for particle separation: a review. Lab Chip 14(21):4139–4158. doi:10.1039/c4lc00939h

Miansari M, Qi A, Yeo LY, Friend JR (2015) Vibration-induced deagglomeration and shear-induced alignment of carbon nanotubes in air. Adv Funct Mater 25(7):1014–1023. doi:10.1002/adfm.201402976

Morijiri T, Sunahiro S, Senaha M, Yamada M, Seki M (2011) Sedimentation pinched-flow fractionation for size- and density-based particle sorting in microchannels. Microfluid Nanofluid 11(1):105–110. doi:10.1007/s10404-011-0785-6

Morton KJ, Loutherback K, Inglis DW, Tsui OK, Sturm JC, Chou SY, Austin RH (2008) Hydrodynamic metamaterials: microfabricated arrays to steer, refract, and focus streams of biomaterials. Proc Natl Acad Sci USA 105(21):7434–7438. doi:10.1073/pnas.0712398105

Neild A, Oberti S, Dual J (2007) Design, modeling and characterization of microfluidic devices for ultrasonic manipulation. Sens Actuato B Chem 121(2):452–461. doi:10.1016/j.snb.2006.04.065

Park S, Zhang Y, Wang TH, Yang S (2011) Continuous dielectrophoretic bacterial separation and concentration from physiological media of high conductivity. Lab Chip 11(17):2893–2900. doi:10.1039/c1lc20307j

Petersson F, Nilsson A, Holm C, Jonsson H, Laurell T (2005) Continuous separation of lipid particles from erythrocytes by means of laminar flow and acoustic standing wave forces. Lab Chip 5(1):20–22. doi:10.1039/b405748c

Riera-Franco de Sarabia E, Gallego-Juárez JA, Rodríguez-Corral G, Elvira-Segura L, González-Gómez I (2000) Application of high-power ultrasound to enhance fluid/solid particle separation processes. Ultrasonics 38(1–8):642–646. doi:10.1016/s0041-624x(99)00129-8

Sajeesh P, Sen AK (2013) Particle separation and sorting in microfluidic devices: a review. Microfluid Nanofluid 17(1):1–52. doi:10.1007/s10404-013-1291-9

Schmid L, Weitz DA, Franke T (2014) Sorting drops and cells with acoustics: acoustic microfluidic fluorescence-activated cell sorter. Lab Chip 14(19):3710–3718. doi:10.1039/c4lc00588k

Sesen M, Alan T, Neild A (2014) Microfluidic on-demand droplet merging using surface acoustic waves. Lab Chip 14(17):3325–3333. doi:10.1039/c4lc00456f

Shi J, Huang H, Stratton Z, Huang Y, Huang TJ (2009) Continuous particle separation in a microfluidic channel via standing surface acoustic waves (SSAW). Lab Chip 9(23):3354–3359. doi:10.1039/b915113c

Shields CW, Reyes CD, Lopez GP (2015) Microfluidic cell sorting: a review of the advances in the separation of cells from debulking to rare cell isolation. Lab Chip 15(5):1230–1249. doi:10.1039/c4lc01246a

Shiokawa S, Matsui Y, Ueda T (1989) Liquid streaming and droplet formation caused by leaky Rayleigh waves. In: Ultrasonics symposium, 1989. Proceedings., IEEE 1989, 3–6 Oct 1989, vol 641, pp 643–646. doi:10.1109/ULTSYM.1989.67063

Sivanantha N, Ma C, Collins DJ, Sesen M, Brenker J, Coppel RL, Neild A, Alan T (2014) Characterization of adhesive properties of red blood cells using surface acoustic wave induced flows for rapid diagnostics. Appl Phys Lett 105(10):103704. doi:10.1063/1.4895472

Skowronek V, Rambach RW, Schmid L, Haase K, Franke T (2013) Particle deflection in a poly(dimethylsiloxane) microchannel using a propagating surface acoustic wave: size and frequency dependence. Anal Chem 85(20):9955–9959. doi:10.1021/ac402607p

Tartaj P, del Puerto Morales M, Veintemillas-Verdaguer S, González-Carreño T, Serna CJ (2003) The preparation of magnetic nanoparticles for applications in biomedicine. J Phys D Appl Phys 36(13):R182

Wang Y, Zhao Y, Cho SK (2007) Efficient in-droplet separation of magnetic particles for digital microfluidics. J Micromech Microeng 17(10):2148

Wei Hou H, Gan HY, Bhagat AA, Li LD, Lim CT, Han J (2012) A microfluidics approach towards high-throughput pathogen removal from blood using margination. Biomicrofluidics 6(2):24115–2411513. doi:10.1063/1.4710992

Wiklund M, Gunther C, Lemor R, Jager M, Fuhr G, Hertz HM (2006) Ultrasonic standing wave manipulation technology integrated into a dielectrophoretic chip. Lab Chip 6(12):1537–1544. doi:10.1039/b612064b

Witte C, Reboud J, Wilson R, Cooper JM, Neale SL (2014) Microfluidic resonant cavities enable acoustophoresis on a disposable superstrate. Lab Chip 14(21):4277–4283. doi:10.1039/c4lc00749b

Xia N, Hunt TP, Mayers BT, Alsberg E, Whitesides GM, Westervelt RM, Ingber DE (2006) Combined microfluidic-micromagnetic separation of living cells in continuous flow. Biomed Microdevices 8(4):299–308. doi:10.1007/s10544-006-0033-0

Yamada M, Seki M (2005) Hydrodynamic filtration for on-chip particle concentration and classification utilizing microfluidics. Lab Chip 5(11):1233–1239. doi:10.1039/b509386d

Yeo LY, Friend JR (2009) Ultrafast microfluidics using surface acoustic waves. Biomicrofluidics 3(1):12002. doi:10.1063/1.3056040

Yeo LY, Friend JR (2014) Surface acoustic wave microfluidics. Annu Rev Fluid Mech 46(1):379–406. doi:10.1146/annurev-fluid-010313-141418

Chapter 4

Acoustic Tweezing of Particles using Decaying Opposing Travelling Surface Acoustic Waves (DOTSAW)

4.1 Overview

In this chapter, investigation of using another novel acoustic wave field to achieve particle tweezing is carried out. Acoustic particle tweezing refers to the trapping of particles and then the subsequent movement of them by translation of the sound field. Whilst this is possible using BAW, where the sound field is usually generated by exciting resonances in the fluid body, it requires the careful suppression of reflected waves to obtain the required control over the pressure field. However, SAW lends itself more naturally to this process due to the weak reflections present, displacement of the particles once trapped in a standing wave can be achieved by frequency or phase changes. The result is a movement of the pattern of particles created in the standing wave. A common factor in approaches to date is the use of a single excitation frequency at any moment of time. The foundation of this work relies on challenging two prevalent assumptions about two counter-propagating waves. The first assumption is two counter-propagating waves always superpose and form standing waves, which generate periodic traps for suspended particles. Since our work is not of a SSAW system but of a TSAW system, the second assumption is that a typical TSAW system possesses monodirectional quality, where particles are always pushed away in a single direction. Two different frequency travelling waves are excited in this work, our analysis shows that under such conditions a standing wave is not produced, rather a single trapping location exists for the suspended particles, (similar to optical tweezers that can trap particles over multiple wavelengths in a single location). This single trap's location can be altered very simply by adjusting the relative power of excitation of the two waves.

4.2 Publication

The following publication was reproduced [154] by permission of The Royal Society of Chemistry.

Lab on a Chip

PAPER

Acoustic tweezing of particles using decaying opposing travelling surface acoustic waves (DOTSAW)†

Jia Wei Ng, Citsabehsan Devendran [iD] and Adrian Neild [iD] *

Surface acoustic waves offer a versatile and biocompatible method of manipulating the location of suspended particles or cells within microfluidic systems. The most common approach uses the interference of identical frequency, counter propagating travelling waves to generate a standing surface acoustic wave, in which particles migrate a distance less than half the acoustic wavelength to their nearest pressure node. The result is the formation of a periodic pattern of particles. Subsequent displacement of this pattern, the prerequisite for tweezing, can be achieved by translation of the standing wave, and with it the pressure nodes; this requires changing either the frequency of the pair of waves, or their relative phase. Here, in contrast, we examine the use of two counterpropagating traveling waves of different frequency. The non linearity of the acoustic forces used to manipulate particles, means that a small frequency difference between the two waves creates a substantially different force field, which offers significant advantages. Firstly, this approach creates a much longer range force field, in which migration takes place across multiple wavelengths, and causes particles to be gathered together in a single trapping site. Secondly, the location of this single trapping site can be controlled by the relative amplitude of the two waves, requiring simply an attenuation of one of the electrical drive signals. Using this approach, we show that by controlling the powers of the opposing incoherent waves, 5 μm particles can be migrated laterally across a fluid flow to defined locations with an accuracy of ±10 μm.

Introduction

Suspended matter in a microfluidic systems can be manipulated through a range of mechanisms including using optical,[1][3] magnetic,[4,5] dielectrophoretic[6,7] or acoustic forces.[8][11] Among these, acoustic forces offer the benefits of easy integration into a miniaturised system and excellent bio compatibility with minimal effect on the viability and function of biological cells,[10,12][15] in addition no tagging or labelling of the particles is required. Particle manipulation allows trapping of particles in defined positions enabling tasks such as concentration,[16,17] sorting[18,19] and imaging,[4,20] however it is also possible to define particle trajectory rather than position. Whilst, recently, predefined trajectory control has been shown by use of phase gradients established through acoustic holography,[21] the term acoustic tweezing is usually reserved for systems in which there is the freedom to actively move trapped particles, offering user defined trajectory control.[22,23]

Acoustic particle manipulation is often achieved through the excitation of a resonant standing wave in a fluid body using a single excitation source.[24] In this con figuration, bulk acoustic waves are used to excite the pres sure field, and suspended particles will migrate to the pressure nodes or antinodes depending on their physical properties.[25][28] As the fields which are excited using bulk acoustic waves are resonant modes, and there are a limited number of modes available, it is very challenging to subsequently displace the field and as such the trapped particles, to enable tweezing. To gain the control over the pressure field which is required for tweezing, it is preferable to excite a standing wave field using multiple wave sources. This has been demonstrated using bulk acoustic wave transducers which excite counter propagating waves. By suppressing undesired reflections and altering the relative phase of excitation, a standing wave field can be displaced to move trapped particles over desired trajectories.[29][31]

Surface acoustic waves offer an alternative excitation method, here a periodic pattern of electrodes, an interdigitated transducer (IDT), is used to excite a wave which propagates across the surface of a piezoelectric wafer, from where it can couple into an adjacent fluid body.[32,33] When

Department of Mechanical and Aerospace Engineering, Monash University, Clayton, Victoria 3800, Australia. E-mail: adrian.neild@monash.edu
† Electronic supplementary information (ESI) available. See DOI: 10.1039/c7lc00862g

71

the fluid body is contained within a PDMS channel, the absorption of acoustic waves in the PDMS ensures that re flections of the waves are substantially reduced, allowing greater freedom in the design of the sound field.[34] As such a single set of electrodes can create a travelling wave, capa ble of near field particle patterning,[35] pushing suspended particles,[36 38] droplets[39] or fluid interfaces.[40,41] Whilst, multiple sets of electrodes can create standing waves for particle sorting[42 45] and patterning.[46 49] With wave reflec tion suppressed, changes in the relative phase of wave ex citation allows tweezing *via* movement of the sound field.[50 52] The use of more complex electrode designs of fers additional approaches, for example, chirped IDTs al low a range of frequencies to be excited, so that the nodes of the sound wave can be displaced by change of excitation frequency.[53,54]

The overriding similarity in the systems described is that a single frequency is used for all the waves which are ex cited. Even when tweezing is achieved by shifting the fre quency of excitation, at any given moment of operation a single frequency is being excited. Indeed, this condition is required to establish the standing waves used to trap the particles.

Here we propose a new technique for acoustic tweezing by employing two opposing travelling surface acoustic waves with distinct frequencies. We show that the differ ence in frequency, a form of incoherence, means that a standing wave isn't established, the interference of the two waves doesn't cause nodes and antinodes to form. However, trapping can be achieved as, effectively, the waves act as a pair of independent travelling waves, with each wave exerting a pushing force on the particles in op posing directions. The strength of the force generated by each wave is spatially varying due to attenuation, as such a single stable force potential minimum is achieved. This enables stable particle trapping, at the location at which each opposing force has the same magnitude. We term this new form of acoustic trap decaying opposing travel ling surface acoustic waves (DOTSAW), as it arises from decaying opposing travelling surface acoustic waves. As well as creating a single trapping location in which all particles are gathered (rather than the multiple periodic trapping of a standing wave), this approach also offers the advantage of simple displacement of the particles once trapped, the prerequisite for tweezing, by adjustment of the relative amplitudes of the waves. Finally, the differ ence in frequency required between the waves is so small that it falls within the bandwidth of a linear IDT set, so there is no need for chirped IDTs which are non optimal in terms of energy transduction efficiency. To demonstrate this, we show that 5 μm radius particles can be manipu lated to any desired position across the width of a chan nel (so transverse to the flow) by modulating the ampli tude ratio between the opposing identical transducers, and we characterise the relationship between location and rela tive power. Experimentally, the system provides large spa

tial range (>400 μm) along with excellent accuracy (±10 μm) (Fig. 1).

System principle

A surface acoustic wave (SAW) is generated when an alternat ing current (AC) electrical signal is applied to the IDTs pat terned on a piezoelectric substrate. When driven at the fre quency given by $f = c_s/\lambda_{SAW}$, where c_s is the sound speed of the surface wave on the substrate and λ_{SAW} is the distance be tween periodic features in the IDTs, the mechanical displace ments emanating from one set of finger pairs constructively interfere with those emerging neighbouring ones, resulting in a high displacement SAW.

The resulting surface wave will efficiently travel along the surface of the substrate with minimal loses.[55] If however a fluid is located on the substrate, energy will "leak" from the surface wave into that fluid. This coupling of energy into the fluid, resulting in a wave emerging from the substrate at the Rayleigh angle,[56] in turn causes an exponential decay in the amplitude of the surface acoustic wave. The attenuation coef ficient of this decay, C_d, is given by:[14,57]

$$C_d = \frac{\rho_0 c_0}{\rho_{LN} c_{LN} \lambda_{SAW}} \tag{1}$$

where ρ_0 and ρ_{LN} are the density of water and lithium niobate substrate respectively, c_0 and c_{LN} are their respective sound speed, and λ_{SAW} is the SAW wavelength.

The coupling of energy into the fluid is essential for acoustofluidic applications; as it is the waves passing through the fluid which affect suspended particle and fluid behav iour. In the case of particle manipulation the force field arises from the time average of the pressure squared and fluid particle velocity squared terms at any given location, with the acoustic radiation force, F^{rad}, being given by:[58]

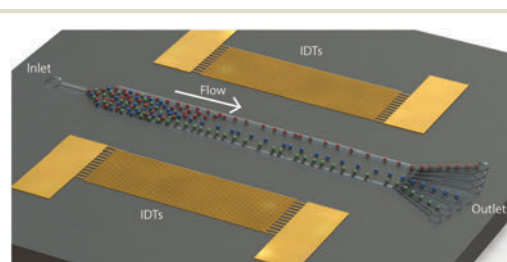$$F^{rad} = \quad \nabla U^{rad} \tag{2a}$$

Fig. 1 Sketch of the DOTSAW device operating principle: accurate positioning of particles can be achieved through an acoustic field created by two opposing sets of interdigitated transducers (IDTs) on a piezoelectric lithium niobate (LN) substrate. The different coloured particles represent the trajectories the particle take under different operating conditions.

$$U^{\mathrm{rad}} = \frac{4\pi}{3} a^3 \left[f_1 \frac{1}{2} \kappa_0 \left\langle p_{\mathrm{in}}^2 \right\rangle - f_2 \frac{3}{4} \rho_0 \left\langle v_{\mathrm{in}}^2 \right\rangle \right] \qquad (2b)$$

$$f_1(\tilde{\kappa}) = 1 - \tilde{\kappa}, \quad \text{with } \tilde{\kappa} = \frac{\kappa_{\mathrm{p}}}{\kappa_0} \qquad (2c)$$

$$f_2(\tilde{\rho}) = \frac{2(\tilde{\rho}-1)}{2\tilde{\rho}+1}, \quad \text{with } \tilde{\rho} = \frac{\rho_{\mathrm{p}}}{\rho_0} \qquad (2d)$$

where U^{rad} is the acoustic potential, $\langle p_{\mathrm{in}}^2 \rangle$ and $\langle v_{\mathrm{in}}^2 \rangle$ are the temporal average second ordered fluid pressure and velocity at the particle's location, and κ and ρ are the compressibility and density, respectively, of the particle or the fluid with the subscript p or 0 accordingly. This equation assumes that the particles are below the Rayleigh limit, meaning that they are considerably smaller than the wavelength. There are however some issues around the application of it on certain sound fields. Settnes and Bruus[59] who derived the equation noted that it is only the imaginary parts of factors f_1 and f_2 (arising from viscous effects) which contribute to the force when the equation is applied to the special case of a travelling wave. Whilst Gor'kov, who performed an earlier study in which the fluid was assumed to be inviscid (an assumption we also make), noted directly an issue with application of his equations to plane travelling waves.[60]

As a result we apply the formula with care. In this section, we examine the way that terms from each of the two waves are connected in the force expression after time averaging. When the solution relates to plane travelling waves (with no decay) we calculate a zero net force. However, the key here is understanding how the time averaging is affected by a frequency shift to one of the waves at a conceptual level, rather than the actual force calculated. In the Results and discussion section, we include a decay term which means the wave is no longer a pure plane travelling wave. This allows us to calculate the actual (non zero) forces in our system. Further validation is offered by comparison with the experimental data.

There have been two main approaches to using surface acoustic waves to manipulate particles the first uses a single IDT source and the emerging travelling surface acoustic wave (TSAW) to couple into the fluid, the result is the migration of particles away from the source.[61] The second approach uses two IDT sources which produce counter propagating waves at the same frequency, the interference of which yields a standing surface acoustic wave (SSAW), it too couples into the fluid, where the result is a form of standing acoustic field. In this case particles are held in periodic locations due to the periodicity of the standing wave.[32] Hence, the addition of the second surface acoustic wave makes a large difference to the nature of the force field, going from mono directional to periodic. The reason lies in the relationship of the acoustic radiation force with the pressure and particle velocity squared, this non linearity means that whilst the pressure field from the two waves can be linearly superposed, the resultant forces from the two waves cannot.

Two counter propagating waves (for this discussion we ignore the decay in amplitude) can be expressed mathematically in terms of the velocity potential, Φ, as:

$$\Phi_{\mathrm{a}} = \phi_{\mathrm{A}} e^{i(\omega_{\mathrm{a}}t - k_{\mathrm{a}}x)} \qquad (3a)$$

$$\Phi_{\mathrm{b}} = \phi_{\mathrm{B}} e^{i(\omega_{\mathrm{b}}t + k_{\mathrm{b}}x)} \qquad (3b)$$

where ϕ_{A} and ϕ_{B} are the peak amplitudes, k_{a} and k_{b} the wavenumbers and ω_{a} and ω_{b} the angular frequencies. The pressure can then be calculated using $p = \rho \partial \Phi / \partial t$ and summed to give:

$$p = \rho \phi_{\mathrm{A}} i \omega_{\mathrm{a}} e^{i(\omega_{\mathrm{a}}t - k_{\mathrm{a}}x)} + \rho \phi_{\mathrm{B}} i \omega_{\mathrm{b}} e^{i(\omega_{\mathrm{b}}t - k_{\mathrm{b}}x)} \qquad (4)$$

what is important for this discussion is that in summing the pressures, a linear process, the subscript a terms are clustered together, as are the subscript b terms. The next stage in calculating the component of the force potential related to $\langle p^2 \rangle$, is to square the real component of the pressure, here the terms have been expanded out so the time components are clearly stated which gives rise to the rather unwieldy:

$$
\begin{aligned}
& \left[\Re(p) \right]^2 \\
&= \rho^2 \phi_{\mathrm{A}}^2 \omega_{\mathrm{a}}^2 \left[\sin^2 \omega_{\mathrm{a}}t \cos^2 k_{\mathrm{a}}x \right. \\
& + \cos^2 \omega_{\mathrm{a}}t \sin^2 k_{\mathrm{a}}x \\
& \left. -2\sin \omega_{\mathrm{a}}t \cos k_{\mathrm{a}}x \cos \omega_{\mathrm{a}}t \sin k_{\mathrm{a}}x \right] \\
& + \rho^2 \phi_{\mathrm{B}}^2 \omega_{\mathrm{b}}^2 \left[\sin^2 \omega_{\mathrm{b}}t \cos^2 k_{\mathrm{b}}x \right. \\
& + \cos^2 \omega_{\mathrm{b}}t \sin^2 k_{\mathrm{b}}x \\
& \left. -2\sin \omega_{\mathrm{b}}t \cos k_{\mathrm{b}}x \cos \omega_{\mathrm{b}}t \sin k_{\mathrm{b}}x \right] \\
& + 2\rho^2 \phi_{\mathrm{A}} \phi_{\mathrm{B}} \omega_{\mathrm{a}} \omega_{\mathrm{b}} \left[\sin \omega_{\mathrm{a}}t \cos k_{\mathrm{a}}x \sin \omega_{\mathrm{b}}t \cos k_{\mathrm{b}}x + \sin \omega_{\mathrm{a}}t \cos k_{\mathrm{a}}x \cos \omega_{\mathrm{b}}t \sin k_{\mathrm{b}}x \right. \\
& \left. - \cos \omega_{\mathrm{a}}t \sin k_{\mathrm{a}}x \sin \omega_{\mathrm{b}}t \cos k_{\mathrm{b}}x - \cos \omega_{\mathrm{a}}t \sin k_{\mathrm{a}}x \cos \omega_{\mathrm{b}}t \sin k_{\mathrm{b}}x \right]
\end{aligned}
\qquad (5)
$$

73

Here the key feature is that in the third square bracket there are terms with both a and b subscripts, so in contrast to the linear pressure, the effect of wave a and b can't simply be added.

In performing the time average, $\cos^2 \omega t$ will become 1/2 (as $\cos^2 A = \frac{1}{2} + \frac{1}{2}\cos 2A$), whilst $\cos \omega t \sin \omega t$ is equated to zero ($\cos A \sin A = \frac{1}{2}\sin 2A$). Hence, when ω_a is set to be equal to ω_b, then the time average of the pressure squared is given by:

$$\langle p^2 \rangle = 2\rho^2 \phi^2 \omega^2 \cos^2 kx \qquad (6)$$

which shows the spatial periodicity related to the standing wave produced by two counter propagating waves of equal frequency. For a discussion of the role of decay in this case see a previous studies.[42]

If the frequencies of the two waves differ, then the $\cos \omega_a t \cos \omega_b t$ and the $\sin \omega_a t \sin \omega_b t$ expressions will become negligible when averaged over a long time period, T (see Fig. S1 in the ESI†). We assume that $T \gg \frac{2\pi}{\omega_a - \omega_b}$, and that this T is small in comparison to the timescale of the net motion of the particles. Using this assumption, all the terms within the third square bracket will time average to zero. Hence, there is a separation of the subscript a and b terms. In fact, the force potential related to $\langle p^2 \rangle$ is that due to the sum of terms related to the two individual waves, the same is true for $\langle v^2 \rangle$, so we can sum the forces from each individual wave, provided they are of different frequency. Note that if the two frequencies of operation are very close together (in the order of a few Hertz), this assumption will breakdown, and example of this has been seen in an earlier study which used two orthogonal standing waves of different frequencies.[48]

In this case, in which no decay is considered, the simplification of the expression yields to a trivial result, in that there is no spatial variation in the force potential, and hence no force. This again fits with the addition of the forces from independent travelling waves, in the absence of decay this force would be spatially uniform, hence two counter propagating waves will yield equal and opposite forces, thus, no net force. Here, under dual frequency operation, the decay of the travelling waves is required to impose a net force, as it introduces a spatial distribution in the time averaged pressure field. Whilst the underlying principle of the DOTSAW system has been discussed, it is in the results section that a full characterisation, including the effect of SAW decay, is given.

Methodology

To investigate the use of the DOTSAW system experimentally, suitable devices have been fabricated. The experimental system consists of a piezoelectric 128° Y cut X propagating lith-

ium niobate (LN) substrate patterned with straight interdigitated transducers (IDTs). Each set of IDTs has 12 finger pairs with a SAW wavelength of $\lambda_{SAW} = 50$ μm and aperture of 1600 μm. Note that the two IDT sets are identical, having the same nominal operational frequency, however there is enough bandwidth in the response to allow them to be excited at frequencies sufficiently separated to observe the DOTSAW effect. The microfluidic channel is created by soft lithography replica moulding of polydimethylsiloxane (PDMS) and subsequently bonded, after exposure to an air plasma, to the LN substrate. The depth and the width of the microchannel used in this system is designed to be 25 μm and 400 μm respectively.

To demonstrate DOTSAW performance, the SAW devices were used for a series of experiments conducted under a fluorescence microscope (Olympus BX43, Tokyo, Japan). In which, fluorescent polystyrene particles (Magsphere, Pasadena, CA, USA) of 10 μm diameter were diluted using deionised water (Milli Q 18.2 MΩ cm, Millipore, Billerica, MA) with 2% w/w polyethylene glycol (PEG) to prevent particle adhesion, before being injected into the microfluidic channel using a syringe pump (KD Scientific Legato 210, Holliston, MA, USA). For system actuation, two incoherent signals were produced by a two channel power signal generator (BelektroniG F20 Power Saw, Freital, Germany) and were applied to the two sets of IDTs to generate opposing SAWs at two different frequencies. A 5 MPixel C mount camera (PixeLink PL B872CU, Ottawa, Canada) was connected to the microscope to monitor particle behaviour. The videos were post processed and analysed using a custom MATLAB (MathWorks) program, in which the fluorescence intensity of the particles was profiled at the end of the channel to yield quantitative data about the particle manipulation distance for each video frame (this was conducted over a time frame of approximately 1 min).

This experimental data is compared against numerical predictions. MATLAB is used to generate this numerical data, by evaluation of expressions describing the pressure field including energy decay due to coupling into the fluid, and the subsequent calculation of the acoustic radiation forces. The parameters used for this numerical study are given in the Table S1.†

Results and discussion

The system concept description demonstrated the difference of having counter propagating coherent (SSAW) and incoherent waves (DOTSAW). Namely, that in the latter the forces generated arise from a straightforward summation of terms arising from each individual wave. However, for the purpose of demonstrating this principle without additional complexity, the spatial decay of the waves was ignored. The result was that the two frequency system resulted in no net forces. Here, we use a numerical approach to examine the effect of this decay in both the equal and differing frequency scenarios. This

74

allows the DOTSAW concept to be more comprehensively demonstrated.

In a system with two opposing exponentially decaying traveling waves with the same frequency, coherent interference will occur and result in a standing wave. The shape of the time averaged pressure squared is that of a sinusoid, so displaying multiple troughs (Fig. 2a), the amplitude of which increases at each side of the field due to the proximity to the nearest IDT set.

Fig. 2c shows the resulting force field, on a 5 μm radius particle, which, as with the pressure squared plot, has a strong periodicity. In this force field the particles can be expected to collect at locations corresponding to zero force and a negative gradient in the force profile (such that the locations are stable force potential minima).

In contrast, the time averaged pressure squared field which results from DOTSAW has a single minimum at the centre of the field, as shown in Fig. 2b. This results in a force field which has a single zero force location, Fig. 2d, meaning that all particles are collected in that one location. Due to the larger spatial scale of the time averaged pressure field, the resulting force is lower than that of the SSAW system, however, despite this, powers well below the maximum available can achieve particle collection.

There are two key features of the DOTSAW system, firstly the single collection location, and secondly the ease with which this minimum can be translated. Fig. 3 demonstrates that by application of different excitation amplitudes to each of the IDTs, the minimum can be displaced. Whilst such displacement is also possible for SSAW, this requires an electrically more complex shift in phase or frequency.
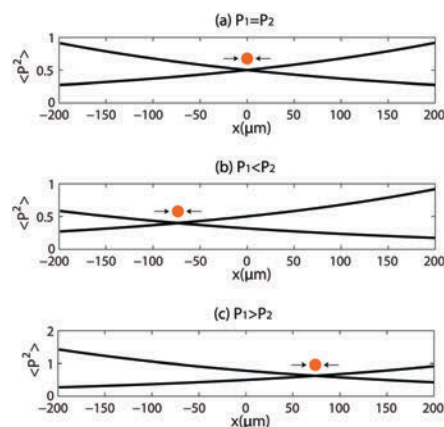

Fig. 3 Schematic diagram showing working mechanism of particle manipulation using amplitude modulation of DOTSAW: (a) equal power, (b) lower power from the left, (c) higher power from the left.

The adjustment of the relative amplitudes can cause the force minimum to move over a large spatial range, as shown in Fig. 4.

Here, the particle collection locations are plotted against the logarithmic power ratio, Γ, which is given as:

$$\Gamma = \log_e \left(\frac{P_a}{P_b} \right)^2 \qquad (8)$$

where the power input is equivalent to the square of pressure amplitude ratio. As shown in the plot, after the exclusion of
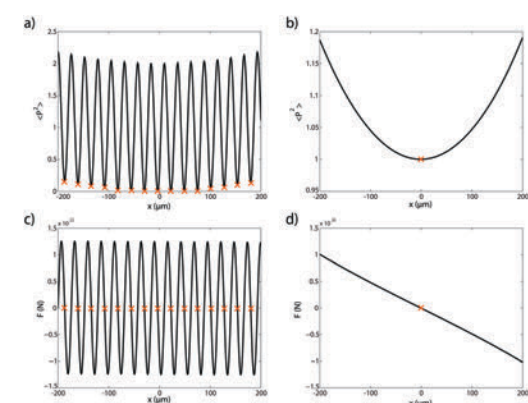

Fig. 2 Comparison of standing wave field and opposing travelling wave field. (a and b) Show the time averaged pressure squared field for SSAW and DOTSAW respectively. (c and d) Show the spatial variation of forces exerted on suspended particles. A zero net force and a negative slope in the force indicates the locations where the particles are collected. The orange cross represents the particle collection locations in each field.
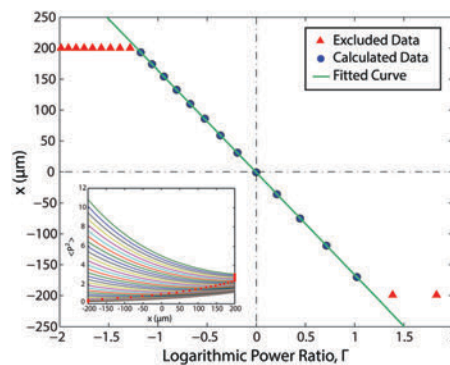
Fig. 4 Theoretical relationship for power ratio between the opposing IDTs pair and particle collection locations. The relationship is linearised by applying logarithm to the power ratio, denoted by the green line. Data are excluded from the curve fitting due to the limit of the size of the channel, which is shown by the red triangles. Inset shows the effect of different combination of power from both IDTs pair to the second-order pressure squared field. The red asterisk indicates the lowest point of the pressure field of each power combination, which represents the locations where particles are collected.

the data which is out of bounds, which occurs when the trapping location is outside the channel dimensions (red triangles), a linear relationship exists between x, the distance from the midpoint between the two IDTs to the trap, and the power ratio. This is shown to be related directly to the decay term, such that, for frequencies which differ only slightly:

$$x = -\frac{\Gamma}{4C_d}, \qquad (9)$$

Using this relationship, we can accurately control the particles position by changing the power ratio between the two opposing IDTs. The inset in Fig. 4 shows the source of the data in the main graph, of the time averaged pressure is shown for each amplitude combination, with the minimum denoted by a red asterisk, the actual powers used (for each power ratio) have been chosen such that each line can be clearly seen. The effect of coherence of the pressure sources on the particle trajectories is examined experimentally and illustrated in Fig. 5.

For coherent sources, where the SAW generated has constant phase difference and identical frequency, fluorescent particles exit the channel in an ordered manner along multiple routes separated by the same distance (Fig. 5a) as predicted in Fig. 2c. Note in Fig. 5a, we can only see the collection locations if a particle happens to enter the channel in the nearby vicinity, hence some force potential minima have no particle present.

In contrast, for the scenario of incoherent sources, particles are seen to be displaced towards a single location (the channel centre) from each side, that is by both incident travelling waves (Fig. 5b). The frequencies applied to each of the IDT sets is 76.2 MHz and 75.8 MHz respectively, while the input power is equal for both at 508 mW. In this case the behaviour matches that predicted in Fig. 2d.

Fig. 5c shows the S11 curve of the IDTs used in the experiment. The S11 parameter represents the reflection coefficient, which is measured using the signal generator in the network analyser mode. 76 MHz is chosen as the centre frequency as it has the lowest reflection coefficient. This frequency is used in the SSAW field. Two off peak frequencies of 75.8 MHz and 76.2 MHz are selected as the incoherent sources. These two frequencies has very similar S11 values, which makes it suitable to be used in the DOTSAW field as it does not have an inherent bias towards a particular IDT set.

A further analysis is performed on the trajectory of single particles experiencing the DOTSAW field. 4 particles of distinct starting location prior to the acoustic exposure region is investigated frame by frame. The trajectories of each particle is fitted using an exponential curve (Fig. 6a). The force field across the channel width (Fig. 6b) is then obtained from the viscous Stokes drag force, $F^{drag} = 6\pi\eta a v_p$, using the calculated velocity field from the fitted curve. The linear force field shows that the particles migrate towards the location of least acoustic pressure, which corroborates the theoretical force graph in Fig. 2d.

To show that the particle position can be manipulated, different power ratios were applied to the opposing IDTs pair. This was achieved by fixing the power input of the top IDTs set, while manipulating the bottom IDTs set's power input and the same procedure is repeated but with the connections to the IDTs reversed. One input power is fixed at 508 mW, whilst the other has a range from 508 mW to 1640 mW, with the interval of ~100 mW are investigated in the experiments. A stacked image (Fig. 7) shows a series of particle trajectories (dictated by various colours) affected by the power ratio. Each colour represents particle motions with different power ratios, with red, orange, yellow, green, blue, indigo and violet showing logarithmic power ratio of 2.22, 1.80, 0.36, 0, 0.67, 1.39 and 2.34 respectively. Note separate images were acquired for the trajectories arising from each power ratio, the colour of each image was then adjusted so that when stacked the difference in trajectory is clearly seen. This superimposed image successfully shows that the particles affected by the DOTSAW field can be focused and manipulated to any location *via* amplitude modulation. As such, tweezing, of all particles in the fluid, at controlled locations is achieved.
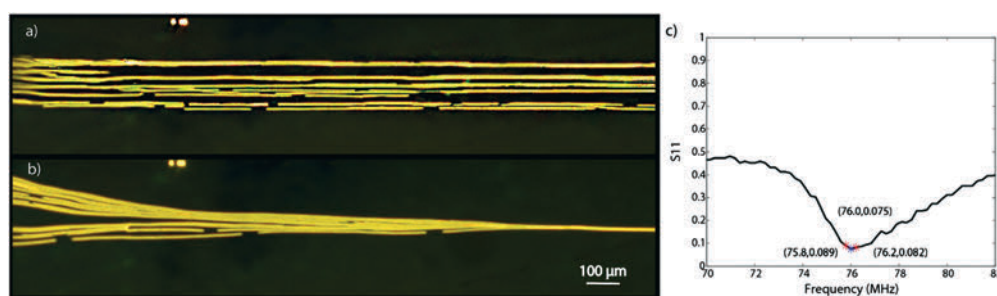
Fig. 5 Stacked images of particle trajectories from experiments. (a) SSAW field, with $f_1 = f_2 = 76$ MHz; where multiple equidistant particle trapping location can be seen. (b) DOTSAW field, with $f_1 = 75.8$ MHz and $f_2 = 76.2$ MHz; where particles are focused to the channel centre. The whole frame of the two images (a and b) takes place within the SAW actuation area. (c) Shows the S11 curve on the IDTs used in the experiments. Blue asterisk represent the centre frequency used in the SSAW field; whereas the red asterisks represent the two off-peak frequencies of 75.8 MHz and 76.2 MHz used in the DOTSAW field, which shows negligible difference in the reflection coefficient S11.

Fig. 6 Single particles analysis (a) particles trajectory (b) calculated radiation force with respect to the distance from the particles' end location. The 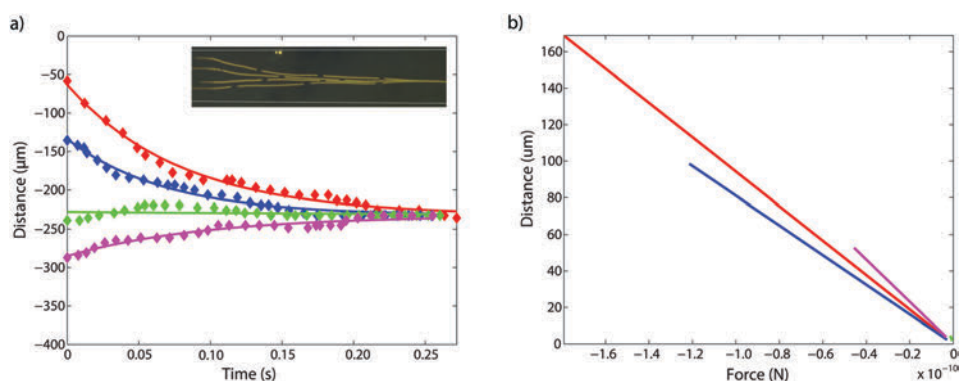power supplied to the top and bottom IDTs are 508 mW and 1040 mW respectively. Inset in (a) shows the stacked image of the particles trajectory.
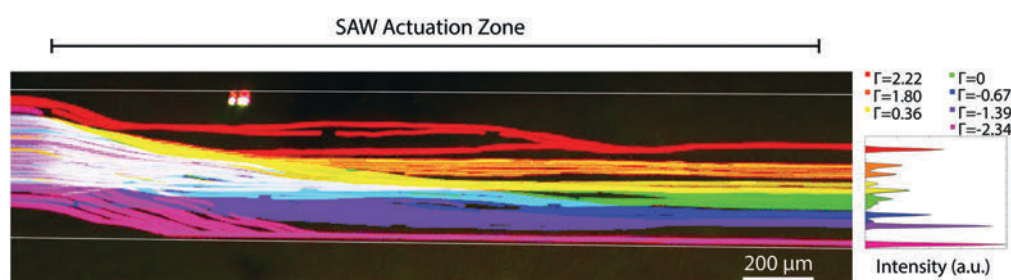

Fig. 7 The superimposed images of particles motions, with each colour being a separate experiment. The trajectories correspond to different power ratios (red: 2.22, orange: 1.80, yellow: 0.36, green: 0, blue: 0.67, indigo: 1.39, violet: 2.34). The channel walls are represented by the white horizontal lines. The flow is from left to right in the image frame, as such it can be seen that under different power ratios the particles leave SAW actuation zone at different lateral locations.

Video analysis is performed to quantify the particle collection data. Fig. 8 shows the relationship between the experimental logarithmic power ratio with the exit location of the particles as well as the theoretical variation of the particle position calculated. One can observe from the experiments that the particle exit location changes almost linearly as a function of logarithmic power ratio, and experimental data has good agreement with the theoretical prediction of the particle position. The experimental data can be fitted using a linear curve with gradient of R square value of 0.85. By comparing the theoretical and experimental curves, their respective equation of curves are $x_{theoretical} = -165\Gamma$ and $x_{experimental} = -163.9\Gamma$. The small discrepancies between the experimental and the theoretical data may be due to the inaccurate pressure amplitude when associated with the particle exit location in the experiments. One of the factors that can cause this is that the power input by the signal generator may not be the same as the power utilised by the IDTs, hence affecting the actual pressure field that determines the particle trapping location. Another reason for the disparities is due to the position of the fluid channel. If the microchannel is slightly off centred and become asymmetrical, there will be a difference in how much the wave amplitude attenuated in the
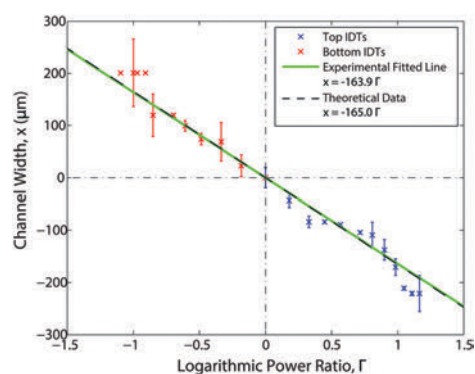

Fig. 8 Experimental particle collection location data as a function of logarithmic power ratio applied and the theoretical location calculated in Fig. 4.

77

PDMS layer before reaching the fluid channel, thus causing error in comparing the particle collection location from the same power input. This inaccuracy can be diminished by minimising the amplitude attenuation due to the lossy SAW transmission at LN PDMS interface using an air filled chamber to completely enclose the IDTs prior to the liquid channel.[62]

Nonetheless, the linear relationship offers accurate predic tion of the final position of the particle subjected to ampli tude modulation. As a result, the particles can be transported and positioned precisely at the locations required for analyti cal processes in lab on a chip systems.

It is important to note that the range of the lateral dis placement of particles affected by DOTSAW field is limited by the size of the channel or the space in between the IDTs pair, and the sensitivity of the system depends on the average power input to the IDTs.

Conclusions

Particle manipulation using amplitude modulation has been successfully demonstrated *via* the use of a novel pressure field that combines two opposing travelling waves without the formation of a standing wave component. This phenome non exploits the nature of superposition of incoherent decaying waves with different frequencies. Such pressure field utilised the tractability of the force potential well to al low dynamic control of particle position. The suspended par ticles are deflected from both sides of the channel that is af fected opposing travelling wave and are trapped at the stable pressure well location which is determined by the point where the energy from both waves are balanced. We demon strate this principle with the simultaneous position control of 5 μm radius particles using different power ratio. With the ability to manoeuvre particles with high sensitivity and range, we anticipate that this system can be implemented in a broad range of applications, such as cytometry, isolation of rare cells, cell focusing and patterning. In addition, it can be eas ily integrated into a miniature fluorescence activated cell sorting (μFACS) system by incorporating fluorescent detec tion and high speed electrical feedback modules.

Conflicts of interest

There are no conflicts to declare.

Acknowledgements

References

1 S. M. Block, L. S. B. Goldstein and B. J. Schnapp, *Nature*, 1990, **348**, 348 352.

2 J. E. Curtis, B. A. Koss and D. G. Grier, *Opt. Commun.*, 2002, **207**, 169 175.

3 M. D. Wang, H. Yin, R. Landick, J. Gelles and S. M. Block, *Biophys. J.*, 1997, **72**, 1335 1346.

4 F. J. Alenghat, B. Fabry, K. Y. Tsai, W. H. Goldmann and D. E. Ingber, *Biochem. Biophys. Res. Commun.*, 2000, **277**, 93 99.

5 B. G. Hosu, K. Jakab, P. Bánki, F. I. Tóth and G. Forgacs, *Rev. Sci. Instrum.*, 2003, **74**, 4158 4163.

6 A. Menachery, D. Graham, S. M. Messerli, R. Pethig and P. J. S. Smith, *IET Nanobiotechnol.*, 2011, **5**, 1 7.

7 T. Schnelle, T. Müller, R. Hagedorn, A. Voigt and G. Fuhr, *Shengwu Huaxue Yu Shengwu Wuli Xuebao*, 1999, **1428**, 99 105.

8 G. Destgeer and H. J. Sung, *Lab Chip*, 2015, **15**, 2722 2738.

9 J. Nam, H. Lim and S. Shin, *Korea Aust. Rheol. J.*, 2012, **23**, 255 267.

10 D. Bazou, R. Kearney, F. Mansergh, C. Bourdon, J. Farrar and M. Wride, *Ultrasound Med. Biol.*, 2011, **37**, 321 330.

11 C. Devendran, T. Albrecht, J. Brenker, T. Alan and A. Neild, *Lab Chip*, 2016, **16**, 3756 3766.

12 O. Manneberg, B. Vanherberghen, B. Onfelt and M. Wiklund, *Lab Chip*, 2009, **9**, 833 837.

13 H. Bruus, J. Dual, J. Hawkes, M. Hill, T. Laurell, J. Nilsson, S. Radel, S. Sadhal and M. Wiklund, *Lab Chip*, 2011, **11**, 3579 3580.

14 M. Gedge and M. Hill, *Lab Chip*, 2012, **12**, 2998 3007.

15 J. Hultström, O. Manneberg, K. Dopf, H. M. Hertz, H. Brismar and M. Wiklund, *Ultrasound Med. Biol.*, 2007, **33**, 145 151.

16 X. Xuan, J. Zhu and C. Church, *Microfluid. Nanofluid.*, 2010, **9**, 1 16.

17 J. Shi, S. Yazdi, S. C. Steven Lin, X. Ding, I. K. Chiang, K. Sharp and T. J. Huang, *Lab Chip*, 2011, **11**, 2319 2324.

18 J. G. Kralj, M. T. W. Lis, M. A. Schmidt and K. F. Jensen, *Anal. Chem.*, 2006, **78**, 5019 5025.

19 H. Lei, Y. Zhang and B. Li, *Opt. Express*, 2012, **20**, 1292 1300.

20 H. M. Davey and D. B. Kell, *Microbiol. Rev.*, 1996, **60**, 641 696.

21 A. Marzo, S. A. Seah, B. W. Drinkwater, D. R. Sahoo, B. Long and S. Subramanian, *Nat. Commun.*, 2015, **6**, 8661.

22 J. Shi, D. Ahmed, X. Mao, S. C. Lin, A. Lawit and T. J. Huang, *Lab Chip*, 2009, **9**, 2890 2895.

23 C. R. P. Courtney, C. E. M. Demore, H. Wu, A. Grinenko, P. D. Wilcox, S. Cochran and B. W. Drinkwater, *Appl. Phys. Lett.*, 2014, **104**, 154103.

24 A. Lenshof, M. Evander, T. Laurell and J. Nilsson, *Lab Chip*, 2012, **12**, 684 695.

25 S. V. Kothapalli, M. Wiklund, B. Janerot Sjoberg, G. Paradossi and D. Grishenkov, *Ultrasonics*, 2016, **70**, 275 283.

26 Z. Mao, Y. Xie, F. Guo, L. Ren, P. H. Huang, Y. Chen, J. Rufo, F. Costanzo and T. J. Huang, *Lab Chip*, 2016, **16**, 515 524.

27 F. Petersson, A. Nilsson, C. Holm, H. Jonsson and T. Laurell, *Lab Chip*, 2005, **5**, 20 22.

28 T. Laurell, F. Petersson and A. Nilsson, *Chem. Soc. Rev.*, 2007, **36**, 492 506.

29 B. W. Drinkwater, *Lab Chip*, 2016, **16**, 2360 2375.

30 M. S. Scholz, B. W. Drinkwater, T. M. Llewellyn Jones and R. S. Trask, *IEEE Trans. Ultrason. Ferroelectr. Freq. Control*, 2015, **62**, 1845 1855.

31 A. L. Bernassau, C. K. Ong, Y. Ma, P. G. A. Macpherson, C. R. P. Courtney, M. Riehle, B. W. Drinkwater and D. R. S. Cumming, *IEEE Trans. Ultrason. Ferroelectr. Freq. Control*, 2011, **58**, 2132 2138.

32 X. Ding, P. Li, S. C. Lin, Z. S. Stratton, N. Nama, F. Guo, D. Slotcavage, X. Mao, J. Shi, F. Costanzo and T. J. Huang, *Lab Chip*, 2013, **13**, 3626 3649.

33 L. Y. Yeo and J. R. Friend, *Annu. Rev. Fluid Mech.*, 2014, **46**, 379 406.

34 D. J. Collins, T. Alan and A. Neild, *Lab Chip*, 2014, **14**, 1595 1603.

35 C. Devendran, D. J. Collins, Y. Ai and A. Neild, *Phys. Rev. Lett.*, 2017, **118**, 154501.

36 G. Destgeer, K. H. Lee, J. H. Jung, A. Alazzam and H. J. Sung, *Lab Chip*, 2013, **13**, 4210 4216.

37 G. Destgeer, A. Alazzam and H. J. Sung, *J. Mech. Sci. Technol.*, 2016, **30**, 3945 3952.

38 G. Destgeer, B. H. Ha, J. H. Jung and H. J. Sung, *Lab Chip*, 2014, **14**, 4665 4672.

39 M. Sesen, T. Alan and A. Neild, *Lab Chip*, 2015, **15**, 3030 3038.

40 J. C. Brenker, D. J. Collins, H. Van Phan, T. Alan and A. Neild, *Lab Chip*, 2016, **16**, 1675 1683.

41 D. J. Collins, T. Alan, K. Helmerson and A. Neild, *Lab Chip*, 2013, **13**, 3225 3231.

42 J. W. Ng, D. J. Collins, C. Devendran, Y. Ai and A. Neild, *Microfluid. Nanofluid.*, 2016, **20**, 151.

43 A. Fakhfouri, C. Devendran, D. J. Collins, Y. Ai and A. Neild, *Lab Chip*, 2016, **16**, 3515 3523.

44 X. Ding, Z. Peng, S. C. S. Lin, M. Geri, S. Li, P. Li, Y. Chen, M. Dao, S. Suresh and T. J. Huang, *Proc. Natl. Acad. Sci. U. S. A.*, 2014, **111**, 12992 12997.

45 P. Li, Z. Mao, Z. Peng, L. Zhou, Y. Chen, P. H. Huang, C. I. Truica, J. J. Drabick, W. S. El Deiry, M. Dao, S. Suresh and T. J. Huang, *Proc. Natl. Acad. Sci. U. S. A.*, 2015, **112**, 4970 4975.

46 D. J. Collins, C. Devendran, Z. Ma, J. W. Ng, A. Neild and Y. Ai, *Sci. Adv.*, 2016, **2**.

47 D. J. Collins, B. Morahan, J. Garcia Bustos, C. Doerig, M. Plebanski and A. Neild, *Nat. Commun.*, 2015, **6**, 8686.

48 S. Oberti, A. Neild and J. Dual, *J. Acoust. Soc. Am.*, 2007, **121**, 778 785.

49 F. Gesellchen, A. L. Bernassau, T. Dejardin, D. R. Cumming and M. O. Riehle, *Lab Chip*, 2014, **14**, 2266 2275.

50 X. Ding, S. C. Lin, B. Kiraly, H. Yue, S. Li, I. K. Chiang, J. Shi, S. J. Benkovic and T. J. Huang, *Proc. Natl. Acad. Sci. U. S. A.*, 2012, **109**, 11105 11109.

51 A. Riaud, M. Baudoin, O. Bou Matar, L. Becerra and J. L. Thomas, *Phys. Rev. Appl.*, 2017, **7**, 024007.

52 F. Guo, Z. Mao, Y. Chen, Z. Xie, J. P. Lata, P. Li, L. Ren, J. Liu, J. Yang, M. Dao, S. Suresh and T. J. Huang, *Proc. Natl. Acad. Sci. U. S. A.*, 2016, **113**, 1522 1527.

53 X. Ding, S. C. Lin, M. I. Lapsley, S. Li, X. Guo, C. Y. Chan, I. K. Chiang, L. Wang, J. P. McCoy and T. J. Huang, *Lab Chip*, 2012, **12**, 4228 4231.

54 C. Devendran, N. R. Gunasekara, D. J. Collins and A. Neild, *RSC Adv.*, 2016, **6**, 5856 5864.

55 J. Friend and L. Y. Yeo, *Rev. Mod. Phys.*, 2011, **83**, 647 704.

56 L. Y. Yeo and J. R. Friend, *Biomicrofluidics*, 2009, **3**, 12002.

57 M. B. Dentry, L. Y. Yeo and J. R. Friend, *Phys. Rev. E: Stat., Nonlinear, Soft Matter Phys.*, 2014, **89**, 013203.

58 H. Bruus, *Lab Chip*, 2012, **12**, 1014 1021.

59 M. Settnes and H. Bruus, *Phys. Rev. E: Stat., Nonlinear, Soft Matter Phys.*, 2012, **85**, 016327.

60 L. Gorkov, *Dokl. Akad. Nauk SSSR*, 1961, **140**, 88 92.

61 G. Destgeer, B. H. Ha, J. Park, J. H. Jung, A. Alazzam and H. J. Sung, *Phys. Procedia*, 2015, **70**, 34 37.

62 D. J. Collins, A. Neild and Y. Ai, *Lab Chip*, 2016, **16**, 471 479.

79

Acoustic tweezing of particles using decaying opposing travelling surface acoustic waves (DOTSAW)

JIA WEI NG, CITSABEHSAN DEVENDRAN and ADRIAN NEILD
Laboratory for Micro Systems (LMS), Department of Mechanical and Aerospace
Engineering, Monash University, Clayton, Victoria 3800, Australia

*Corresponding author: Laboratory for Micro Systems, Department of Mechanical and Aerospace Engineering, Monash
University, Clayton, Victoria 3800, Australia.; E-mail: adrian.neild@monash.edu

1. Time averaging

When time averaging a function, care needs to be taken in the selection of a suitable time window. In acoustofluidics, typically a single frequency sound wave is used, the period of which is several orders of magnitude shorter than the time scale of particle motion. The effect of increasing the time frame of the time integral of $\cos^2 \omega_1 t$ is shown Fig. S1 (red line), as can be seen, at a timescale of such smaller than that of particle motion (tenths of a second) the value of this time average has settled to 0.5. When two frequencies are used the time required to settle at a fixed value is longer, in the case of the two frequencies used in our experiments, 76.2 and 75.8MHz, a settled value is obtained over a time frame of milliseconds (blue line). However, it is worth noting that when two frequencies are very close together (differing by 20Hz in Fig. S1, green line) the time required for the time average to settle can be larger than that of particle motion, in this scenario constant motion of the particle will occur.
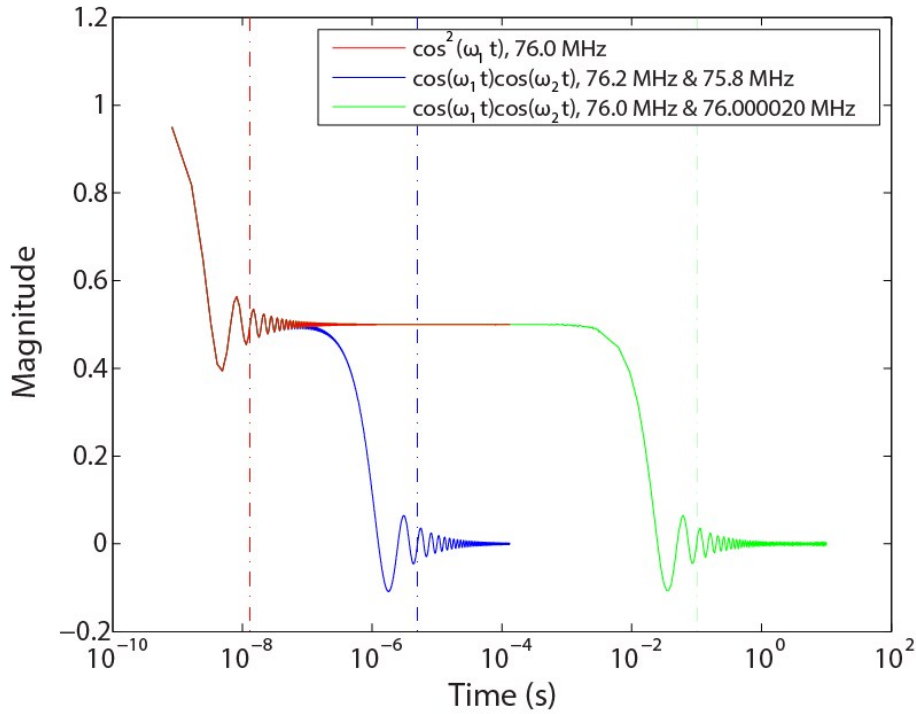
Fig. S1 This figure shows the value of the time averaged trigonometric functions $\cos^2 \omega_1 t$ and $\cos \omega_1 t \cos \omega_2 t$ with varying averaging period. For the term with same frequency $\cos^2 \omega_1 t$, the time averaged value with settles at 0.5, the vertical dotted line indicates the time period of the oscillation. As for the terms with different frequencies, $\cos \omega_1 t \cos \omega_2 t$, the time average values started with 0.5 but will eventually breakdown at a certain time averaging point depending on the difference in frequencies, and settles at zero. Here, the dotted lines show $T = \dfrac{2\pi}{\omega_1 - \omega_2}$. In our case (the one in blue), this time period T is small ($\sim 10^{-5}$ s) in comparison to the timescale of the net motion of the particles. We can safely assume that the trigonometric term will time average to zero. This assumption will breakdown when the two operational frequencies are very close together, as depicted by the green curve, where the time average value only settles at zero at around 1s.

*Corresponding author: Laboratory for Micro Systems, Department of Mechanical and Aerospace Engineering, Monash University, Clayton, Victoria 3800, Australia.; E-mail: adrian.neild@monash.edu

81

2. Parameters

Table S1 lists the parameters used in the simulations presented in this work.

Table S1 Parameters used in theoretical calculations

Water		
Density	ρ_0	997 kg m^{-3}
Speed of sound	c_0	1497 m s^{-1}
Compressibility	κ_0	448 TPa^{-1}
Lithium Niobate		
Speed of sound	ρ_{LN}	3994 m s^{-1}
Density	c_{LN}	4700 kg m^{-3}
Polystyrene		
Density	ρ_p	1050 kg m^{-3}
Speed of sound	c_p	2350 m s^{-1}
Poisson's ratio	σ_p	0.35
Compressibility	κ_p	249 TPa^{-1}
SAW actuation parameters		
SAW wavelength (at resonance)	λ_{SAW}	50 μm
Excitation frequency (top)	f_1	76.2 MHz
Excitation frequency (bottom)	f_2	75.8 MHz

*Corresponding author: Laboratory for Micro Systems, Department of Mechanical and Aerospace Engineering, Monash University, Clayton, Victoria 3800, Australia.; E-mail: adrian.neild@monash.edu

Chapter 5

Multiple Outcome Particle Sorting using Cascaded Surface Acoustic Wave (CSAW) Manipulation

5.1 Overview

Sorting cells by type in a sample is a key step in many life sciences processes. Fluorescent activated cell sorters, FACS, are ubiquitous, rapid and can sort based on many different markers simultaneously. FACS are extremely important especially in purifying specific cell population based on phenotypes. This is different from the acoustic sorting platform form Chapter 3, where the cell population are indiscriminately sorted based on size. To enable this, fluorescent tags are used, which bind to cells based on specific active sites, resulting in chemical specificity. Once the fluorescent marker response is determined using an optic sensor, the cell is individually deterministically sorted based on this response. This is usually achieved by using electrical deflection of the sample containing the cell in nebulised droplet form into one of multiple destinations. On-chip FACS sorters with similar high performance have been receiving significant research effort due to the ability to eliminate the contamination concern in conventional FACS system. As the optical detection technologies are well developed, the key challenge is an actuation method capable of a rapid and multichannel response. Surface acoustic waves (SAW) offer an effective way of generating a sound field which is capable of exerting forces on suspended particles and cells.

When SAW has been used for FACS, it has either been by use of TSAW, from a single electrode set, or has used SSAW to nudge the particle into a new trajectory. Here in this work, we use multiple pairs of electrode sets, that are offset laterally, to produce independent sound fields in close proximity. Different combinations of actuation of electrode pairs produce pressure field of different shape. This cascaded surface acoustic wave (CSAW) manipulation scheme dictates the particle trajectories. The

reconfigurability of this system is what allows the multiple sorting outcomes. Experimentally, 5 μm radius particles are sorted into four distinct outlets on a single microfluidic chip using different actuation permutation of electrodes.

5.2 Publication

This article is currently in review with *Lab on a Chip*. The article included here is formatted using the template from The Royal Society of Chemistry.

ARTICLE

Multiple Outcome Particle Sorting using Cascaded Surface Acoustic Wave (CSAW) Manipulation

Jia Wei Ng,[a] and Adrian Neild [a]

On-chip flourescent activates cell sorting (FACS) requires the optical indentification of a cell s type followed by the selective displacement of that particle from the incoming streamline, the number of displacement choices available dictate the number of different sort outcomes which are obtained. Surface acoustic waves (SAW) offer an effective way of generating a sound field which is capable of exerting forces on suspended particles and cells. The SAW couples into the fluid contained within a microfluidic channel. A single SAW source can cause a travelling wave which pushes particles in the direction of propagation, whilst a pair of sources can give rise to a standing wave which moves particles to pressure nodes. By pulsing the SAW field on, both approaches have been used to displace selected particles, either by pushing particles to the channel wall furthest along the propagation direction, or moving them to the nearest pressure node. However, this work shows that multiple outcomes can be obtained by successive source pairs, each spatially offset from each other, the result is a cascaded manipulation yielding, in this demonstration, four possible outcomes.

Introduction

Cell and particle sorting is essential for many biological studies and clinical medical applications.[1-7] A widespread method is fluorescence-activated cell sorting (FACS), in which different subsets of cells in a heterogenous cell population are selectively marked using fluorescent tags. Each cell is then individually carried by a fluid flow through an optical sensor. Based on the optical response, the cell type can be determined because of the specificity of each fluorescent tag. The selected cells are encapsulated in small liquid droplets, electrically charged and deflected into one of multiple receptacles using large electrical fields based on the knowledge gained optically.[8] Commercial FACS systems are used to sort multiple cell types at high rates, but they are typically expensive and require large sample sizes. They also risk sample contamination and biosafety issues attributed to the final step.[9]

There is increasing interest in miniaturisation of the process onto a microfluidic chip, as that would allow minimal sample size and not require the generation of a charged, cell-encapsulating sprays of droplets. Furthermore, the on-chip sorting system can be integrated with other multiple inexpensive on-chip capabilities, acting as the first stage of a more complex automated workflow.[10, 11]

The confined nature of microfluidic system, which minimises contamination, also restricts the interaction with the suspended cells. So, in order to guide cells, in the case of on-chip FACS this would be after optical identification, a range of microscale actuation systems have been developed. These externally applied force fields can be generated through magnetic, electric and acoustics approaches.[12-16] Of these, acoustic fields appear to be an excellent method for cell sorting as they are applicable to all suspended matter and are widely considered biocompatible,[17-23] especially if that actuation is restricted in duration and power.[24]

Acoustic-based manipulation methods can be split into two general types: bulk acoustic waves (BAW)[25-29] and surface acoustic waves (SAW)[30-32]. The former is generated by a bulk wave mode transducer adhered to a fluid containing resonant chamber. The latter, SAW, uses a spatially periodic interdigitated transducers (IDTs) to create a resonant condition on a piezoelectric substrate. In the case of BAW, by choosing a suitable excitation frequency a resonant standing wave can be formed, this pushes suspended particles[33-37] or droplets[29] to either the pressure nodal or antinodal planes.[38] However, the options for pressure field design are limited to the resonant modes of the fluid volume. SAW has gained popularity in the field of acoustofluidics as it is easy to integrate with microfluidic systems, and offers a far broader range of acoustic fields. These fields can yield forces which push or capture particles, as well as strong fluid flows (acoustic streaming) which occur both within the aperture of the IDTs and at the periphery of them.[39]

SAW systems can be broadly classified as either travelling SAWs (TSAWs) or standing SAWs (SSAWs), though hybrid fields can also exist.[40] The former, TSAW, is a wave generated by a single

set of IDTs, which propagates through the system; the latter, SSAW, are formed by two coherent counter propagating waves, formed from two opposite sets of IDTs. Travelling waves are usually used to push particles,[41, 42] droplets[43, 44] or fluid interfaces[45] away from the source.[9, 41, 46-48] Whilst SSAW creates standing wave traps, which hold particles[23, 49] or droplets[50, 51] in multiple stable locations.

To use such forcing mechanisms to sort particles there are two main approaches. One uses continuous actuation, the other pulsed actuation. The former has been used to sort cells by size[47, 48, 52-55] and stiffness[41, 42, 56-58] by designing a system in which those parameters dictate the final trajectory of a cell through the force field. However, for on-chip FACS, it is pulsed methods which are pertinent; once the type of cell is determined using optical detection of the fluorescent tag, a decision is made on whether the acoustic field should be pulsed on or remain off. This yields a binary outcome, capable of sorting two cell types[9, 44, 59-61], a process which can be sped up through using highly focussed IDTs or constricted channels[9, 46].

There have been very few efforts to surpass the possibility of a binary outcome. One recent work uses standing SAW generated by electrodes that vary in pitch spatially. Here, droplets are pushed to different outlet channels depending on the frequency of excitation.[51] The downside is that such chirped electrode are less efficient, and so more capable of moving droplets than cells, than single frequency designs, which better match the impedance of the driving amplifier accurately.

Whilst a wide range of SAW excitation methods have been explored, the use multiple electrode sets to produce independent sound fields in close proximity is very rare. Here, we examine the use of several pairs of single frequency electrodes to create a cascaded surface acoustic wave (CSAW) manipulation scheme.

Each pair of electrodes are laterally displaced from each other along the length of the channel. We show that, despite their proximity, they behave independently. With, for example, little effect of the acoustic streaming field generated at the edge of one electrode set on the behaviour of particles in the next set. In addition, they are also aligned such that they create pressure nodes which are slightly offset across the width of the channel, we demonstrate how this offset of the electrodes is highly accurately reproduced in the sound field. We show that this results in the capability of using different combinations of actuation of electrode pairs to dictate multiple particle trajectories. Such multiple trajectory control has the potential for combination with optical detection for multi-cell line on-chip FACS sorting, in which post-detection, a cells trajectory is dictated by the combination of electrodes pairs which are pulsed on for the duration of the passage of the cells passed the electrodes, surpassing the standard binary set of outcomes.
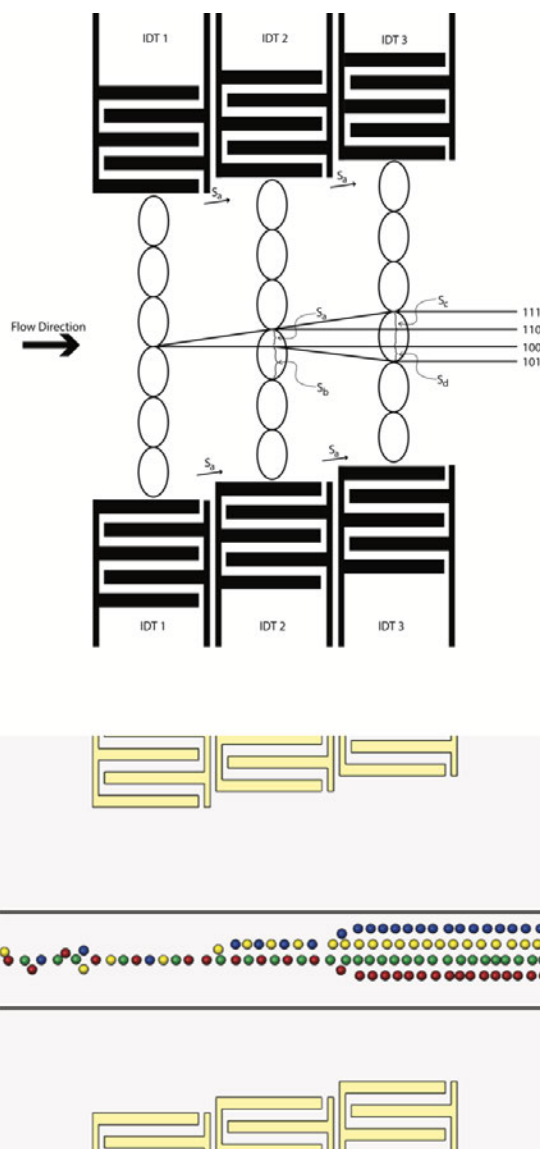
Figure 1 Schematic diagram showing working mechanism of the particle outcome manipulation using binary actuation combination of Cascade SAW device. Each colour refers to the path taken by a single particle, governed by the imposed force fields. The first set of IDTs are used to locate the particles in the first node, while the second and third sets of IDTs are the sorting IDTs that is used to create a cascaded surface acoustic wave response (CSAW).

System description

The acoustic radiation force (F^{rad}) is responsible for the sorting of suspended particles in standing wave field, with the equation given by:[38]

$$F^{rad} = -\left(\frac{\pi p_0{}^2 V_c \beta_w}{2\lambda}\right).\phi(\beta,\phi).\sin(2kx) \qquad (1)$$

$$\phi(\beta,\phi) = \frac{5\rho_c - 2\rho_w}{2\rho_c + \rho_w} - \frac{\beta_c}{\beta_w} \qquad (2)$$

where p_0 is the acoustic pressure amplitude and V_c is the particle volume. The wavenumber, k, is defined by $2\pi/\lambda$ and x is the distance from a pressure node. The acoustic contrast factor, ϕ, depends on the particle density and compressibility (ρ_c, β_c) in relation to the corresponding properties of the surrounding fluid (ρ_w, β_w). The sign of an acoustic contrast factor determines the direction of the acoustic force acting on the particle or cell, and thus influencing whether the particle or cell will move the standing wave pressure node or the antinode. Most solid particles in an aqueous media have a positive ϕ-factor and are translated to a pressure node. For such particles, the force at the antinode is also zero, but this is an unstable minima.

However, in our system we do not use a single sound field, but have the option of multiple independent fields. Equation 1 is for a perfect standing wave, with pressure field which consists of a sinusoidal spatial fluctuation along one-dimension. Such a field is generated using bulk acoustic wave actuators, as it is one of the resonant modes which can be excited within the fluid.[62] To give us more freedom in the design of the field, we instead use surface acoustic wave excitation. In this case the sound field is more complex, having a variation in three dimensions, however, across a plane parallel to the substrate a predominately one-dimensional field will exist, and the results section will confirm that the principles discussed here apply to our more complex systems, for the particle size used.

We use the freedom that surface acoustic wave actuation offers to assume that spatially offsetting one pair of IDTs from another will create a sound field which is sufficiently accurately defined that the nodes are also spatially offset. Again, this assumption will be tested experimentally. First, however, we examine the role of the size of this offset.

To accurately bump the particle from the node of one sound field to the node of the next, a distance bias is required between the particle location in the first field and the pressure node (PN) location in the second. In order to create this bias, we have to design the offset that satisfy the following conditions:

$$s_p = s_a + s_b = s_c + s_d = \frac{\lambda_{SAW}}{2} \qquad (3)$$

$$s_c = 2s_a \qquad (4)$$

$$s_d = s_b - s_a \qquad (5)$$

$$s_a < s_b \qquad (6)$$

$$s_d < s_c \qquad (7)$$

$$\frac{\lambda_{SAW}}{8} < s_a < \frac{\lambda_{SAW}}{4} \qquad (8)$$

where, as shown in Figure 1, s_a is the offset distance; s_p is the internodal distance, which is half a SAW wavelength. Since we want the nodal shift to be kept constant, s_c is twice the length of the pressure nodes offset. To ensure the downward deflection of particles (in terms of the image plane) every second electrode, provided the previous electrode is not actuated, the bottom pressure node has to be closer to the initial position compared to the top pressure node, which gives the condition that s_d has to be greater than s_c. By solving the inequalities, the offset is found to be between $\lambda_{SAW}/8$ and $\lambda_{SAW}/4$.

By selective actuation of multiple pairs of electrodes, various particle trajectory outcomes can be obtained, each one pertaining to the permutations of on and off cases applied to each IDT pair. To maximise the number of possible outcomes with minimal number of sorting IDTs, the golden ratio is used as an inspiration for the design as it is considered the most irrational number.[63] This is to ensure that the periodicity of the pressure nodes and the constant nodal offset does not contribute to a repetition of possible particle manipulation outcome. For this cascaded pressure field, the region or

Table 1 Table listing the possible location outcomes corresponds to the number of Sorting IDTs. The zeroth IDT pair is used to centre particles before they enter the sorting IDTs.

Number of Sorting IDTs	0	1	2	3	4
Number of Possible Location Outcome	1	2	4	6	9
Possible Location Outcomes	0	0	0	0	0
		s_a	s_a	s_a	s_a
			$2s_a$	$2s_a$	$2s_a$
			$2s_a - s_p$	$2s_a - s_p$	$2s_a - s_p$
				$3s_a$	$3s_a$
				$3s_a - s_p$	$3s_a - s_p$
					$4s_a$
					$4s_a - s_p$
					$4s_a - 2s_p$
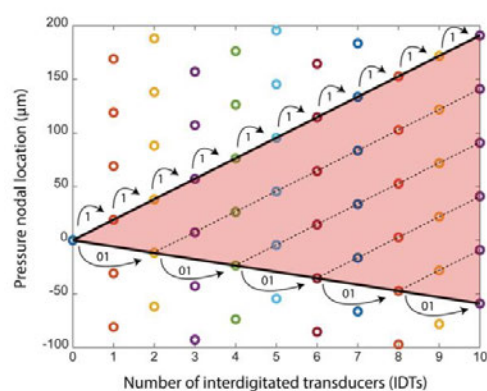
Figure 2 Graph showing the relationship between the number of sorting IDTs and the particle outcome location. The highlighted pink triangle is all the available particle outcome correspond to the number of IDTs. The larger the number of IDTs, the larger the triangle encapsulating the particle outcome. To travel upwards from the adjacent pressure node location, the subsequent IDT can be turned on (1); to travel downwards, the binary combination of (01) can be applied to the next two IDTs. By controlling the movement direction of the particles, the particle outcome location can be determined. In the depiction it is assumed that each new additional IDT added is activated, hence for two IDTs only the combination of actuation 11, 01 is shown, in addition the possibility 10 and 00 is possible, these relate to the locations already described for 0 IDTs and 1 IDT, hence what is depicted for 2 IDTs are the additional locations which adding a second IDT pair offers.

boundaries that the particles are affected depending on the number of sorting IDTs pair is portrayed in Figure 2. The highlighted triangle, containing all the pressure nodes, showing the unique possible outcomes. Table 1 also tabulate the possible pressure nodes location at electrode that are active with the number of electrodes. As with Figure 2, this table shows the additional set of locations which is added by the use of each additional IDT pair, so the total number of outcomes for n IDTs is a summation of those afforded by the use of 0 to n IDTs. In Figure 1, the first IDT is used for alignment, the following two are sorting IDTS, and hence four possible outcomes are depicted.

The relationship between the numbers of sorting IDTs set to the number of outcomes is shown with the following equation:

$$Outcome(n) = \sum_{i=0}^{i=n} \left(\frac{3 + 2i + (-1)^i}{4} \right) \qquad (9)$$

where n is the number of sorting electrodes. To accurately sort particles to any one of the outcomes, we can use different actuation combination of the electrodes. A single particle sorting outcome may have more than a single combination of activated IDTs; however, the most straightforward combination can be found by looking at Figure 2 and Table 1. From Figure 2, we can see within the triangle, there are lines slanted upwards and a line pointing downward. For the top boundaries of the triangle, by switching on every adjacent IDTs, the particles are shifted upwards with the offset distance, s_a. By switching on every alternate IDTs, with the binary combination (01), the particles can shift downwards. The sorting outcome lies on the lines within the triangle, this also represents the simplest trajectory and actuation combination of the IDTs.

In our experiment, only two pairs of sorting IDTs are actuated to create the cascaded SAW, while a pair of IDTs are actuated prior to the sorting region to set the initial location of the particles on the first node. In order to simplify the design while producing the same results (having four distinct outcomes), we turn to the Fibonacci sequence [0,1,1,2,3,5, …] that closely related to the golden ratio. The 3rd and 4th number from the sequence is selected as the ratio (2:1) to form the offset distance of $\lambda_{SAW}/6$, while still satisfying the offset distance criteria. This allows the particles to be 1 part closer to the desired pressure node and two parts away from the subsequent pressure node.

Methods

Device Fabrication

The piezoelectric substrate is made from 128° Y-cut lithium niobate (LN), chosen for its optical transparency and excellent electrical-mechanical coupling efficiency. The IDTs are composed of a 10 nm thick chromium (Cr) adhesive layer, and a 200 nm thick aluminium (Al) conductive layer on top of that. A 200 nm thick layer of silicon dioxide (SiO_2) is further coated on the substrate to insulate the IDTs from corrosion and to
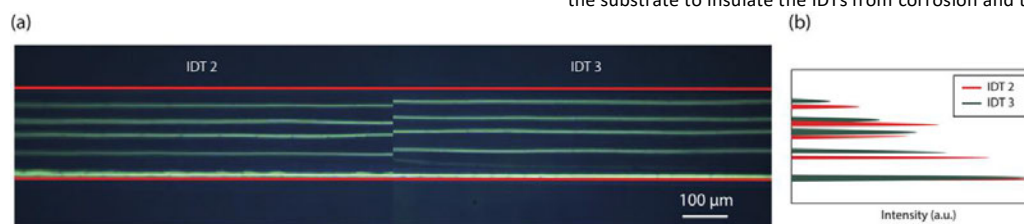
Figure 3 (a) Stacked Image of particles motion without sheath flow. Particle lines up with the nodal lines when exposed to the acoustic field. **(b)** The nodal lines in the later actuation zone is offset by $\lambda_{SAW}/6$ from the previous actuation region.
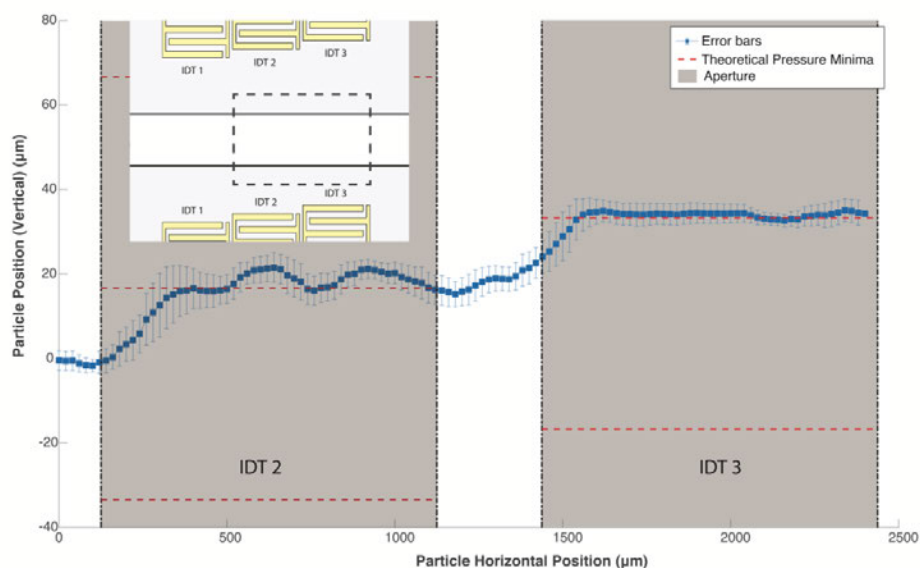
Figure 4 shows the trajectory of the particles under IDT2 and IDT3 when the all the IDTs are being actuated. This plot shows that the particles can be accurately manipulated without noticeable effect by the acoustic streaming on the edge of IDTs where they are usually the strongest. The red dotted line represents the acoustic pressure minima where the particles may be collected, while the grey zones represent the apertures for the IDTs. The error bar is calculated with 2 standard deviation and a pooled standard deviation shows that the spread of the data along the trajectory is only 3.48 µm. The top left insert highlights the location particles where the trajectory data is investigated.

promote channel bonding to the substrate. Each IDTs has the same pitch of 100 µm, producing a working frequency of 40 MHz, and an aperture of 1000 µm. Two identical IDTs are separated by a distance of 12.5 λ (1250 µm) apart to form an opposing IDTs set; and by patterning three of this opposing sets on the LN substrate forms the sorting system. These opposing IDTs set are shifted up $\lambda_{SAW}/6$ from one another.

The microfluidic channel is made up of polymethylsiloxane (PDMS) (SYLGARD© 184, Dow Corning, 1:10 ratio of curing agent/ polymer) and is fabricated by soft lithography replica moulding. An air-filled chamber encloses the IDTs to limit leakage of acoustic energy into the PDMS superstructure, and so maximise acoustic energy transmitting into the liquid in the channel. The fluid chamber of 200 µm width and 25 µm height is then exposed to an air plasma and bonded to the LN substrate.

Experimental Procedure

The device is held under a microscope (Olympus BX43) using a 3D printed frame where spring loaded contact pins make contact with the electrode pads on the LN substrate. The experiments are recoded using a microscope mounted camera (PixieLink PL-B872CU, Ottawa, Canada). The electrical signal is provided by a combined signal generator and amplifier

(PowerSAW Belektronig F20). This generator is also a network analyser, capable of assessing the S11 values, a measure of input port voltage reflection coefficient. This can show the efficiency of the examined IDTs and about how much power is transmitted into the LN to generate SAW.

A solution of fluorescent polystyrene particles with diameters of 5 µm, was injected into the microfluidic channel by syringe pumps (KD Scientific Legato 210). They are hydrodynamically focused to the centre of the main channel by two side sheath flows before entering the IDTs actuation region. The first IDT pair is then used to refine that alignment prior to the other two pairs being used to dictate the final trajectory. The flow rates of the sample flow and the sheath flow were 5 ul/min and 2 µl/min respectively. The buffer solution consists of deionised water (Milli-Q 18.2 MΩcm, Millipore) with 2% w/w polyethylene glycol (PEG) to prevent particle/ particle or particle/ wall adhesion.

Results and discussion

The functionality of the trajectory control requires that the spatial offset of each IDT pair is accurately replicated in the sound field and so the position of the particles as they travel along the channel. To test this, two of the offset sorting IDTs
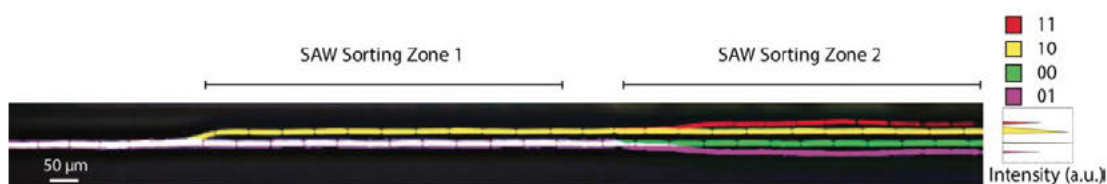
Figure 5 Superimposed images of the motion of a small number of particles, with each colour being a different experiment. The trajectories the particles changes with different actuation scheme (Red: 11, Yellow: 10, Green: 00, Violet: 01). The fluid flow is from left to right in the image frame. The initial position of the particles is fixed by using hydrodynamic focusing and acoustic focusing by the first IDT set. The intensity plot across the width of the channel gives a good representation of the accuracy and repeatability of this positioning over a larger number of particles.

(IDT 2, IDT 3) are actuated (sequentially) without any sheath flow. Particles are collected in the pressure nodes in the SAW working region. In the Figure 3a, the set of nodal lines are shifted between the two IDTs . This bodes well for the creation of a cascaded response. The images are produced by video stacking of the continuous flow system.

Using image analysis in MATLAB, the quantitative data about the manipulation distance of the particles is acquired by profiling the fluorescence intensity of the particles at the end of each IDT actuation region. The shift in the nodal lines is found to be ~17 μm, which is comparable to the shift in the offset sorting IDTs (16.7 μm), as seen in Figure 3b.

In the concept of this system, we have assumed that the field shift matches the IDT pair offset. But we have also assumed that streaming does not affect the system, rather that acoustic radiation force dominates to the extent that the particles are highly accurately located (at least for particles of a size similar to that of cells – 5 μm are used here). We have seen that the average location of the particles is offset to within a micrometer of the IDT pair offset. The data (Figure 4) also shows us that the spread of the location of the particles along the trajectory is just 3.48μm, under the diameter of the particle, calculated using the pooled standard deviation. However, the expectation is that the strongest streaming will occur at the periphery of the IDT aperture, both the data in Figure 4 and the straight lines seen in Fig 3 suggest this is not an issue, indeed the largest deviation observed in Fig 4 is in the centre of the IDTs. Furthermore, we observe the particle behaviour of the final IDT set is now worse, rather better, than in IDT 2, suggesting the addition of further IDTs would not see an increase in error.

To show that particle outcome can be manipulated, different actuation combinations were applied to the sorting IDTs. This was achieved by first fixing the initial position of the particles before the cascade sorting region via focusing the particle with the help of hydrodynamic sheath flow and the first IDTs set. The sheath flow puts the particle in one nodal range and the first IDTs set focuses the particle more accurately. Another way of setting the particle's initial position precisely would be to use DOTSAW, a new type of field that holds particles in a single location which is easily controlled via relative amplitude modulation.[64] Next, the remaining two sorting IDTs sets were

actuated with different binary combination, and the trajectories imaged.

A stacked image (Fig. 5) shows a series of particle trajectories (indicated by various colours) affected by the actuation combination. Each colour represents particle motions with different actuation combination, with red, yellow, green and violet showing binary actuation combination of 11, 10, 00, 01 respectively. Note separate images were acquired for the trajectories arising from each actuation combination, the colour of each image was then adjusted so that when stacked the difference in trajectory is clearly seen. This superimposed image successfully shows that the particles can be manipulated to any location when exposed to the cascaded SAW field via different actuation combination. The intensity plot shows the accuracy which can be obtained in this positioning over a larger number of particles (approx. 400).

Particle collection data is acquired by performing video analysis. Figure 6 shows the relationship between actuation combination and the particle outcome as well as the theoretical particle position, excellent agreement is seen, with the particles positioned to an accuracy range smaller than their own diameter.
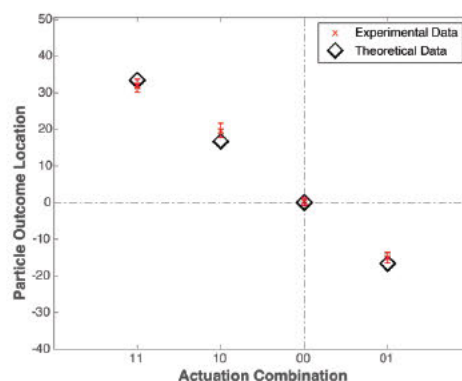
Figure 6 Experimental and theoretical particle outcome location as a function of actuation combination.
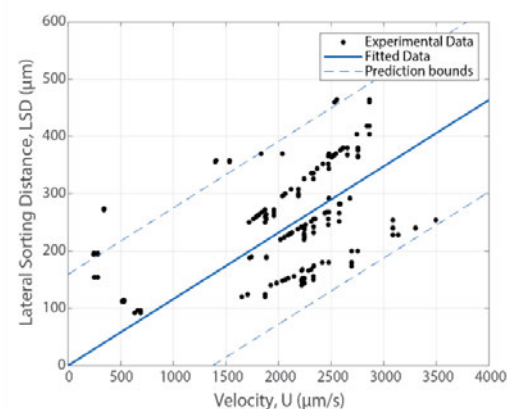
Figure 7 shows the relationship between the distance the particle travels along the channel whilst displacing laterally across the channel, with the particle velocity.

Having established the accuracy that can be obtained, we now examine what parameters effect the speed of displacement. Each set of IDTs is independently actuated, so could be handling different particle simultaneously. As such, we examine the time taken to move a particle to its final position in a single IDT pair. Figure 7 shows the distance travelled along the channel before a particle has moved to its desired lateral location, this is plotted as a function of the velocity the particle is travelling along the channel, the data is built up over several experiments with different flow rates. It is worth noting that the cluster of data points is related to low temporal resolution. It can be seen, that a line can be fitted to the data. The slope of this fitted line shows that the time taken to reach the final location is 0.11 s. However, the IDT can only be repurposed to sort the next particle once the initial particle has exited the aperture. To achieve this, the ideal flow rate is chosen such that by the time the lateral displacement is complete, a distance of 1 mm, the size of the aperture, has been covered. For these operating conditions this would be 9 mm/s.

The sort time could be reduced by increasing the acoustic radiation force, the power used here, 232 mW, is significantly lower than in many works, especially those using pulsed actuation, and the acoustic radiation force will scale linearly with applied power. Hence the sorting time will be inversely proportional to the applied power. To harness this benefit the flow speed would need to be adjusted such that the lateral displacement takes place across the full aperture of the IDT. In addition, it could also be possible to reduce the distance that needs to be traversed, this has been shown as highly effective for systems with binary outputs using travelling acoustic waves. In which the distance is subsequently magnified by a channel expansion. Here the mode of operation would require a higher frequency of operation, noting that frequencies with resulting wavelengths in the order of three particle diameters have been shown to be capable of accurate particle positioning.[23]

Conclusions

In conclusion, we have successfully demonstrated a tuneable sorting method that is SSAW using a novel cascade pressure field. Our device is able to sort 5 μm radius particles into four distinct outlets on a single microfluidic chip using different actuation combination. We show that the acoustic field generated by each pair of IDTs can accurately move particles with the same offset as the physical location of the IDTs, and that streaming at the periphery of each IDT is not detrimental to this. Depending on the application, we show how the number of possible sorting outcome is dictated by the number of independent IDT sets. Finally, we examine the speed of collection and identify how this can be further improved now that the principle of operation has been demonstrated. With the ability to control the trajectory simply by switching on the appropriate IDTs set, we anticipate that it can be easily integrated into a miniature fluorescence-activated cell sorting (μFACS) system.

Conflicts of interest

There are no conflicts to declare.

Acknowledgements

References

1.   C. Alix-Panabières and K. Pantel, 2014, **14**, 57-62.
2.   N. S. Barteneva, K. Ketman, E. Fasler-Kan, D. Potashnikova and I. A. Vorobjev, *Biochimica et Biophysica Acta (BBA) - Reviews on Cancer*, 2013, **1836**, 105-122.
3.   E. Fung, P. Sugianto, J. Hsu, R. Damoiseaux, T. Ganz and E. Nemeth, *Molecular Pharmacology*, 2013, **83**, 681-690.
4.   W. Qi, C. Zhao, L. Zhao, N. Liu, X. Li, W. Yu and L. Wei, 2014, **14**, 3.
5.   T. Segers and M. Versluis, 2014, **14**, 1705.
6.   B. L. Wang, A. Ghaderi, H. Zhou, J. Agresti, D. A. Weitz, G. R. Fink and G. Stephanopoulos, *Nature Biotechnology*, 2014, **32**, 473-478.
7.   M. Eisenstein, *Nature*, 2006, **441**, 1179-1179.
8.   W. A. Bonner, H. R. Hulett, R. G. Sweet and L. A. Herzenberg, *Review of Scientific Instruments*, 1972, **43**, 404-409.
9.   Z. Ma, Y. Zhou, D. J. Collins and Y. Ai, *Lab on a Chip*, 2017, **17**, 3176-3185.
10.   A. Y. Fu, C. Spence, A. Scherer, F. H. Arnold and S. R. Quake, *Nature Biotechnology*, 1999, **17**, 1109-1111.
11.   P. Li, Z. Mao, Z. Peng, L. Zhou, Y. Chen, P.-H. Huang, C. I. Truica, J. J. Drabick, W. S. El-Deiry, M. Dao, S. Suresh and T. J. Huang, *Proceedings of the National Academy of Sciences*, 2015, **112**, 4970-4975.

Chapter 6

Conclusion and Future Work

This chapter will discuss the conclusions of the work presented in this thesis. This will be followed by detailed discussion of the research outcomes. To conclude, recommendations of future work are presented.

6.1　Conclusions

The thesis described the use of three novel SAW fields to achieve on-chip particle/ cell manipulation techniques. These new types of sound field with unique properties and capabilities, offer enhanced flexible and tuneable, particle manipulation functionalities, so that almost any specific study could be performed with ease. In the following paragraphs, the primary contributions of this thesis are summarised.

The first innovative SAW field, as discussed in Chapter 3, combines the favourable properties of a standing wave and travelling wave in a microfluidic system. This acoustic field arises from the superposition of two highly attenuated SAW traveling in opposite direction. This enables the sorting of particles that is size deterministic. The behaviour of particles of varying size in this hybrid field are predicted using finite element analysis in COMSOL Multiphysics. The particles in the travelling wave-dominant region are deflected and sorted based on size and are subsequently trapped at stable pressure node locations, resulting in distinct exit locations that is flow rate independent. Finally, this principle is demonstrated experimentally, and continuous sorting of 5.1 μm, 6.1 μm and 7.0 μm particles is achieved.

The second new sound field is introduced in Chapter 4. This SAW field does not possess the properties of a conventional travelling wave, where the particles are pushed away from the source; or a standing wave that gathers the particles in a periodic pattern. Instead, this unique acoustic field has a single trapping site, which the location can be easily controlled. This phenomenon arises from the superposition of opposing incoherent

waves and the amplitude modulation of the waves. MATLAB has been used to describe the behaviour of the particles numerically in this novel pressure field. Experimentally, simultaneous position control of 5 μm radius particle with an accuracy of is shown with ± 10 μm.

Chapter 6 explored the use of a novel and combinatorial acoustic field in manipulation of particles. Multiple pair of electrode sets are placed in close proximity to generate independent sound fields. The sound fields have pressure nodes that are spatially offset from each other. Multiple particle trajectories can be produced by selecting the appropriate sound field combination. In the experiments, sorting of 5 μm particles in to four distinct outlets on a single microfluidic chip using different electrode actuation combination.

6.2   Future Work

In Chapter 3, it is demonstrated that particles can be sorted based on size by using TSAW and SSAW hybrid field. The ability to sort multiple particle population in a way that is insensitive to flow rate and deterministic is useful for a wide range of applications, especially in systems where flow rates cannot be controlled precisely. Further work can be exploring the use of passive pumping mechanism in this hybrid field, eliminating the use of bulky equipment (syringe pumps) that usually accompanies SAW microfluidic methods.

As discussed in Chapter 4, 1D trajectory control serves as a precursor towards developing a 2D acoustic tweezing system. Thus, this work will be further developed by introducing 2 extra orthogonal transducers. Additionally, the uses of this general platform, where a 2D acoustic field is generated by opposing sets of IDTs, has not been fully explored. This reconfigurability of this 2D acoustic tweezing can then be used in application such as tissue engineering and 3D printing.

Using the SAW manipulation mechanisms described in Chapters 4 and 5, further work can include the integration into a miniature fluorescence-activated cell sorting

(μFACS) system. This can be achieved by incorporating fluorescent detection and high-speed electrical feedback modules. Possible work also includes applying the manipulation methods discussed in Chapters 3, 4, and 5 for biological applications. For example, simultaneous sorting of red blood cells, white blood cells, platelets and plasma is very important in the subsequent blood component analysis.

Appendix A

Conference paper

The conference paper 'FLOW-RATE INSENSITIVE DETERMINISTIC PARTICLE SORTING USING A COMBINATION OF TRAVELLING AND STANDING SURFACE ACOUSTIC WAVES' was presented at the 20th International Conference on Miniaturized Systems for Chemistry and Life Sciences ("µTAS") in Dublin, Ireland on October 9-13, 2016. This paper, largely simplifying the material in Chapter 3, is presented on the following page.

FLOW-RATE INSENSITIVE DETERMINISTIC PARTICLE SORTING USING A COMBINATION OF TRAVELLING AND STANDING SURFACE ACOUSTIC WAVES

Jia Wei Ng[1], David J. Collins[2], Citsabehsan Devendran[1], Ye Ai[2], and Adrian Neild[2]
[1]Lab for Microsystems, Monash University, AUSTRALIA and
[2]Engineering Product Design Pillar, Singapore University of Technology and Design, SINGAPORE

ABSTRACT

Acoustic fields offer a versatile and non-contact method for particle and cell manipulation, where several acoustofluidic systems have been developed for the purpose of sorting. Many acoustic sorting systems rely on either standing waves (SW)[1] or travelling waves (TW)[2, 3] individually and require specific exposure times to the acoustic field, fine-tuned by manipulating the bulk flow rate. Due to the temporal nature of these separations, they are rendered inappropriate for use in systems that require a high degree of flow rate control downstream. Herein, we report a flowrate insensitive size-deterministic sorting system, permitting the continuous separation of 5.1μm, 6.1μm and 7.0μm particles.

KEYWORDS: Particle Sorting, Microfluidics, Lab on a Chip, Acoustofluidics, Surface Acoustic Waves (SAW), Standing Waves, Travelling Waves, Acoustic Radiation Forces

INTRODUCTION

In this work, the device employs a pressure field that utilises both TW and SW components, whose non-uniform spatial distribution arises from the attenuation of a leaky surface acoustic wave (SAW). Particles within their corresponding TW dominant region migrate across multiple wavelengths, drifting into the SW dominant region, where the particles are confined within distinct nodal positions (i.e. stable location) corresponding to their size.

THEORY

This hybrid field is created by counter propagating SAWs, excited by two sets of interdigitated transducers (IDTs) with distance between periodic features, $\lambda_{saw}= 40$μm from either side of a 1200μm wide fluid channel. This design (Figure 1), incorporates a large contrast between the channel width and the typical decay length of the SAW (~ 10 λ_{saw})[4, 5], making the role of attenuation highly significant. The use of higher operational frequency systems reduces the acoustic wavelength, λ_{ac}. When the particle size, r approaches λ_{ac}, the presence of the suspended particle distorts the local pressure field in the surrounding medium, resulting in different force relationships when subjected to a TW or SW pressure field, thus giving rise to novel mechanisms that enables enhanced size-deterministic particle sorting capabilities.

Figure 1: Sketch of the SAW device operating principle: particles with different sizes pass through an acoustic field created by two opposing sets of interdigitated transducers (IDTs) on a piezoelectric Lithium Niobate (LN) substrate.

EXPERIMENTAL

To demonstrate the effect of a mixed wave field in a complex system, a simplified 2D model in COMSOL Multiphysics was used. The model incorporates the effect of TW and SW forces allowing the fundamental principles of operation to be probed. In the experiment, fluorescent polystyrene particles with 5.1, 6.1 and 7.0 μm diameters were injected into the microfluidic channel and are hydrodynamically focused to the sides of the main channel by a central sheath flow with a flow rate of 6 μl/min prior to the continuously SAW field being applied.
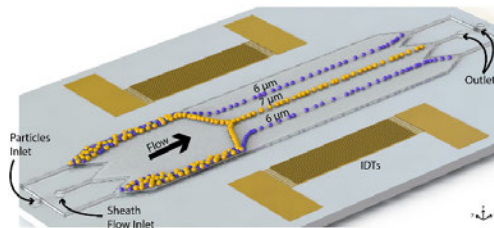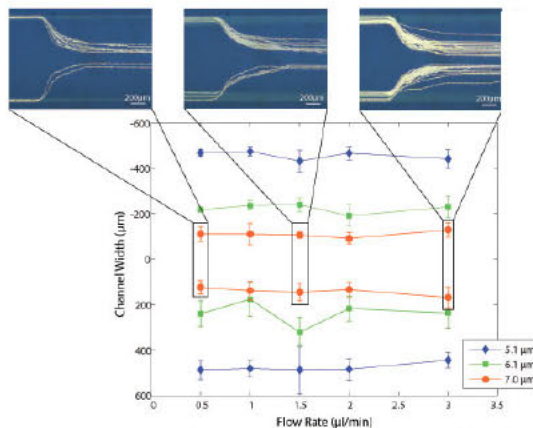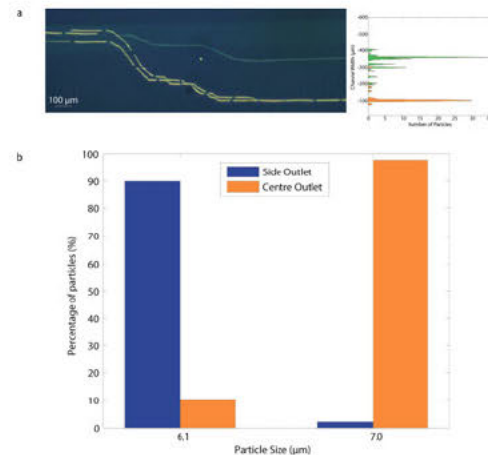
Figure 2: Lateral position of the polystyrene beads of size 5.1 μm (blue), 6.1 μm (green) and 7.0 μm (orange) after their egress from the working region as a function of flow rate.

Figure 3: (a) Continuous distinct separation of fluorescent polystyrene beads of 6.1 μm (green) and 7.0 μm (yellow) diameter. (b) Separation efficiency that is analysed by measuring the distribution of the fluorescence intensity.

RESULTS AND DISCUSSION

From the finite element models, we find that the stable locations for larger particles are at a higher SW to TW ratio (i.e. closer to the central region of the channel) regions. This finding is supported experimentally in Figure 3a, which illustrates the trajectories of the 6.1μm and 7.0μm sized particles exposed to the hybrid pressure field. Using the device, the flow rate has a negligible effect (Figure 2) on the exit locations of the particles as it establishes a unique and stable end location for a given particle size. The separation efficiency of the particles are found to be 90% for 6.1μm and 98% for 7μm beads, as shown in Figure 3b.

CONCLUSION

It was demonstrated that the final confinement location for the particles is dependent on the particle size, and independent of the force field exposure time and thus the flow rate, permitting the continuous separation of 5.1μm, 6.1μm and 7.0μm particles. Omitting the need to precisely control the bulk flow rate potentially enables sorting in a wide range of applications especially in systems which flow is not driven by an external pump.

ACKNOWLEDGEMENTS

REFERENCES

[1] Shi, J., et al., "Continuous particle separation in a microfluidic channel via standing surface acoustic waves (SSAW), " *Lab Chip*, **9**(23): p. 3354-9, 2009.

[2] Destgeer, G., et al., "Submicron separation of microspheres via travelling surface acoustic waves," *Lab Chip*, **14**(24): p. 4665-72, 2014.

[3] Destgeer, G., et al., "Continuous separation of particles in a PDMS microfluidic channel via travelling surface acoustic waves (TSAW)," *Lab Chip*, **13**(21): p. 4210-6, 2013.

[4] Shiokawa, S., Y. Matsui, and T. Ueda, "Liquid streaming and droplet formation caused by leaky Rayleigh waves," *Ultrasonics Symposium, Proceedings, IEEE 1989*, 1989.

[5] Dentry, M.B., L.Y. Yeo, and J.R. Friend, "Frequency effects on the scale and behavior of acoustic streaming," *Phys Rev E Stat Nonlin Soft Matter Phys*, **89**(1): p. 013203, 2014.

CONTACT

* Jia Wei Ng; phone:+J.Q. Public; phone: + 61399050422; jia.wei.ng@monash.edu

1518

Appendix B

Conference paper

The conference paper 'TRAVELLING SURFACE ACOUSTIC WAVES FOR PARTICLE TWEEZING' was presented at the 14th Conference on Acoustofluidics in San Diego, United States of America on August 28-29, 2017. This paper, largely simplifying the material in Chapter 4, is presented on the following page.

Travelling Surface Acoustic Waves for Particle Tweezing

Jia Wei Ng[1] and Citsabehsan Devendran,[1] Adrian Neild[1]

[1] Laboratory for Microsystems, Department of Mechanical and Aerospace Engineering, Monash University, Clayton, Victoria 3800, Australia
E-mail: adrian neild@monash.edu, URL: http://www.labformicrosystems.com/

Introduction
Particle manipulation can be achieved using bulk acoustic waves (BAW) or surface acoustic waves (SAW), both of which harness the acoustic radiation force generated by interaction of a suspended particle with an ultrasonic sound field. In the case of BAW the sound field is usually generated by exciting resonances in the fluid body, under such conditions waves reflected at the interfaces of the fluid constructively interfere creating a standing wave field the shape of which is related to the geometry of the fluid volume. In SAW systems reflections of fluid interfaces are usually weak as the fluid is typically enclosed in PDMS which has a similar acoustic impedance to water. Consequently, the standing waves required to trap particles in patterns, are produced using two separately generated counter propagating travelling waves.

Acoustic particle tweezing refers to the trapping of particles and then the subsequent movement of them by translation of the sound field. Whilst this is possible using BAW, it requires the careful suppression of reflected waves to obtain the required control over the pressure field [1]. However, SAW lends itself more naturally to this process due to the weak reflections present, displacement of the particles once trapped in a standing wave can be achieved by frequency or phase changes [2]. The result is movement of the pattern of particles created in the standing wave. A common factor in approaches to date is the use of a single excitation frequency at any moment of time. In this work, two different frequency travelling waves are excited, our analysis shows that under such conditions a standing wave is not produced, rather a single trapping location exists for the suspended particles, and this single trap's location can be altered very simply by adjusting the relative power of excitation of the two waves.

Working Principle
The acoustic radiation force exerted on a suspended particle can be found using [3]:

$$\boldsymbol{F}^{rad} = -\boldsymbol{\nabla} U^{rad} \tag{1a}$$

$$U^{rad} = \frac{4\pi}{3} a^3 \left[f \frac{1}{2} \kappa_0 \langle p_{in}^2 \rangle - f_3 \frac{3}{4} \rho_0 \langle v_{in}^2 \rangle \right] \tag{1b}$$

$$f(\tilde{\kappa}) = 1 - \tilde{\kappa}, with \ \tilde{\kappa} = \frac{\kappa_p}{\kappa_0} \quad f_2(\tilde{\rho}) = \frac{2(\tilde{\rho} - 1)}{2\tilde{\rho} + 1}, with \ \tilde{\rho} = \frac{\rho_p}{\rho_0} \tag{1c}$$

where U^{rad} is the acoustic potential, $\langle p_{in}^2 \rangle$ and $\langle v_{in}^2 \rangle$ are the temporal average second ordered fluid pressure and velocity at the particle's location, κ and ρ are the compressibility and density of the particle or the fluid with the subscript p or 0.

The difference in the shape of the force field generated by two counter-propagating waves is considered for two cases, that of two identical frequencies and that of two different frequencies. The pressure generated by the two counter propagating waves can be expressed as:

$$p = \rho \phi_A i \omega_a e^{i(\omega_a t - k_a x)} + \rho \phi_B i \omega_b e^{i(\omega_b t + k_b x)} \tag{2}$$

where ϕ_A and ϕ_B are the amplitudes, k_a and k_b are the wavenumbers and ω_a and ω_b are the angular frequencies. The decay of each wave is neglected in this equation. The total pressure is simply a linear summation of the pressures generated by each of the two waves. However, the forces generated are a non-linear effect, so no such superposition can be used. Once the real terms are taken, expanded out and squared, the following unwieldy expression is obtained:

$$
\begin{aligned}
[\Re(p)]^2 &= \rho^2 \phi_A^2 \omega_a^2 [\sin^2 \omega_a t \cos^2 k_a x + \cos^2 \omega_a t \sin^2 k_a x - 2 \sin \omega_a t \cos k_a x \cos \omega_a t \sin k_a x] \\
&\quad + \rho^2 \phi_B^2 \omega_b^2 [\sin^2 \omega_b t \cos^2 k_b x + \cos^2 \omega_b t \sin^2 k_b x - 2 \sin \omega_b t \cos k_b x \cos \omega_b t \sin k_b x]
\end{aligned}
\tag{3}
$$

$$+2\rho^2\phi_A\phi_B\omega_a\omega_b[\sin\omega_a t\cos k_a x\sin\omega_b t\cos k_b x+\sin\omega_a t\cos k_a x\cos\omega_b t\sin k_b x$$
$$-\cos\omega_a t\sin k_a x\sin\omega_b t\cos k_b x-\cos\omega_a t\sin k_a x\cos\omega_b t\sin k_b x]$$

The first square bracket expression is related to only terms related to wave a, the second to wave b, and the third to a mixture of a and b terms. When the time average is taken, it is the $\sin^2\omega t$ and $\cos^2\omega t$ which are non-zero and so contribute to the acoustic force. These are the first two terms in the first two of the square brackets. However, in the third square bracket, containing the mixed subscript a and b terms, the time average depends on whether $\omega_a=\omega_b$. If this is the case, then the first and final terms in the third square bracket contributes to the acoustic radiation force, and the expression can be reduced to $\langle p^2\rangle=2\rho^2\phi^2\omega^2\cos^2 kx$, which predicts a periodicity in the particle patterning which aligns with the periodicity of the standing wave which is produced. However, if the frequencies are not equal, then none of the terms in the third square brackets are non-zero. This means that despite the non-linearity of the acoustic radiation force, the total value of $\langle p^2\rangle$ is simple the summation of the $\langle p^2\rangle$ of each individual wave. As the same can be shown for $\langle v^2\rangle$ the total force is simply the summation of the force generated by the two individual travelling waves. In the case of equation 3, in which no decay is included in the strength of the travelling wave, the total force will be zero as an equal and opposite force is generated from each of the counter-propagating waves, if, however, decay is included a single collection location is achieved at the location at which the forces generated from each of the two waves equate. Under such a scenario, the location of this single trap location can be moved by adjusting the relative amplitude of the two waves.

Experimental Results

An experimental demonstration of the use of two different frequency travelling waves, each decaying due to attenuation of the surface wave as energy is coupled into the fluid, is shown in figure 1. With a comparison of the standing surface acoustic waves (SSAW) and decaying opposing travelling surface acoustic waves (DOTSAW), as well as the trajectory control via altering the relative amplitude of the two waves.
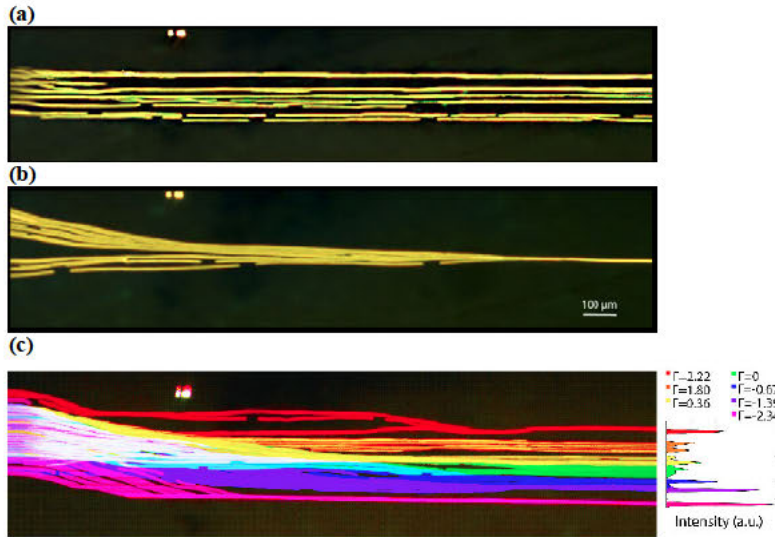
Figure 1: Stacked images of particle trajectories from experiments. (a) SSAW field; where multiple equidistant particle trapping location can be seen in a field generated by two counter-propagating waves of equal frequency. (b) DOTSAW field; where particles are focused to the channel center, in a file generated by decaying, opposing travelling waves of two different frequencies. (c) The trajectories of particles within DOTSAW fields with different relative wave amplitudes, each colour coming from a different experiment.

Conclusion

The use of two different frequency counter-propagating travelling waves has been shown to produce a force field distinctly different to that generated in a standing wave excited when identical frequencies are used. As a result of the properties of this type of excitation, the DOTSAW system can trap particles in a single location, and that location can be displaced via alteration of the relative amplitudes of the two waves.

References
[1] C. R. P. Courtney, C. E. M. Demore, H. Wu, A. Grinenko, P. D. Wilcox, S. Cochran and B. W. Drinkwater, Applied Physics Letters, **104**, 154103 (2014).
[2] F. Guo, Z. Mao, Y. Chen, Z. Xie, J. P. Lata, P. Li, L. Ren, J. Liu, J. Yang, M. Dao, S. Suresh and T. J. Huang, Proceedings of the National Academy of Sciences, **113**, 1522-1527 (2016).
[3] H. Bruus, Lab on a Chip, **12**, 1014-1021 (2012).

Bibliography

[1]   N.-T. Nguyen, S. T. Wereley, and S. A. M. Shaegh, *Fundamentals and applications of microfluidics*. Artech house, 2019.

[2]   H. A. Stone, A. D. Stroock, and A. Ajdari, "Engineering Flows in Small Devices: Microfluidics Toward a Lab-on-a-Chip," *Annual Review of Fluid Mechanics,* vol. 36, no. 1, pp. 381-411, 2004/01/21 2004, doi: 10.1146/annurev.fluid.36.050802.122124.

[3]   N. Gadegaard, S. Mosler, and N. B. Larsen, "Biomimetic Polymer Nanostructures by Injection Molding," vol. 288, no. 1, pp. 76-83, 2003, doi: 10.1002/mame.200290037.

[4]   B. Löchel, "Ultraviolet Depth Lithography and Galvanoforming for Micromachining," *Journal of The Electrochemical Society,* vol. 143, no. 1, p. 237, 1996, doi: 10.1149/1.1836415.

[5]   J. Elders, H. V. Jansen, M. Elwenspoek, and W. Ehrfeld, "DEEMO: a new technology for the fabrication of microstructures," in *Proceedings IEEE Micro Electro Mechanical Systems. 1995*, 1995: IEEE, p. 238.

[6]   D. Janasek, J. Franzke, and A. Manz, "Scaling and the design of miniaturized chemical-analysis systems," *Nature,* vol. 442, no. 7101, pp. 374-380, 2006, doi: 10.1038/nature05059.

[7]   C. D. Meinhart and H. Zhang, "The flow structure inside a microfabricated inkjet printhead," vol. 9, no. 1, pp. 67-75, 2000, doi: 10.1109/84.825779.

[8]   C. Q. Choi, ""Memjet" Momentum," *Scientific American,* vol. 296, no. 6, pp. 24-26, 2007. [Online]. Available: www.jstor.org/stable/26069292.

[9]   J. Heikenfeld *et al.*, "Electrofluidic displays using Young–Laplace transposition of brilliant pigment dispersions," *Nature Photonics,* vol. 3, no. 5, pp. 292-296, 2009, doi: 10.1038/nphoton.2009.68.

[10]   J. Wang, "Microchip devices for detecting terrorist weapons," *Analytica Chimica Acta,* vol. 507, no. 1, pp. 3-10, 2004, doi: 10.1016/j.aca.2003.08.031.

[11]   C. M. B. Ho, S. H. Ng, K. H. H. Li, and Y.-J. Yoon, "3D printed microfluidics for biological applications," *Lab on a Chip,* vol. 15, no. 18, pp. 3627-3637, 2015, doi: 10.1039/c5lc00685f.

[12]   P. Yager *et al.*, "Microfluidic diagnostic technologies for global public health," *Nature,* vol. 442, no. 7101, pp. 412-418, 2006, doi: 10.1038/nature05064.

[13]   C. D. Chin, V. Linder, and S. K. Sia, "Lab-on-a-chip devices for global health: Past studies and future opportunities," *Lab Chip,* vol. 7, no. 1, pp. 41-57, 2007, doi: 10.1039/b611455e.

[14]   J. Knight, "Honey, I shrunk the lab," *Nature,* vol. 418, no. 6897, pp. 474-475, 2002/08/01 2002, doi: 10.1038/418474a.

[15]   S. Haeberle and R. Zengerle, "Microfluidic platforms for lab-on-a-chip applications," *Lab on a Chip,* 10.1039/B706364B vol. 7, no. 9, pp. 1094-1110, 2007, doi: 10.1039/B706364B.

[16]   S. Schumacher *et al.*, "Highly-integrated lab-on-chip system for point-of-care multiparameter analysis," *Lab on a Chip,* vol. 12, no. 3, pp. 464-473, 2012.

[17]   L. J. Carter *et al.*, "Assay Techniques and Test Development for COVID-19 Diagnosis," *ACS Central Science,* vol. 6, no. 5, pp. 591-605, 2020/05/27 2020, doi: 10.1021/acscentsci.0c00501.

[18]   A. S. Fauci, H. C. Lane, and R. R. Redfield, "Covid-19—navigating the uncharted," ed: Mass Medical Soc, 2020.

[19]   E. Morales-Narváez and C. Dincer, "The impact of biosensing in a pandemic outbreak: COVID-19," *Biosensors and Bioelectronics,* vol. 163, p. 112274, 2020/09/01/ 2020, doi: https://doi.org/10.1016/j.bios.2020.112274.

[20]   M. J. Loeffelholz and Y.-W. Tang, "Laboratory diagnosis of emerging human coronavirus infections – the state of the art," *Emerging Microbes & Infections,* vol. 9, no. 1, pp. 747-756, 2020/01/01 2020, doi: 10.1080/22221751.2020.1745095.

[21]   G. Mboowa, "Current and emerging diagnostic tests available for the novel COVID-19 global pandemic," *AAS Open Research,* vol. 3, 2020.

[22]   J. C. Rife, M. I. Bell, J. S. Horwitz, M. N. Kabler, R. C. Y. Auyeung, and W. J. Kim, "Miniature valveless ultrasonic pumps and mixers," vol. 86, no. 1-2, pp. 135-140, 2000, doi: 10.1016/s0924-4247(00)00433-7.

[23]   J. H. Jerman, "Electrically-Activated, Micromachined Diaphragm Valves," in *Micro System Technologies 90*, Berlin, Heidelberg, H. Reichl, Ed., 1990// 1990: Springer Berlin Heidelberg, pp. 806-811.

[24]   P. Rogers and A. Neild, "Selective particle trapping using an oscillating microbubble," *Lab on a Chip,* 10.1039/C1LC20459A vol. 11, no. 21, pp. 3710-3715, 2011, doi: 10.1039/C1LC20459A.

[25]   J. N. Tan and A. Neild, "Microfluidic mixing in a Y-junction open channel," *AIP Advances,* vol. 2, no. 3, p. 032160, 2012, doi: 10.1063/1.4750483.

[26]   W. Wang *et al.*, "Controllable microfluidic production of multicomponent multiple emulsions," vol. 11, no. 9, p. 1587, 2011, doi: 10.1039/c1lc20065h.

[27]   F. Gattiker, F. Umbrecht, J. Neuenschwander, U. Sennhauser, and C. Hierold, "Novel ultrasound read-out for a wireless implantable passive strain sensor (WIPSS)," vol. 145-146, pp. 291-298, 2008, doi: 10.1016/j.sna.2007.09.003.

[28]   T. M. Squires and S. R. Quake, "Microfluidics: Fluid physics at the nanoliter scale," *Reviews of Modern Physics,* vol. 77, no. 3, pp. 977-1026, 10/06/ 2005, doi: 10.1103/RevModPhys.77.977.

[29]   H. Yun, K. Kim, and W. G. Lee, "Cell manipulation in microfluidics," *Biofabrication,* vol. 5, no. 2, p. 022001, 2013/02/13 2013, doi: 10.1088/1758-5082/5/2/022001.

[30]   H. Song and R. F. Ismagilov, "Millisecond Kinetics on a Microfluidic Chip Using Nanoliters of Reagents," *Journal of the American Chemical Society,* vol. 125, no. 47, pp. 14613-14619, 2003, doi: 10.1021/ja0354566.

[31]   B. Zhao, "Surface-Directed Liquid Flow Inside Microchannels," *Science,* vol. 291, no. 5506, pp. 1023-1026, 2001, doi: 10.1126/science.291.5506.1023.

[32]   E. Berthier and D. J. Beebe, "Flow rate analysis of a surface tension driven passive micropump," *Lab on a Chip,* 10.1039/B707637A vol. 7, no. 11, pp. 1475-1478, 2007, doi: 10.1039/B707637A.

[33]   A. Karimi, S. Yazdi, and A. M. Ardekani, "Hydrodynamic mechanisms of cell and particle trapping in microfluidics," *Biomicrofluidics,* vol. 7, no. 2, p. 021501, 2013, doi: 10.1063/1.4799787.

[34]   D. Huh *et al.*, "Gravity-Driven Microfluidic Particle Sorting Device with Hydrodynamic Separation Amplification," *Analytical Chemistry,* vol. 79, no. 4, pp. 1369-1376, 2007, doi: 10.1021/ac061542n.

[35]   A. A. S. Bhagat, H. W. Hou, L. D. Li, C. T. Lim, and J. Han, "Pinched flow coupled shear-modulated inertial microfluidics for high-throughput rare blood cell separation," *Lab on a Chip,* 10.1039/C0LC00633E vol. 11, no. 11, pp. 1870-1878, 2011, doi: 10.1039/C0LC00633E.

[36]   Z. Wu and K. Hjort, "Microfluidic hydrodynamic cell separation: a review," *Micro and Nanosystems,* vol. 1, no. 3, pp. 181-192, 2009.

[37]   D. W. Inglis, J. A. Davis, R. H. Austin, and J. C. Sturm, "Critical particle size for fractionation by deterministic lateral displacement," *Lab on a Chip,* vol. 6, no. 5, p. 655, 2006, doi: 10.1039/b515371a.

[38]   A. A. S. Bhagat, S. S. Kuntaegowdanahalli, and I. Papautsky, "Continuous particle separation in spiral microchannels using dean flows and differential migration," *Lab on a Chip,* vol. 8, no. 11, p. 1906, 2008, doi: 10.1039/b807107a.

[39]   M. Zborowski, P. S. Malchesky, T. F. Jan, and G. S. Hall, "Quantitative separation of bacteria in saline solution using lanthanide Er(III) and a magnetic field," *Journal of General Microbiology,* vol. 138, no. 1, pp. 63-68, 1992, doi: 10.1099/00221287-138-1-63.

[40]   C. Wilhelm *et al.*, "Binding of biological effectors on magnetic nanoparticles measured by a magnetically induced transient birefringence experiment," *Physical Review E,* vol. 65, no. 3, p. 031404, 02/19/ 2002, doi: 10.1103/PhysRevE.65.031404.

[41]   , "Magnetophoresis: Fundamentals and Applications," in *Wiley Encyclopedia of Electrical and Electronics Engineering*, pp. 1-23.

[42]   A. Hultgren, M. Tanase, C. S. Chen, G. J. Meyer, and D. H. Reich, "Cell manipulation using magnetic nanowires," *Journal of Applied Physics,* vol. 93, no. 10, pp. 7554-7556, 2003, doi: 10.1063/1.1556204.

[43]   N. Pamme and C. Wilhelm, "Continuous sorting of magnetic cells via on-chip free-flow magnetophoresis," *Lab on a Chip,* vol. 6, no. 8, p. 974, 2006, doi: 10.1039/b604542a.

[44]   A. Egatz-GóMez *et al.*, "Discrete magnetic microfluidics," vol. 89, no. 3, p. 034106, 2006, doi: 10.1063/1.2227517.

[45]   P. Dunnill and M. D. Lilly, "Purification of enzymes using magnetic bio-affinity materials," *Biotechnology and Bioengineering,* vol. 16, no. 7, pp. 987-990, 1974, doi: 10.1002/bit.260160710.

[46]   K. Mosbach and L. Andersson, "Magnetic ferrofluids for preparation of magnetic polymers and their application in affinity chromatography," vol. 270, no. 5634, pp. 259-261, 1977, doi: 10.1038/270259a0.

[47]   A. Kondo, H. Kamura, and K. Higashitani, "Development and application of thermo-sensitive magnetic immunomicrospheres for antibody purification," *Applied Microbiology and Biotechnology,* vol. 41, no. 1, pp. 99-105, 1994, doi: 10.1007/bf00166089.

[48]   U. Lehmann, C. Vandevyver, V. K. Parashar, and M. A. M. Gijs, "Droplet-Based DNA Purification in a Magnetic Lab-on-a-Chip," *Angewandte Chemie International Edition,* vol. 45, no. 19, pp. 3062-3067, 2006, doi: 10.1002/anie.200503624.

[49] S. Kwakye and A. Baeumner, "A microfluidic biosensor based on nucleic acid sequence recognition," *Analytical and Bioanalytical Chemistry,* vol. 376, no. 7, pp. 1062-1068, 2003/08/01 2003, doi: 10.1007/s00216-003-2063-2.

[50] W. H. Grover and R. A. Mathies, "An integrated microfluidic processor for single nucleotide polymorphism-based DNA computing," *Lab on a Chip,* 10.1039/B505840F vol. 5, no. 10, pp. 1033-1040, 2005, doi: 10.1039/B505840F.

[51] X. Wang, X.-B. Wang, and P. R. C. Gascoyne, "General expressions for dielectrophoretic force and electrorotational torque derived using the Maxwell stress tensor method," vol. 39, no. 4, pp. 277-295, 1997, doi: 10.1016/s0304-3886(97)00126-5.

[52] D. S. Clague and E. K. Wheeler, "Dielectrophoretic manipulation of macromolecules: The electric field," *Physical Review E,* vol. 64, no. 2, p. 026605, 07/18/ 2001, doi: 10.1103/PhysRevE.64.026605.

[53] P. R. C. Gascoyne and J. Vykoukal, "Particle separation by dielectrophoresis," *ELECTROPHORESIS,* vol. 23, no. 13, pp. 1973-1983, 2002, doi: 10.1002/1522-2683(200207)23:13<1973::Aid-elps1973>3.0.Co;2-1.

[54] H. A. Pohl, "Dielectrophoresis: Applications to the Characterization and Separation of Cells," in *Methods of Cell Separation*, N. Catsimpoolas Ed. Boston, MA: Springer US, 1977, pp. 67-169.

[55] G. Fuhr, T. Müller, V. Baukloh, and K. Lucas, "High-frequency electric field trapping of individual human spermatozoa," *Human Reproduction,* vol. 13, no. 1, pp. 136-141, 1998, doi: 10.1093/humrep/13.1.136.

[56] T. Heida, W. L. C. Rutten, and E. Marani, "Dielectrophoretic trapping of dissociated fetal cortical rat neurons," *IEEE Transactions on Biomedical Engineering,* vol. 48, no. 8, pp. 921-930, 2001, doi: 10.1109/10.936368.

[57] M. Mischel, F. Roug , I. Lamprecht, C. Aubert, and G. Prota, "Dielectrophoresis of malignant human melanocytes," vol. 275, no. 3, pp. 141-143, 1983, doi: 10.1007/bf00510042.

[58] B. H. Lapizco-Encinas, B. A. Simmons, E. B. Cummings, and Y. Fintschenko, "Dielectrophoretic Concentration and Separation of Live and Dead Bacteria in an Array of Insulators," *Analytical Chemistry,* vol. 76, no. 6, pp. 1571-1579, 2004/03/01 2004, doi: 10.1021/ac034804j.

[59] S. P. Desai and J. Voldman, "Measuring the impact of dielectrophoresis on cell physiology using a high-content screening platform," in *Proceedings of the Micro Total Analysis Systems*, 2008, vol. 8, pp. 1308-1310.

[60] A. Ashkin, J. M. Dziedzic, J. E. Bjorkholm, and S. Chu, "Observation of a single-beam gradient force optical trap for dielectric particles," *Optics Letters,* vol. 11, no. 5, p. 288, 1986, doi: 10.1364/ol.11.000288.

[61] J. Lee, K. Ha, and K. K. Shung, "A theoretical study of the feasibility of acoustical tweezers: Ray acoustics approach," *The Journal of the Acoustical Society of America,* vol. 117, no. 5, pp. 3273-3280, 2005, doi: 10.1121/1.1886387.

[62] K. Dholakia, P. Reece, and M. Gu, "Optical micromanipulation," *Chem. Soc. Rev.,* vol. 37, no. 1, pp. 42-55, 2008, doi: 10.1039/b512471a.

[63] A. Ashkin, "Trapping of Atoms by Resonance Radiation Pressure," *Physical Review Letters,* vol. 40, no. 12, pp. 729-732, 1978, doi: 10.1103/physrevlett.40.729.

[64] A. Ashkin, K. Schütze, J. M. Dziedzic, U. Euteneuer, and M. Schliwa, "Force generation of organelle transport measured in vivo by an infrared laser trap," *Nature,* vol. 348, no. 6299, pp. 346-348, 1990, doi: 10.1038/348346a0.

[65]   M. Dao, C. T. Lim, and S. Suresh, "Mechanics of the human red blood cell deformed by optical tweezers," *Journal of the Mechanics and Physics of Solids,* vol. 51, no. 11-12, pp. 2259-2280, 2003, doi: 10.1016/j.jmps.2003.09.019.

[66]   K. C. Neuman, E. H. Chadd, G. F. Liou, K. Bergman, and S. M. Block, "Characterization of photodamage to Escherichia coli in optical traps," (in eng), *Biophys J,* vol. 77, no. 5, pp. 2856-2863, 1999, doi: 10.1016/S0006-3495(99)77117-1.

[67]   G. Leitz, E. Fällman, S. Tuck, and O. Axner, "Stress response in Caenorhabditis elegans caused by optical tweezers: wavelength, power, and time dependence," (in eng), *Biophys J,* vol. 82, no. 4, pp. 2224-2231, 2002, doi: 10.1016/S0006-3495(02)75568-9.

[68]   M. Bregnhøj, A. Blázquez-Castro, M. Westberg, T. Breitenbach, and P. R. Ogilby, "Direct 765 nm Optical Excitation of Molecular Oxygen in Solution and in Single Mammalian Cells," *The Journal of Physical Chemistry B,* vol. 119, no. 17, pp. 5422-5429, 2015/04/30 2015, doi: 10.1021/acs.jpcb.5b01727.

[69]   P. Haro-González *et al.*, "Quantum Dot-Based Thermal Spectroscopy and Imaging of Optically Trapped Microspheres and Single Cells," *Small,* vol. 9, no. 12, pp. 2162-2170, 2013, doi: 10.1002/smll.201201740.

[70]   A.-I. Bunea and J. Glückstad, "Strategies for Optical Trapping in Biological Samples: Aiming at Microrobotic Surgeons," *Laser & Photonics Reviews,* vol. 13, no. 4, p. 1800227, 2019, doi: 10.1002/lpor.201800227.

[71]   Z. Liu *et al.*, "Optical funnel for living cells trap," *Optics Communications,* vol. 431, pp. 196-198, 2019/01/15/ 2019, doi: https://doi.org/10.1016/j.optcom.2018.09.023.

[72]   B. Koss, S. Chowdhury, T. Aabo, S. Gupta, and W. Losert, "Indirect optical gripping with triplet traps," *JOSA B,* vol. 28, no. 5, pp. 982-985, 2011.

[73]   D. Débarre, N. Olivier, W. Supatto, and E. Beaurepaire, "Mitigating phototoxicity during multiphoton microscopy of live Drosophila embryos in the 1.0-1.2 μm wavelength range," (in eng), *PLoS One,* vol. 9, no. 8, pp. e104250-e104250, 2014, doi: 10.1371/journal.pone.0104250.

[74]   C. Macias-Romero, V. Zubkovs, S. Wang, and S. Roke, "Wide-field medium-repetition-rate multiphoton microscopy reduces photodamage of living cells," (in eng), *Biomed Opt Express,* vol. 7, no. 4, pp. 1458-1467, 2016, doi: 10.1364/BOE.7.001458.

[75]   M. P. Landry, P. M. McCall, Z. Qi, and Y. R. Chemla, "Characterization of photoactivated singlet oxygen damage in single-molecule optical trap experiments," (in eng), *Biophys J,* vol. 97, no. 8, pp. 2128-2136, 2009, doi: 10.1016/j.bpj.2009.07.048.

[76]   T. L. Min, P. J. Mears, L. M. Chubiz, C. V. Rao, I. Golding, and Y. R. Chemla, "High-resolution, long-term characterization of bacterial motility using optical tweezers," (in eng), *Nat Methods,* vol. 6, no. 11, pp. 831-835, 2009, doi: 10.1038/nmeth.1380.

[77]   M. Swoboda *et al.*, "Enzymatic oxygen scavenging for photostability without pH drop in single-molecule experiments," (in eng), *ACS Nano,* vol. 6, no. 7, pp. 6364-6369, 2012, doi: 10.1021/nn301895c.

[78]   H. Mao, J. R. Arias-Gonzalez, S. B. Smith, I. Tinoco, Jr., and C. Bustamante, "Temperature control methods in a laser tweezers system," (in eng), *Biophys J,* vol. 89, no. 2, pp. 1308-1316, 2005, doi: 10.1529/biophysj.104.054536.

[79]   S. Deshmukh, Z. Brzozka, T. Laurell, and P. Augustsson, "Acoustic radiation forces at liquid interfaces impact the performance of acoustophoresis," *Lab on a*

Chip, 10.1039/C4LC00572D vol. 14, no. 17, pp. 3394-3400, 2014, doi: 10.1039/C4LC00572D.

[80]   P. Augustsson, J. T. Karlsen, H.-W. Su, H. Bruus, and J. Voldman, "Iso-acoustic focusing of cells for size-insensitive acousto-mechanical phenotyping," (in eng), *Nat Commun,* vol. 7, pp. 11556-11556, 2016, doi: 10.1038/ncomms11556.

[81]   J. T. Karlsen, P. Augustsson, and H. Bruus, "Acoustic force density acting on inhomogeneous fluids in acoustic fields," *Physical review letters,* vol. 117, no. 11, p. 114504, 2016.

[82]   H. Bruus, "Acoustofluidics 2: Perturbation theory and ultrasound resonance modes," *Lab on a Chip,* 10.1039/C1LC20770A vol. 12, no. 1, pp. 20-28, 2012, doi: 10.1039/C1LC20770A.

[83]   K. Yosioka and Y. Kawasima, "Acoustic radiation pressure on a compressible sphere," *Acta Acustica United with Acustica,* vol. 5, no. 3, pp. 167-173, 1955.

[84]   L. P. Gor'kov, "On the forces acting on a small particle in an acoustical field in an ideal fluid," in *Sov. Phys. Dokl.*, 1962, vol. 6, pp. 773-775.

[85]   H. Bruus, "Acoustofluidics 7: The acoustic radiation force on small particles," *Lab on a Chip,* vol. 12, no. 6, p. 1014, 2012, doi: 10.1039/c2lc21068a.

[86]   S. J. Lighthill, "Acoustic streaming," *Journal of Sound and Vibration,* vol. 61, no. 3, pp. 391-418, 1978/12/08/ 1978, doi: https://doi.org/10.1016/0022-460X(78)90388-7.

[87]   J. W. Strutt, "On the circulation of air observed in kundt’s tubes, and on some allied acoustical problems," *Proceedings of the Royal Society of London,* vol. 36, no. 228-231, pp. 10-11, 1883, doi: doi:10.1098/rspl.1883.0075.

[88]   P. B. Muller *et al.*, "Ultrasound-induced acoustophoretic motion of microparticles in three dimensions," *Physical Review E,* vol. 88, no. 2, p. 023006, 08/08/ 2013, doi: 10.1103/PhysRevE.88.023006.

[89]   H. Schlichting, "Berechnung ebener periodischer Grenzschichtstromungen," *Phys. z.,* vol. 33, pp. 327-335, 1932.

[90]   P. Tho, R. Manasseh, and A. Ooi, "Cavitation microstreaming patterns in single and multiple bubble systems," *Journal of Fluid Mechanics,* vol. 576, pp. 191-233, 2007, doi: 10.1017/s0022112006004393.

[91]   C. Eckart, "Vortices and Streams Caused by Sound Waves," *Physical Review,* vol. 73, no. 1, pp. 68-76, 01/01/ 1948, doi: 10.1103/PhysRev.73.68.

[92]   A. Riaud, M. Baudoin, O. Bou Matar, J. L. Thomas, and P. Brunet, "On the influence of viscosity and caustics on acoustic streaming in sessile droplets: an experimental and a numerical study with a cost-effective method," *Journal of Fluid Mechanics,* vol. 821, pp. 384-420, 2017, doi: 10.1017/jfm.2017.178.

[93]   J. Eisener, A. Lippert, T. Nowak, C. Cairós, F. Reuter, and R. Mettin, "Characterization of Acoustic Streaming Beyond 100 MHz," *Physics Procedia,* vol. 70, pp. 151-154, 2015/01/01/ 2015, doi: https://doi.org/10.1016/j.phpro.2015.08.075.

[94]   J. Stuart, "Double boundary layers in oscillatory viscous flow," *Journal of Fluid Mechanics,* vol. 24, no. 4, pp. 673-687, 1966.

[95]   P. B. Muller, R. Barnkob, M. J. H. Jensen, and H. Bruus, "A numerical study of microparticle acoustophoresis driven by acoustic radiation forces and streaming-induced drag forces," *Lab on a Chip,* 10.1039/C2LC40612H vol. 12, no. 22, pp. 4617-4627, 2012, doi: 10.1039/C2LC40612H.

[96]   R. Barnkob, P. Augustsson, T. Laurell, and H. Bruus, "Acoustic radiation- and streaming-induced microparticle velocities determined by microparticle image

velocimetry in an ultrasound symmetry plane," *Physical Review E,* vol. 86, no. 5, p. 056307, 11/13/ 2012, doi: 10.1103/PhysRevE.86.056307.

[97]   S. Shiokawa, Y. Matsui, and T. Ueda, "Liquid streaming and droplet formation caused by leaky Rayleigh waves," in *Proceedings., IEEE Ultrasonics Symposium*, 3-6 Oct. 1989 1989, pp. 643-646 vol.1, doi: 10.1109/ULTSYM.1989.67063.

[98]   A. Fakhfouri, C. Devendran, A. Ahmed, J. Soria, and A. Neild, "The size dependant behaviour of particles driven by a travelling surface acoustic wave (TSAW)," *Lab on a Chip,* 10.1039/C8LC01155A vol. 18, no. 24, pp. 3926-3938, 2018, doi: 10.1039/C8LC01155A.

[99]   V. Bjerknes, *Die Kraftfelder* (no. 28). F. Vieweg, 1909.

[100]   W. König, "Hydrodynamisch-akustische Untersuchungen," *Annalen der Physik,* vol. 278, no. 4, pp. 549-563, 1891, doi: 10.1002/andp.18912780404.

[101]   R. Habibi and A. Neild, "Sound wave activated nano-sieve (SWANS) for enrichment of nanoparticles," *Lab on a Chip,* vol. 19, no. 18, pp. 3032-3044, 2019, doi: 10.1039/c9lc00369j.

[102]   B. Hammarström, T. Laurell, and J. Nilsson, "Seed particle-enabled acoustic trapping of bacteria and nanoparticles in continuous flow systems," *Lab on a Chip,* 10.1039/C2LC40697G vol. 12, no. 21, pp. 4296-4304, 2012, doi: 10.1039/C2LC40697G.

[103]   M. Evander, O. Gidlöf, B. Olde, D. Erlinge, and T. Laurell, "Non-contact acoustic capture of microparticles from small plasma volumes," *Lab on a Chip,* vol. 15, no. 12, pp. 2588-2596, 2015, doi: 10.1039/c5lc00290g.

[104]   P. Ohlsson *et al.*, "Integrated Acoustic Separation, Enrichment, and Microchip Polymerase Chain Reaction Detection of Bacteria from Blood for Rapid Sepsis Diagnostics," *Analytical Chemistry,* vol. 88, no. 19, pp. 9403-9411, 2016/10/04 2016, doi: 10.1021/acs.analchem.6b00323.

[105]   M. Tenje *et al.*, "Acoustic trapping as a generic non-contact incubation site for multiplex bead-based assays," *Analytica Chimica Acta,* vol. 853, pp. 682-688, 2015, doi: 10.1016/j.aca.2014.07.008.

[106]   F. Trampler, S. A. Sonderhoff, P. W. S. Pui, D. G. Kilburn, and J. M. Piret, "Acoustic Cell Filter for High Density Perfusion Culture of Hybridoma Cells," *Bio/Technology,* vol. 12, no. 3, pp. 281-284, 1994/03/01 1994, doi: 10.1038/nbt0394-281.

[107]   J. Friend and L. Y. Yeo, "Microscale acoustofluidics: Microfluidics driven via acoustics and ultrasonics," *Reviews of Modern Physics,* vol. 83, no. 2, pp. 647-704, 06/20/ 2011, doi: 10.1103/RevModPhys.83.647.

[108]   C. R. P. Courtney *et al.*, "Manipulation of microparticles using phase-controllable ultrasonic standing waves," *The Journal of the Acoustical Society of America,* vol. 128, no. 4, pp. EL195-EL199, 2010, doi: 10.1121/1.3479976.

[109]   C. R. P. Courtney *et al.*, "Independent trapping and manipulation of microparticles using dexterous acoustic tweezers," *Applied Physics Letters,* vol. 104, no. 15, p. 154103, 2014, doi: 10.1063/1.4870489.

[110]   T. Kozuka, T. Tuziuti, H. Mitome, T. Fukuda, and F. Arai, "Control of position of a particle using a standing wave field generated by crossing sound beams," in *1998 IEEE Ultrasonics Symposium. Proceedings (Cat. No. 98CH36102)*, 1998, vol. 1: IEEE, pp. 657-660.

[111]   A. Grinenko, C. K. Ong, C. R. P. Courtney, P. D. Wilcox, and B. W. Drinkwater, "Efficient counter-propagating wave acoustic micro-particle

manipulation," *Applied Physics Letters,* vol. 101, no. 23, p. 233501, 2012, doi: 10.1063/1.4769092.

[112] M. Ward, P. Turner, M. DeJohn, and G. Kaduchak, "Fundamentals of Acoustic Cytometry," *Current Protocols in Cytometry,* vol. 49, no. 1, pp. 1.22.1-1.22.12, 2009, doi: 10.1002/0471142956.cy0122s49.

[113] D. Kamsma and G. J. L. Wuite, "Single-Molecule Measurements Using Acoustic Force Spectroscopy (AFS)," in *Single Molecule Analysis: Methods and Protocols*, E. J. G. Peterman Ed. New York, NY: Springer New York, 2018, pp. 341-351.

[114] L. Rayleigh, "On Waves Propagated along the Plane Surface of an Elastic Solid," *Proceedings of the London Mathematical Society,* vol. s1-17, no. 1, pp. 4-11, 1885, doi: 10.1112/plms/s1-17.1.4.

[115] D. J. Collins, A. Neild, and Y. Ai, "Highly focused high-frequency travelling surface acoustic waves (SAW) for rapid single-particle sorting," *Lab on a Chip,* 10.1039/C5LC01335F vol. 16, no. 3, pp. 471-479, 2016, doi: 10.1039/C5LC01335F.

[116] G. Destgeer, B. H. Ha, J. H. Jung, and H. J. Sung, "Submicron separation of microspheres via travelling surface acoustic waves," *Lab on a Chip,* 10.1039/C4LC00868E vol. 14, no. 24, pp. 4665-4672, 2014, doi: 10.1039/C4LC00868E.

[117] G. Destgeer, B. H. Ha, J. Park, J. H. Jung, A. Alazzam, and H. J. Sung, "Microchannel Anechoic Corner for Size-Selective Separation and Medium Exchange via Traveling Surface Acoustic Waves," *Analytical Chemistry,* vol. 87, no. 9, pp. 4627-4632, 2015/05/05 2015, doi: 10.1021/acs.analchem.5b00525.

[118] R. Shilton, M. K. Tan, L. Y. Yeo, and J. R. Friend, "Particle concentration and mixing in microdrops driven by focused surface acoustic waves," *Journal of Applied Physics,* vol. 104, no. 1, p. 014910, 2008/07/01 2008, doi: 10.1063/1.2951467.

[119] J. Shi, D. Ahmed, X. Mao, S.-C. S. Lin, A. Lawit, and T. J. Huang, "Acoustic tweezers: patterning cells and microparticles using standing surface acoustic waves (SSAW)," *Lab on a Chip,* 10.1039/B910595F vol. 9, no. 20, pp. 2890-2895, 2009, doi: 10.1039/B910595F.

[120] M. Sesen, T. Alan, and A. Neild, "Microfluidic plug steering using surface acoustic waves," *Lab on a Chip,* 10.1039/C5LC00468C vol. 15, no. 14, pp. 3030-3038, 2015, doi: 10.1039/C5LC00468C.

[121] Z. Guttenberg *et al.*, "Planar chip device for PCR and hybridization with surface acoustic wave pump," *Lab on a Chip,* 10.1039/B412712A vol. 5, no. 3, pp. 308-317, 2005, doi: 10.1039/B412712A.

[122] M. Cecchini, S. Girardo, D. Pisignano, R. Cingolani, and F. Beltram, "Acoustic-counterflow microfluidics by surface acoustic waves," *Applied Physics Letters,* vol. 92, no. 10, p. 104103, 2008/03/10 2008, doi: 10.1063/1.2889951.

[123] W.-K. Tseng, J.-L. Lin, W.-C. Sung, S.-H. Chen, and G.-B. Lee, "Active micro-mixers using surface acoustic waves on Y-cut 128° LiNbO3," *Journal of Micromechanics and Microengineering,* vol. 16, no. 3, pp. 539-548, 2006/02/06 2006, doi: 10.1088/0960-1317/16/3/009.

[124] T. Frommelt, M. Kostur, M. Wenzel-Schäfer, P. Talkner, P. Hänggi, and A. Wixforth, "Microfluidic Mixing via Acoustically Driven Chaotic Advection," *Physical Review Letters,* vol. 100, no. 3, p. 034502, 01/24/ 2008, doi: 10.1103/PhysRevLett.100.034502.

[125] R. J. Shilton, L. Y. Yeo, and J. R. Friend, "Quantification of surface acoustic wave induced chaotic mixing-flows in microfluidic wells," *Sensors and Actuators B: Chemical,* vol. 160, no. 1, pp. 1565-1572, 2011/12/15/ 2011, doi: https://doi.org/10.1016/j.snb.2011.09.007.

[126] J. O. Castro, S. Ramesan, A. R. Rezk, and L. Y. Yeo, "Continuous tuneable droplet ejection via pulsed surface acoustic wave jetting," *Soft Matter,* 10.1039/C7SM02534C vol. 14, no. 28, pp. 5721-5727, 2018, doi: 10.1039/C7SM02534C.

[127] D. J. Collins, O. Manor, A. Winkler, H. Schmidt, J. R. Friend, and L. Y. Yeo, "Atomization off thin water films generated by high-frequency substrate wave vibrations," *Physical Review E,* vol. 86, no. 5, p. 056312, 11/20/ 2012, doi: 10.1103/PhysRevE.86.056312.

[128] M. Kurosawa, T. Watanabe, A. Futami, and T. Higuchi, "Surface acoustic wave atomizer," *Sensors and Actuators-A-Physical Sensors,* vol. 50, no. 1, pp. 69-74, 1995.

[129] J. R. Friend, L. Y. Yeo, D. R. Arifin, and A. Mechler, "Evaporative self-assembly assisted synthesis of polymeric nanoparticles by surface acoustic wave atomization," *Nanotechnology,* vol. 19, no. 14, p. 145301, 2008/03/04 2008, doi: 10.1088/0957-4484/19/14/145301.

[130] W. Tsung-Tsong, T. He-Tai, C. Yung-Yu, and L. Pei-Ling, "Analysis and design of focused interdigital transducers," *IEEE Transactions on Ultrasonics, Ferroelectrics, and Frequency Control,* vol. 52, no. 8, pp. 1384-1392, 2005, doi: 10.1109/TUFFC.2005.1509798.

[131] X. Ding *et al.*, "On-chip manipulation of single microparticles, cells, and organisms using surface acoustic waves," *Proceedings of the National Academy of Sciences,* vol. 109, no. 28, p. 11105, 2012, doi: 10.1073/pnas.1209288109.

[132] H. Yatsuda, "Design techniques for SAW filters using slanted finger interdigital transducers," *IEEE Transactions on Ultrasonics, Ferroelectrics, and Frequency Control,* vol. 44, no. 2, pp. 453-459, 1997, doi: 10.1109/58.585130.

[133] T. Laurell and A. Lenshof, *Microscale Acoustofluidics*. Royal Society of Chemistry, 2014.

[134] J. D. N. Cheeke, *Fundamentals and applications of ultrasonic waves*. CRC press, 2017.

[135] G. Destgeer, B. H. Ha, J. H. Jung, and H. J. Sung, "Submicron separation of microspheres via travelling surface acoustic waves," *Lab Chip,* vol. 14, no. 24, pp. 4665-4672, 2014, doi: 10.1039/c4lc00868e.

[136] V. Skowronek, R. W. Rambach, L. Schmid, K. Haase, and T. Franke, "Particle Deflection in a Poly(dimethylsiloxane) Microchannel Using a Propagating Surface Acoustic Wave: Size and Frequency Dependence," *Analytical Chemistry,* vol. 85, no. 20, pp. 9955-9959, 2013/10/15 2013, doi: 10.1021/ac402607p.

[137] G. Destgeer, S. Im, B. Hang Ha, J. Ho Jung, M. Ahmad Ansari, and H. Jin Sung, "Adjustable, rapidly switching microfluidic gradient generation using focused travelling surface acoustic waves," *Applied Physics Letters,* vol. 104, no. 2, p. 023506, 2014/01/13 2014, doi: 10.1063/1.4862322.

[138] Y. Chen *et al.*, "Standing surface acoustic wave (SSAW)-based microfluidic cytometer," *Lab Chip,* vol. 14, no. 5, pp. 916-923, 2014, doi: 10.1039/c3lc51139a.

[139] Y. Ai, C. K. Sanders, and B. L. Marrone, "Separation of Escherichia coli Bacteria from Peripheral Blood Mononuclear Cells Using Standing Surface

Acoustic Waves," vol. 85, no. 19, pp. 9126-9134, 2013, doi: 10.1021/ac4017715.

[140] Y. Ai, C. K. Sanders, and B. L. Marrone, "Separation of Escherichia coli Bacteria from Peripheral Blood Mononuclear Cells Using Standing Surface Acoustic Waves," *Analytical Chemistry,* vol. 85, no. 19, pp. 9126-9134, 2013/10/01 2013, doi: 10.1021/ac4017715.

[141] X. Ding *et al.*, "Cell separation using tilted-angle standing surface acoustic waves," vol. 111, no. 36, pp. 12992-12997, 2014, doi: 10.1073/pnas.1413325111.

[142] S. Li *et al.*, "Standing surface acoustic wave (SSAW)-based cell washing," *Lab on a Chip,* vol. 15, no. 1, pp. 331-338, 2015, doi: 10.1039/c4lc00903g.

[143] D. J. Collins, B. Morahan, J. Garcia-Bustos, C. Doerig, M. Plebanski, and A. Neild, "Two-dimensional single-cell patterning with one cell per well driven by surface acoustic waves," *Nature Communications,* vol. 6, no. 1, p. 8686, 2015/11/02 2015, doi: 10.1038/ncomms9686.

[144] C. D. Wood *et al.*, "Formation and manipulation of two-dimensional arrays of micron-scale particles in microfluidic systems by surface acoustic waves," *Applied Physics Letters,* vol. 94, no. 5, p. 054101, 2009/02/02 2009, doi: 10.1063/1.3076127.

[145] D. J. Collins, T. Alan, and A. Neild, "Particle separation using virtual deterministic lateral displacement (vDLD)," vol. 14, no. 9, p. 1595, 2014, doi: 10.1039/c3lc51367j.

[146] D. J. Collins, C. Devendran, Z. Ma, J. W. Ng, A. Neild, and Y. Ai, "Acoustic tweezers via sub–time-of-flight regime surface acoustic waves," *Science Advances,* vol. 2, no. 7, p. e1600089, 2016, doi: 10.1126/sciadv.1600089.

[147] D. J. Collins *et al.*, "Self-Aligned Acoustofluidic Particle Focusing and Patterning in Microfluidic Channels from Channel-Based Acoustic Waveguides," *Physical Review Letters,* vol. 120, no. 7, p. 074502, 02/15/ 2018, doi: 10.1103/PhysRevLett.120.074502.

[148] R. T. Smith and F. S. Welsh, "Temperature Dependence of the Elastic, Piezoelectric, and Dielectric Constants of Lithium Tantalate and Lithium Niobate," *Journal of Applied Physics,* vol. 42, no. 6, pp. 2219-2230, 1971/05/01 1971, doi: 10.1063/1.1660528.

[149] J. F. Tressler, S. Alkoy, and R. E. Newnham, "Piezoelectric Sensors and Sensor Materials," *Journal of Electroceramics,* vol. 2, no. 4, pp. 257-272, 1998/12/01 1998, doi: 10.1023/A:1009926623551.

[150] D. Ciplys and R. Rimeika, "Measurements of electromechanical coupling coefficient for surface acoustic waves in proton-exchanged lithium niobate," *Ultragarsas" Ultrasound",* vol. 33, no. 3, pp. 14-20, 1999.

[151] J. C. McDonald *et al.*, "Fabrication of microfluidic systems in poly(dimethylsiloxane)," *ELECTROPHORESIS,* vol. 21, no. 1, pp. 27-40, 2000, doi: 10.1002/(sici)1522-2683(20000101)21:1<27::Aid-elps27>3.0.Co;2-c.

[152] C. f. Chen and K. Wharton, "Characterization and failure mode analyses of air plasma oxidized PDMS–PDMS bonding by peel testing," *RSC Advances,* 10.1039/C6RA25947B vol. 7, no. 3, pp. 1286-1289, 2017, doi: 10.1039/C6RA25947B.

[153] J. W. Ng, D. J. Collins, C. Devendran, Y. Ai, and A. Neild, "Flow-rate-insensitive deterministic particle sorting using a combination of travelling and standing surface acoustic waves," *Microfluidics and Nanofluidics,* vol. 20, no. 11, 2016, doi: 10.1007/s10404-016-1814-2.

[154]   J. W. Ng, C. Devendran, and A. Neild, "Acoustic tweezing of particles using decaying opposing travelling surface acoustic waves (DOTSAW)," *Lab on a Chip,* vol. 17, no. 20, pp. 3489-3497, 2017, doi: 10.1039/c7lc00862g.